Faculdade de Engenharia da Universidade do Porto

Hydrogels Derived from Decellularized Intestines as Platforms for Studying Colorectal Cancer

Carlos José Marinho Botelho

Dissertation for the Master's Degree in Molecular Bioengineering

Supervisor: Mário Barbosa [1,2]
Co-Supervisor: Joana Caldeira [3]

[1] Professor at ICBAS - School of Medicine and Biomedical Sciences
[2] Principal Investigator at Institute for Research and Innovation in Health, i3S
[3] Junior Researcher at Institute for Research and Innovation in Health, i3S

September 15th, 2022

“And once the storm is over, you won’t remember how you made it through, how you managed to survive. You won’t even be sure, whether the storm is really over. But one thing is certain. When you come out of the storm, you won’t be the same person who walked in. That’s what this storm’s all about”

— Haruki Murakami, Kafka on the Shore

Resumo

O cancro colorretal é a terceira forma de cancro mais diagnosticada em ambos os géneros, bem como a segunda principal causa de morte relacionada com cancro em todo o mundo. De facto, nos últimos anos, os avanços científicos e tecnológicos alcançados ao nível das ferramentas de prevenção, deteção e tratamento de cancro colorretal contribuíram para a extensão do nosso conhecimento acerca dos fatores de risco e mecanismos patológicos responsáveis pela transformação maligna do epitélio intestinal. No entanto, apesar dos progressos obtidos, múltiplos desafios permanecem, uma vez que a maioria dos pacientes exibe um quadro clínico desfavorável, devido ao risco elevado de recidiva tumoral. Posto isto, existe uma necessidade de se desenvolverem soluções interdisciplinares que sejam capazes de simular as caraterísticas desta doença e estimar as respostas biológicas dos indivíduos face a uma dada terapia/intervenção.

Recentemente, inúmeros trabalhos demonstraram que os processos envolvidos na iniciação, progressão e metastização de cancro colorretal são fortemente influenciados pelos elementos da matriz extracelular e do microambiente tumoral. Em particular, a matriz extracelular representa um compartimento fisiologicamente ativo, cuja função compreende a manutenção da integridade física e estrutural dos tecidos. Além disso, serve como um reservatório de biomoléculas, possibilitando, deste modo, a preservação dos determinantes bioquímicos envolvidos na comunicação célula-célula/célula-matriz e na monitorização da sobrevivência, proliferação e diferenciação celular. Todavia, independentemente do nosso conhecimento em relação a estas interações, as noções concetuais necessárias para a criação de um modelo pré-clínico capaz de mimetizar a matriz colorretal ainda não estão completamente estabelecidas.

Atualmente, a maioria das culturas celulares de cancro colorretal são estabelecidas em Matrigel®. Todavia, a aplicabilidade deste material é limitada, não só pela sua origem biológica (visto que é extraído de um sarcoma de murganho), como também pela sua heterogeneidade composicional, propriedades mecânicas alteradas e custos elevados. Uma técnica emergente que pode facultar a geração de plataformas de cancro mais pertinentes e representativas consiste na descelularização da matriz extracelular derivada de tecidos e/ou órgãos nativos, através da combinação de tratamentos físicos, químicos ou enzimáticos. Nos últimos anos, as matrizes descelularizadas têm

sido processadas sob a forma de hidrogéis biomiméticos, os quais revelam ser capazes de reproduzir a diversidade comportamental e arquitetural das células cancerígenas e do meio envolvente, respetivamente. Curiosamente, embora possam ser provenientes de tecidos de diversos mamíferos, não existe, até então, nenhum protocolo que descreva a formulação de hidrogéis a partir de intestinos de rato descelularizados. Assim, o objetivo do presente trabalho será produzir uma plataforma *in vitro* e alternativa ao Matrigel® através da descelularização, solubilização e neutralização de matrizes intestinais derivadas de ratos Wistar Hannover.

Os resultados obtidos evidenciaram a eficácia do protocolo de descelularização desenvolvido, independentemente da origem anatómica das amostras de intestino. Na verdade, para além de possibilitarem a remoção do conteúdo celular, genético e nuclear, as lavagens com gradientes de etanol e 75% de isopropanol, aliadas aos tratamentos à base de 0.1% de SDS contribuíram para a preservação da estrutura e da composição da matriz intestinal. Este efeito foi observado nos fragmentos de cécum, intestino delgado e intestino grosso que foram individualmente colocados nas placas de múltiplos poços. Apesar de constituir uma técnica disruptiva, a particulação destes tecidos melhorou substancialmente o processo de descelularização, devido ao aumento da área de contacto com as soluções de limpeza. Ainda assim, em todas as condições experimentais, a avaliação histológica revelou uma redução de glicosaminoglicanos sulfatados, além da conservação da rede de colagénio. Após a solubilização de três quantidades de matrizes descelularizadas (15, 20 e 25 mg) com 2.5 mg/mL de pepsina em 3% de ácido acético e neutralização com 10x PBS e 10 M NaOH, foram obtidos hidrogéis estruturalmente homogéneos e com uma densidade superior à do Matrigel®. A rede polimérica tridimensional destas plataformas foi, ainda, capaz de reticular a 37°C. Particularmente, as duas maiores concentrações de hidrogéis mantiveram a sua integridade ao fim de 7 dias. Após a funcionalização química com sulfato de condroitina modificado, os materiais revelaram uma maior estabilidade e resistência física à deformação. Visto que as propriedades destas estruturas são equiparáveis às do intestino nativo, a manutenção da atividade e viabilidade de uma linha celular de cancro colorretal (SW480) foi assegurada. Esta conclusão foi estipulada para os hidrogéis sem funcionalização. No entanto, espera-se que esta investigação seja posteriormente alargada a hidrogéis funcionalizados, para que se possa estudar o papel do sulfato de condroitina no microambiente tumoral.

Tendo tudo isto em consideração, este trabalho abre portas para o estabelecimento de uma nova geração de modelos 3D *in vitro* de cancro colorretal, cujo potencial pré-clínico poderá ser explorado para a antevisão e/ou modulação das respostas biológicas dos pacientes, assim como para o melhoramento do prognóstico desta doença.

Palavras-chave: Cancro colorretal; matriz extracelular; descelularização; hidrogéis.

This page was intentionally left blank.

Abstract

Colorectal cancer (CRC) represents the third most frequently diagnosed type of cancer. In addition, it is the second leading cause of cancer-associated deaths worldwide. Over the past years, the scientific and technological advances achieved in CRC prevention, discovery, and treatment provided valuable insights into the main causes, risk factors, and pathophysiological mechanisms that are inherent to the malignant transformation of the intestinal epithelium. Nonetheless, despite these improvements, numerous challenges remain, as most individuals evidence rapid tumor development and poor clinical outcomes, due to tumor metastasis and/or recurrence. In this sense, there is a growing demand for an interdisciplinary solution that can recapitulate the features of this disease and assess the biological responses of the affected patients to a given therapy and/or intervention.

More recently, numerous works have demonstrated that the processes involved in the initiation, progression, and invasion of CRC are heavily influenced by the stromal and extracellular matrix (ECM) components of the tumor microenvironment (TME). Particularly, the ECM represents an interwoven compartment, whose function involves the maintenance of the structural integrity of the tissues. Also, it serves as a reservoir for the biochemical and biophysical determinants that are reported to participate in cell-cell and cell-matrix communication, cell survival, growth, proliferation, and differentiation. Regardless of our awareness concerning these interactions, the concepts necessary to design and produce a reliable and representative pre-clinical platform capable of simulating the colorectal ECM are not completely established.

Currently, Matrigel® is the most used platform for cancer cell cultures. Nonetheless, this material is limited in terms of applications because of its biological origin (since it is derived from a murine sarcoma), batch-to-batch variability, modified mechanical properties, and high costs. One emerging technology that supports the formulation of more complex and relevant cancer-related models is the decellularization of the ECM derived from native tissues or organs, through the combination of physical, chemical, and enzymatic treatments. Lately, decellularized ECMs (dECMs) have been engineered to form three-dimensional (3D) biomimetic hydrogels, which are shown to replicate the behavioral and architectural features of CRC cells and their surrounding

landscape, respectively. Although being obtained from a variety of mammalian tissues, there are no methodologies available for producing 3D hydrogels from decellularized rat intestines. Concerning this, the present study will aim at fabricating a 3D *in vitro* platform based on the decellularization, solubilization, and neutralization of the ECMs derived from the intestines of Wistar Hannover rats, which could substitute the use of Matrigel® as a standard cell culture substrate.

The results obtained in this study highlighted the benefits of combining washes in ethanol gradients and 75% isopropanol with the 0.1% SDS-based protocol for the decellularization of the intestines. Indeed, the architectural and compositional characterization of the dECMs confirmed the deletion of the cellular, genetic, and nuclear material from the tissue fragments that were decellularized in multi-well cell culture plates. Moreover, the preservation of the microstructure and macromolecular diversity of the native ECM was achieved, irrespective of the anatomical origin of these samples. In spite of constituting a disruptive technique, the milling of the tissues improved the decellularization process, as a consequence of the increase in the contact surface area with the cleaning solutions. However, in all experimental conditions, histological analysis evidenced a marked reduction in the sulfated glycosaminoglycans (sGAGs) content, aside from the maintenance of the collagen-based network. Following solubilization with 2.5 mg/mL pepsin in 3% acetic acid and neutralization with 10 M NaOH and 10x PBS, three homogeneous hydrogels containing different amounts of dECMs (15, 20, or 25 mg) were obtained. Remarkably, these scaffolds possessed higher tensile strengths when compared to Matrigel®. The resulting polymeric networks were able to crosslink at temperature-controlled environments (37°C), remaining stable for 7 days. This effect was dependent on the concentration of the dECMs, with 20 and 25 mg/mL dECM-based hydrogels revealing the best results. After performing a chemical functionalization with modified chondroitin sulfate (CS), the resulting hybrid biomaterials showed greater stability and resistance to strain. Due to their biomimicry, the dECM-based hydrogels sustained the metabolic activity and viability of cultured CRC cell lines, particularly the SW480. This outcome was only observed in the non-functionalized hydrogels. Nonetheless, in the future, it is expected that this investigation will be extended to the functionalized hydrogels so that the role of CS in the tumor microenvironment can be evaluated.

Bearing all of this in mind, this work opens the door for the establishment of a new generation of *in vitro* models, whose potential can be explored in both fundamental and translational research, for the prediction of therapeutic responses, as well as the improvement of the clinical prognosis of the affected individuals.

Key words: Colorectal cancer; extracellular matrix; decellularization; hydrogels.

Acknowledgments

Os últimos cinco anos foram pautados por muito esforço e dedicação, mas também por vários ensinamentos e momentos de introspeção. Na verdade, ao longo deste ciclo, cresci enquanto pessoa e (futuro) profissional. Aprendi que não há problema em tentar e falhar, em perdermo-nos no caminho e em não sabermos por onde recomeçar. Percebi (muitas vezes à força) que não somos capazes de controlar o que bate à nossa porta, mas que podemos escolher o que entra e o que permanece no lado de fora. Às vezes ganhamos, outras vezes perdemos. Ainda assim, mais importante do que as vezes em que caímos, é a força e a motivação com que nos reerguemos e reinventamos forças para seguir em frente no nosso caminho. E porque as histórias mais bonitas se escrevem no plural, deixo um agradecimento especial a todos aqueles que, direta ou indiretamente, presenciaram de perto o meu percurso e contribuíram para que a superação destes obstáculos fosse possível:

Gostaria de começar por expressar a minha gratidão para com o meu supervisor e mentor, Professor Mário Barbosa. Primeiramente, pela oportunidade de integrar o seu grupo de investigação, que, inevitavelmente, se tornou na minha segunda família. Posteriormente, pela sua disponibilidade e prontidão; pelo interesse com que partilha do seu conhecimento científico; pelas suas palavras sábias, particularmente em momentos de tensão; e pelas suas histórias inspiradoras, que resultam em bons momentos de descontração. Agradeço também à minha co-supervisora, Joana Caldeira, pela simpatia, força de vontade e dedicação, bem como por todo o carinho e apoio demonstrados durante os meus primeiros passos no mundo da investigação.

Ao meu melhor amigo, colega de secretária e companheiro de todas as horas, Nuno Rosa, um especial obrigado. És um modelo a seguir e uma grande inspiração. É também graças a ti que me tornei no Homem que sou hoje, porque "às vezes, precisamos de ser quebrados, para que possamos construir a melhor versão de nós mesmos". Obrigado por me ensinares a fazer a verdadeira ciência e por me mostrares que é possível divertir-me em simultâneo. Obrigado pela tua paciência e motivação, por celebrares comigo as minhas vitórias e por me amparares nas minhas derrotas. Levar-te-ei comigo para o resto da minha vida e estarei sempre do teu lado, para o que der e vier.

Gostaria, ainda, de agradecer à Morena Fiordalisi por me ter integrado e, particularmente, por me ter ensinado a trabalhar num laboratório. Para além disso, agradeço

a sua persistência, a sua vontade e disponibilidade em ajudar o próximo e, finalmente, a sua capacidade de animar uma sala com o seu riso contagioso e boa disposição.

À Beatriz Sousa, Cristiana Couto e Sara Moura um grande obrigado por todo o vosso carinho, bem como pela vossa prontidão para momentos de descontração, acompanhados por boa comida e muita diversão. Especialmente a ti, Beatriz, gostaria de agradecer a ajuda que me deste nos últimos meses. Apesar de cometer erros, os quais eram justificados pela minha "hiperatividade autodiagnosticada", nunca desististe de mim, estando sempre presente (inclusive aos fim-de-semana) para me acompanhar. Agradeço também por esta bonita ligação, que fomos criando com o tempo. É reconfortante saber que tenho comigo alguém único e especial, capaz de aguentar as minhas oscilações de humor e/ou personalidades, bem como os meus picos de energia, estimulados por uma sobredosagem de cafeína.

Gostaria de deixar umas palavras de carinho e de força aos meus queridos MINTi-ons: Beatriz Ribeiro, Catarina Correia, Filipe Nogueira, Inês Sousa, Inês Teixeira e Maria Lopes. Melhor do que ninguém, percebem as dificuldades da luta que estamos em conjunto a travar. Muito obrigado pela vossa amizade e constante companhia, pela força que me deram nos momentos de aflição e, principalmente, por nunca falharem em me fazer rir. Espero que depois disto, tenham todos um futuro brilhante e repleto de muitos sucessos, do qual também eu possa fazer parte.

Finalmente, deixo um agradecimento a todos os elementos do grupo Microenvironments for New Therapies por me terem acolhido de braços abertos e por possuírem um grande espírito de entreajuda. Um especial obrigado à minha colega e grande amiga Kaoutar Chattahy, que mesmo a mais de 2600 km de distância, contribuiu com todo o seu conhecimento, força e motivação, para o sucesso deste projeto. Obrigado por acreditares em mim e por me mostrares que, no final, tudo acaba por correr bem. És, sem dúvida, uma das melhores pessoas que levo comigo para o resto da vida. Para terminar, um grande obrigado aos amigos que fiz durante a minha passagem pelo i3S. Guardo, para todos vocês, um lugar muito especial no meu coração.

Acima de tudo, tenho de agradecer aos meus queridos pais, Carmo e Carlos, por serem um exemplo de força, bondade, coragem e determinação. Obrigado pelo vosso amor, pelos vossos ensinamentos e particularmente pela vossa paciência. Obrigado por nunca me deixarem baixar os braços e por me incentivarem (sempre) a lutar. Obrigado por me mostrarem que que há mais nada vida para além das preocupações, porque, como costumam dizer, "por detrás de milhões de nuvens, há sempre um sol a brilhar". Amo-vos incondicionalmente. Hoje e sempre. Para o resto da vida.

Index

List of Figures

List of Tables

Abbreviations and Acronyms

2D	Two Dimensional
3D	Three Dimensional
5-FU	5-Fluorouracil
ACF	Aberrant Crypt Foci
ACS	Adenoma-Carcinoma Sequence
AFM	Atomic Force Microscopy
AOM	Azoxymethane
APC	Adenomatous Polyposis Coli
BM	Basement Membrane
CAF	Cancer Associated Fibroblast
CAGR	Compound Annual Growth Rate
CDX	Cell Line-Derived Xenograft
CIMP	CpG Island Methylator Phenotype
CIN	Chromosomal Instability
CRC	Colorectal Cancer
CS	Chondroitin Sulfate
CSPG	Chondroitin Sulfate Proteoglycan
CT	Computed Tomographic
DAPI	4',6'-diamino-2-fenil-indol
dECM	Decellularized Extracellular Matrix
DET	Detergent-Enzymatic Treatment
DMAB	3,2′-Dimethyl-4-Aminobiphenyl
DMH	1,2-Dimethylhydrazine

DS	Dermatan Sulfate
ECM	Extracellular Matrix
EMT	Epithelial-Mesenchymal Transition
FAP	Familial Adenomatous Polyposis
FDA	Food and Drug Administration
FIT	Fecal Immunochemical Test
FOBT	Fecal Occult Blood Testing
GAG	Glycosaminoglycan
sGAG	Sulfated Glycosaminoglycan
G'	Storage or Elastic Modulus
G''	Loss or Viscous Modulus
G*	Complex Modulus
GEMM	Genetically Engineered Mouse Model
HA	Hyaluronan
HDI	Human Development Index
H&E	Hematoxylin and Eosin
HNPCC	Hereditary Nonpolyposis Colorectal Cancer
HS	Heparan Sulfate
HSPG	Heparan Sulfate Proteoglycan
IARC	International Agency for Research on Cancer
IBD	Inflammatory Bowel Disease
IM	Interstitial Matrix
IHME	Institute for Health Metrics and Evaluation
KS	Keratan Sulfate
LOX	Lysyl Oxidase
LVR	Linear Viscoelastic Region

MAM	Methylazoxymethanol
MCTS	Multicellular Tumor Spheroid
MHC	Major Histocompatibility Complex
Min	Multiple Intestinal Neoplasia
MMR	Mismatch Repair
MNNG	N-Methyl-N-Nitrosoguanidine
MNU	N-Methyl-N-Nitrosourea
MSI	Microsatellite Instability
mt-sDNA	Multitarget Stool DNA
PCL	Polycaprolactone
PDMS	Polydimethylsiloxane
PDX	Patient-Derived Xenograft
PEG	Polyethylene Glycol
PG	Proteoglycan
PHEMA	Poly(Hydroxyethyl Methacrylate)
PhIP	2-Amino-1-Methyl-6-Phenylimidazo(4,5-b)Pyridine
PLGA	Poly(Lactic-Co-Glycolic Acid)
PS	Polystyrene
RT	Room Temperature
SDC	Sodium Deoxycholate
SDS	Sodium Dodecyl Sulfate
SEM	Scanning Electron Microscopy
SIS	Small Intestine Submucosa
TCPS	Tissue Culture Polystyrene
TEM	Transmission Electron Microscopy
WHO	World Health Organization

This page was intentionally left blank.

Chapter 1

Introduction

1. Colorectal Cancer (CRC)

1.1. Epidemiology

According to the International Agency for Research on Cancer (IARC) and the World Health Organization (WHO), colorectal cancer (CRC) is the third most frequently diagnosed type of cancer worldwide (1.9 million cases in 2020, corresponding to 10.0% of total cancer incidence) and the second leading cause of cancer-associated deaths (0.9 million casualties in 2020, corresponding to 9.4% of total cancer mortality) (Figure 1) (Sung et al., 2021). Although being more identified in men (23.6 *vs.* 16.3 occurrences per 100,000 person-year), women aged ≥ 65 years old are more predisposed to develop tumors at aggressive stages (Kim et al., 2015). This has been recently attributed to the absence of a protective effect that is thought to be exerted by sex hormones, particularly estrogens (17β-estradiol, estriol, and estrone) (Abancens et al., 2020). Furthermore, numerous studies have highlighted patient survival is dependent on the moment at which CRC is identified, with later-stage showing greater fatality. Notably, despite these divergences, age-standardized mortality rates remain superior among men (10.8 *vs.* 7.2 occurrences per 100,000 person-year) (Kim et al., 2015).

The number of CRC cases is conventionally four-fold higher in western regions because of their increased human development index (HDI) (Figure 2) (Cardoso et al., 2021). For example, Europe, Australia, New Zealand, and North America rank first in colon cancer incidence. However, a substantial fraction of these events can be primarily prevented, considering that they are associated with modifiable behavioral and/or nutritional risk factors. In addition, the implementation of long-standing screening programs, including colonoscopies and fecal tests, aids in the early detection and subsequent removal of pre-cancerous wounds (Cardoso et al., 2021).

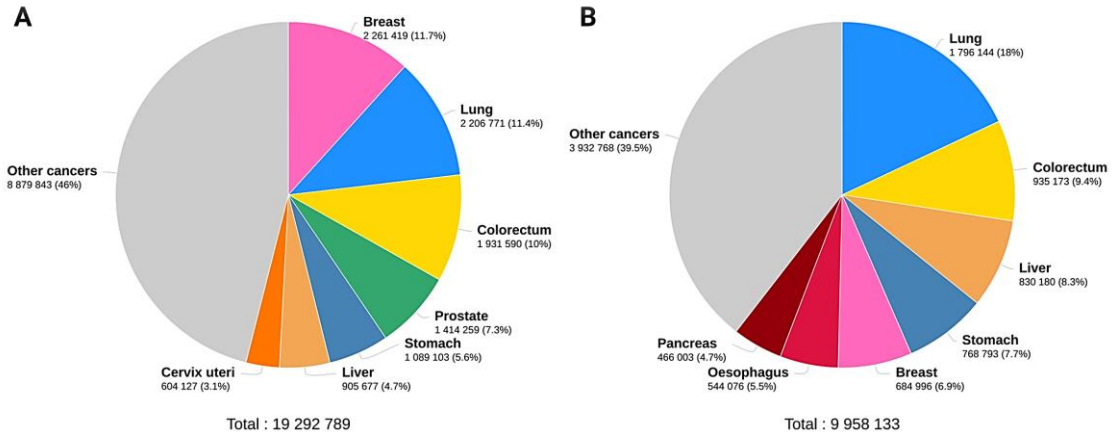

Figure 1 – Worldwide distribution of cancer incidence (A) and mortality (B) in 2020, for both genders, and all ages. Cancer is a leading cause of death, accounting for one in every six casualties every year. In 2020, the most common forms of cancer were breast (11.7%) and lung (11.4%) cancers. In terms of mortality, the latter is also recognized to be the most prominent (18%). On the other hand, colorectal cancer (CRC) represents the third most diagnosed (10%) and the second most mortal (9.4%) type of cancer worldwide. *Adapted from GLOBOCAN 2020, IARC/WHO (Sung et al., 2021).*

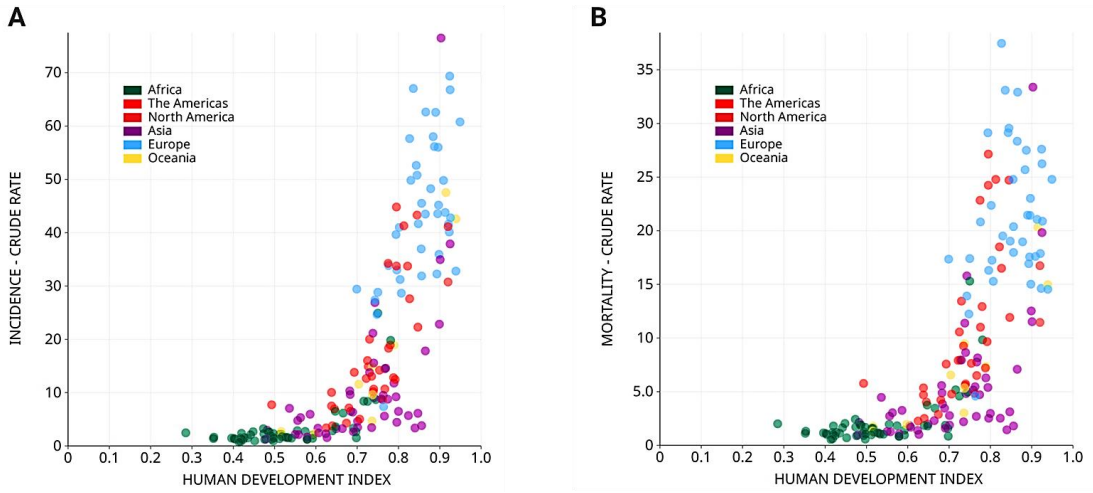

Figure 2 – Regional distribution of colorectal cancer (CRC) incidence (A) and mortality (B) in 2020, for both sexes, and all ages, according to the human development index (HDI). HDI is a composite measurement that considers the three dimensions of human development: the gross national income per capita, the life expectancy, and the access to basic education. The profiles of CRC are shown to vary according to the HDI. Regardless of the technological and scientific advances achieved in this field, most of the CRC burden is still observed in high HDI countries, namely in Europe and North America. In this context, the rapid growth and aging of the population have been pointed out as responsible for the amplification of these trends. *Adapted from GLOBOCAN 2020, IARC/WHO (Sung et al., 2021).*

A similar geographic distribution is observed when looking at the incidence of rectal cancer. Interestingly, for both kinds of lesions, Eastern Asia is reported to be featured among the most affected areas (Cardoso et al., 2021). On the other hand, the

incidence of colon and rectal cancer seems to decrease in Africa and South-Central Asia, due to the lower life expectancy and prominent lethality of other medical conditions. In this context, restrictions on the access of patients to healthcare services, preventive screening programs, healthy foods, and basic education are proven to contribute to the amplification of these trends (Xi & Xu, 2021).

Independently of this heterogeneity, the global burden of CRC is estimated to rise, reaching approximately 3.2 million cases, and surpassing 1.1 million deaths by 2040. This is recognized to be a projection of the rapid growth and aging of the population. Furthermore, as life expectancy increases, the exposure to carcinogenic risk factors, which arise from the westernization of lifestyle and dietary habits, is expected to be observed (Arnold et al., 2020).

1.2. Causes and Main Risk Factors

Over the past decades, CRC has been classified as a highly complex and multistep disease, in which punctual and successive mutations in oncogenes (e.g., *KRAS*, *BRAF*, and *PIK3CA*), tumor-suppressor genes (e.g., *APC, TP53, SMAD2,* and *SMAD4),* and genes involved in the DNA mismatch repair (MMR) system (e.g., *MLH1, MSH2, MSH6*, and *MYH*) lead to genomic instability and acquisition of excessive proliferative capacity. Moreover, many works recognized chromosomal and microsatellite instability (CIN/MSI), and anomalous DNA methylation, also known as CpG island methylator phenotype (CIMP), as plausible molecular pathways that may contribute to the emergence of benign adenomas and the development of malignant invasive adenocarcinomas (Armaghany et al., 2012). Although the genetic origin of CRC is widely accepted, much of its inherent risks have been associated with causes other than unmodifiable DNA errors, including endogenous (e.g., age, gender, genetic susceptibility, hormone levels, and changes in the microbiome), exogenous (e.g., exposures to physical, chemical, and biological carcinogens), and lifestyle (e.g., alcohol consumption, smoking, nutrient imbalance, and sedentarism) risk factors (Mármol et al., 2017). Age represents the primary source of susceptibility, since the onset of CRC increases after the fifth decade of life (Gabriel et al., 2018). Alternatively, personal and/or familial history of neoplastic polyps, inflammatory bowel disease (IBD), Crohn's disease, and ulcerative colitis may also increase the risk of developing lesions in the colorectum (Mármol et al., 2017). Unhealthy nutritional habits (e.g., high intakes of processed foods) and obesity are also found to reinforce CRC predisposition since they are correlated with high levels of visceral fat and secretion of pro-inflammatory cytokines (e.g., IL-8, IL-6, and IL-2) (Choe et al.,

2013). Contrarily, population-based studies have detailed that the consumption of nutrients (e.g., folic acid, calcium, magnesium, and vitamin D), whole grains, and green vegetables provide a protective effect (Thanikachalam & Khan, 2019). Finally, alcohol and tobacco smoke metabolites (acetaldehydes and nicotine, respectively) have been recognized to reach the gastrointestinal epithelium and produce damage to the DNA across the intestinal wall (Amitay et al., 2020).

1.3. Pathophysiology

CRC initiates in the large intestine, particularly the colon and the rectum (Xi & Xu, 2021). Histologically, the large intestine can be divided into the mucosa, submucosa, muscularis propria, and serosa or adventitia (Azzouz & Sharma, 2022). The mucosa is the innermost layer, constituting a physical barrier between the luminal content and the colorectal wall. Underneath is the submucosa, where large blood vessels, lymphatics, and glands support the distribution of nutrients and the production of mucous secretions. Succeeding it is the muscularis propria, whose circular and longitudinal muscle fibers are responsible for the control of the peristaltic movements and the mechanical deformation of the tubular structure. Lastly, the serosa or adventitia provides lubrication through the secretion of the serous fluid (Siri et al., 2020). Based on its structural presentation, the colon can be further segmented into proximal and distal colons (Simon, 2016). The first includes the caecum, ascending colon, hepatic flexure, and transverse colon, while the latter includes the splenic flexure, plus the descending and sigmoid colons (Figure 3) (Baran et al., 2018).

According to Fearon and Vogelstein, the pathological reorganization of the intestinal epithelium follows the adenoma-carcinoma sequence (ACS), whose main steps are initiation, promotion, progression, and metastasis (Figure 4) (Smit et al., 2020). In initiation, irreversible alterations occur at the gene level. The earliest and most prevalent is the loss of function of the adenomatous polyposis coli (*APC*) gene, which is followed by mutations in driver genes (e.g., *KRAS*, *SMAD2, SMAD4*, *TP53*) and signaling pathways (e.g., Wnt/ß-catenin, EGFR, TGF-ß) (Yang et al., 2019). Altogether, these events generate a potential for the affected cells to grow and proliferate, culminating in the emergence of aberrant crypt foci (ACF) (Wargovich et al., 2010). During promotion, the initiated cells are encouraged to divide, prompting the transformation of the ACF into pre-cancerous adenomatous polyps or adenomas (Seely et al., 2022).

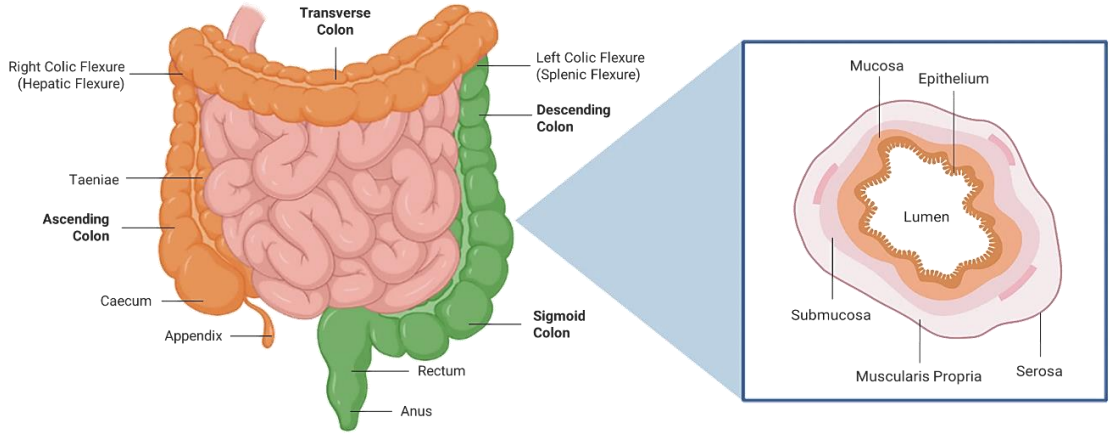

Figure 3 – Schematic representation of the main anatomical and histological regions of the large intestine. The large intestine contains the colon, rectum, and anus. The colon can be divided into proximal (which includes the ascending and transverse portions) and distal colons (which includes the descending and sigmoid portions). Although exhibiting variations in parameters such as pH, microbial loads, and short-chain fatty acids, the multi-layered structure of the colorectal tissue is conserved. Indeed, the structural organization of the mucosa, submucosa, muscularis propria and serosa or adventitia provides the basis for the execution of the main functions of this tissue, also playing an important role in its pathophysiology. *Adapted from Encyclopedia Britannica. Created with Biorender.com.*

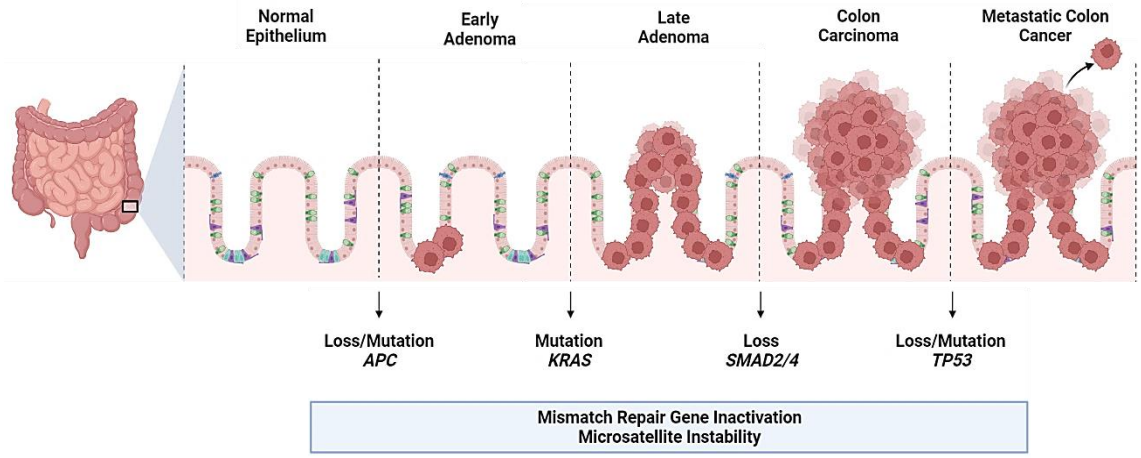

Figure 4 – The adenoma-carcinoma sequence (ACS). Loss of function of the *APC* gene results in abnormal epithelial cell growth and proliferation, leading to the generation of benign adenomatous polyps (or adenomas). Subsequent mutations in *KRAS, SMAD2/4*, and *TP53* driver genes, along with the inactivation of mismatch repair system (MMR) genes and the acquisition of microsatellite instability, are also known to contribute to cancer cell detachment, migration, invasion, and metastasis. Altogether, these events result in the transformation of the previously formed benign adenomas into malignant intestinal adenocarcinomas. *Adapted from (Davies et al., 2005). Created with Biorender.com.*

These structures increase in dimension throughout the progression phase, becoming more heterogeneous and aggressive, as the number of genetic modifications augments (Keum & Giovannucci, 2019). In this context, important features of normal cells,

including the capacity to adhere to their surroundings, are lost. As a result, they break away and invade other tissues and organs through the bloodstream and the lymphatic system (Pretzsch et al., 2019). This phenomenon, known as metastasis, constitutes a key step in the establishment of malignant adenocarcinomas and takes place in a 10 to 15-year period following the appearance of the first neoplasms (Hong et al., 2021). While the ACS accounts for 70 to 90% of colorectal lesions, the serrated pathway is responsible for 10 to 20% of these malignancies. Both events result in microsatellite-stable tumors, yet the latter can give rise to microsatellite instability, which is often a product of the accumulation of mutations in *KRAS* and *BRAF* genes and aberrant methylation of tumor suppressor genes (Dekker et al., 2019).

1.4. Diagnosis and Available Treatments

At the moment, CRC diagnosis is performed in symptomatic patients, who experience abdominal pain, rectal bleeding, and alterations in bowel habits, or following a clinical examination (Walter et al., 2016). In this context, endoscopy represents the gold standard method for the removal of pre-cancerous and/or small cancerous lesions (Swiderska et al., 2014). Since this is an invasive procedure, other alternatives, including fecal occult blood (FOBT), fecal immunochemical (FIT), and multitarget stool DNA (mt-sDNA) tests, have been considered (Simon, 2016). Furthermore, computed tomographic (CT) colonography emerged as an important complementary tool in this field, given that it supports the creation of three-dimensional (3D) images of the colon. Nevertheless, the current guidelines recommend combining it with endoscopy to increase the specificity and sensitivity of the detection (Simon, 2016).

Regarding the available treatments, surgical interventions represent the most explored options for the extraction of early-stage and more advanced colorectal lesions (Xie et al., 2020). Yet, in the last decades, the combination with neoadjuvant therapies (e.g., radiotherapy and chemotherapy) has been required in order to improve the curative effects of these procedures (Xie et al., 2020). Although evidencing high response rates, their success is limited, mainly due to metastasis and tumor recurrence (Ahmad et al., 2021). Accordingly, immune-based and targeted therapies emerged as a solution for the treatment of aggressive CRC lesions. These approaches involve the use of small molecules against receptor and non-receptor tyrosine kinases and monoclonal antibodies, which block immune checkpoints (e.g., PD-1/PDL-1, and CTLA-4) or signaling pathways (e.g., EGFR/RAS, PI3K/AKT, VEGF/VEGFR, and HGF/C-MET). In 2004, the Food and Drug Administration (FDA) approved the first monoclonal antibodies targeting EGFR

(cetuximab) and VEGF-A (bevacizumab) molecules. Ever since, many agents have been formulated and explored in clinical trials (Figure 5) (Xie et al., 2020).

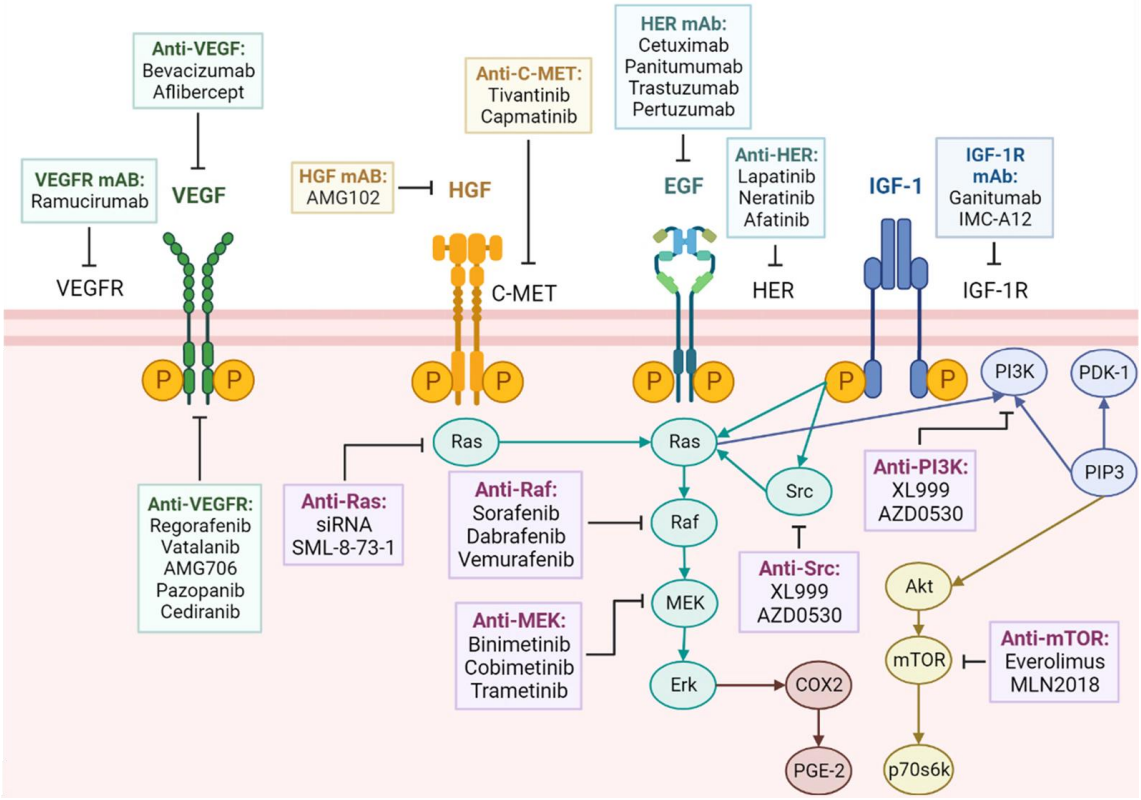

Figure 5 - Overview of the currently available targeted drugs for the treatment of colorectal cancer (CRC) patients. Most targeted therapies involve the use of small molecules (which can easily penetrate inside cancer cells) and monoclonal antibodies (which can recognize specific targets found on the surface of cancer cell membranes). Some monoclonal antibodies mark cancer cells so that they can be more easily identified and eliminated by the immune system. Others directly stop cancer cells from growing by inducing their destruction. *Adapted from (Sartore-Bianchi et al., 2016). Created with Biorender.com.*

1.5. Economic Burden

To understand the economic impact of CRC on patients, healthcare systems, and the United States (U.S.) government, Stukalin *et al.* supported the execution of a comprehensive examination based on data from the Institute for Health Metrics and Evaluation's Disease Expenditure Project (IHME/DEX) (Stukalin et al., 2021). According to this report, the costs of CRC increased 0.9% each year, rising from $8.85 billion in 1996 to $10.50 billion in 2016. Concerning the type of assistance, ambulatory care represented most of the total expenses (65.9%). Regardless, prevalence-adjusted patterns revealed the absolute spending per capita decreased from $8,848 to $8,427 during the forecast period (Stukalin et al., 2021). Similar findings were obtained for Europe, where, in 2015, the economic burden of CRC was equal to €19.1 billion. In this case,

the mean costs for handling individuals with CRC oscillated from €259 to €36,295. While hospitalization and inpatient care represented the largest contributors, a 21.2% reduction was identified from 2009 to 2015. Contrarily, the expenses associated with medication increased 213.7% in specific geographic areas (Henderson et al., 2021). Respecting the CRC drug market, the financial burden of the currently available therapies was $12.77 billion in 2021. This value is presumed to reach $16.43 billion by 2026, with a compound annual growth rate (CAGR) of 4.9%. The number of individuals suffering from this disease might be responsible for the growth of this sector, according to the American Cancer Society (ACS) (Figure 6) (Siegel et al., 2021).

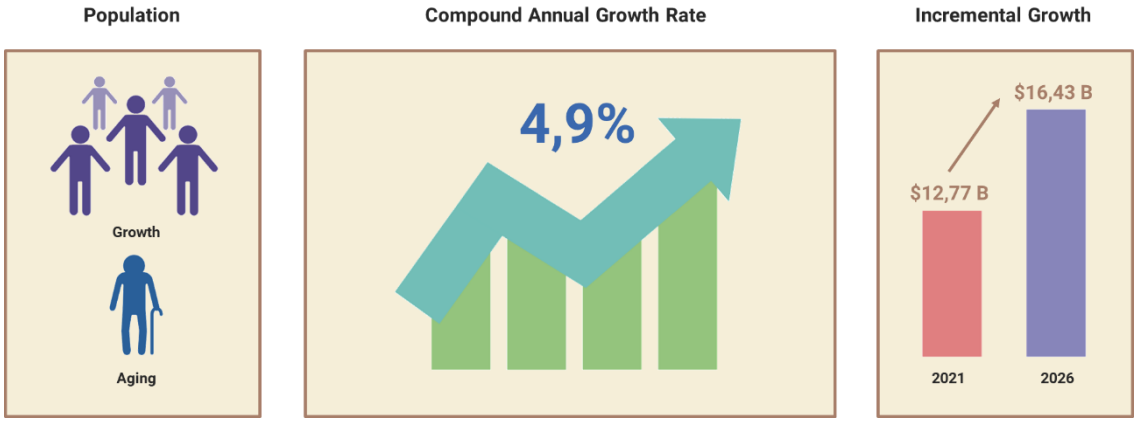

Figure 6 - Analysis of the economic burden associated with the colorectal cancer (CRC) therapeutics market. The global CRC therapeutics market size stood at $12.77 billion in 2021 and is projected to reach $16.43 billion by 2026, with a compound annual growth rate (CAGR) of 4.9%, during this forecast period. These trends are acknowledged to be a result of the continuous growth and aging of the world population. *Adapted from Business Wire. Created with Biorender.com.*

2. Colorectal Extracellular Matrix (ECM)

2.1. Composition and Main Functions

The colorectal extracellular matrix (ECM) consists of two distinct, yet intimately correlated compartments: the basement membrane (BM), which separates the epithelium from the underlying stroma, and the interstitial matrix (IM), which provides structural and functional integrity to the intestinal wall (Pompili et al., 2021). The BM is a network-like structure abundant in type IV collagen (α1, α2, α5, and α6 chains), proteoglycans (e.g., perlecan), and adhesive glycoproteins (e.g., laminin, fibronectin, and nidogens) (Crotti et al., 2017). Type IV collagen constitutes the most prominent element of the BM. Apart from establishing specific interactions with cell receptors, such as integrins, it acts as a mechanical linkage between the ECM and the cell cytoskeleton

(Tanjore & Kalluri, 2006). Perlecan is another key component of the BM. This heparan sulfate proteoglycan (HSPG) possesses a core protein that is attached to glycosaminoglycan (GAGs) chains (N. Afratis et al., 2012). Because perlecan binds to multiple partners, it plays an important role in tissue development and regeneration, as well as in cell adhesion, proliferation, and differentiation (Yamamoto et al., 2013). The molecular composition of the IM is equivalent to that of the BM, yet, in this case, type IV collagen is replaced by type I and III collagens as the most representative constituents (Crotti et al., 2017). These fibrous proteins provide tensile strength, while simultaneously interacting with other collagen isoforms (e.g., type V, XII, XVI, and XIX collagens), ECM modulators (e.g., thrombospondin), and cell membrane receptors (e.g., integrins) (Meran et al., 2017). Besides collagens, fibronectin, elastin, decorin, and hyaluronan (HA) are also a representative fraction of this diverse network. Altogether, these molecules participate in the maintenance of tissue homeostasis and the remodeling of the intestinal epithelium, particularly after injury (Hussey, Cramer, et al., 2018).

2.2. ECM Modifications in CRC

During cancer initiation and progression, the microarchitecture and biomolecular composition of the native ECM are modified, due to the acquisition of malignant features. In CRC, pathological ECM remodeling is typically defined by the anisotropic deposition of proteolytically crosslinked collagen fibrils (e.g., type I, VI, VII, VIII, X, XI, and XVIII), post-translational protein modifications, upregulation of ECM-modifying enzymes (e.g., MMPs, ADAMs, and LOXL1), inactivation of tissue inhibitors (e.g., TIMPs), and increased ECM rigidity (Crotti et al., 2017). Indeed, one of the most common hallmarks of this disease is the loss of the integrity of the BM (Winkler et al., 2020). Aiming at replacing the components that have been lost during this process, an increase in the deposition of organized bundles of collagen fibrils is stimulated (Xu et al., 2019). Along with the upregulation of lysyl oxidases (LOX), which participate in the crosslinking of the recently formed collagen-based network, these events lead to the formation of a denser and stiffer ECM (Crotti et al., 2017). More recently, the changes in the mechanical properties of malignant tissues have been linked to the activation of specific cancer-related signaling pathways. These have been recognized to promote the initiation of epithelial-mesenchymal transitions (EMT), induce a decrease in apoptosis, and, consequently, raise the metastatic potential of CRC cells (Aragona et al., 2013).

2.3. The Role of Chondroitin Sulfate Proteoglycans (CSPGs)

The malignant transformation of the colorectal tissue is characterized by modifications in the structure, expression patterns, metabolism, concentration, and distribution of GAGs (Wei et al., 2020). GAGs are a family of unbranched, negatively-charged polysaccharides that are ubiquitously found on the cell surface and in the ECM, either in a free form or in association with core proteins to form proteoglycans (PGs) (Taylor & Gallo, 2006). According to the variations in their saccharide moieties and the presence/absence of modifications (e.g., sulfation, acetylation, and epimerization) in the functional groups, GAGs can be systematized into four different families: heparin/heparan sulfate (HS), chondroitin sulfate/dermatan sulfate (CS/DS), keratan sulfate (KS), and HA (Morla, 2019). Among cancer-related GAGs, CS/DS chains of chondroitin sulfate proteoglycans (CSPGs) are exceptionally important, as they execute key functions under both normal and pathological conditions (Pudełko et al., 2019). As a matter of fact, CS/DS chains are typically overexpressed in CRC, causing an exaggerated deposition of CSPGs, particularly versican and decorin (Wei et al., 2020). Previous works have also demonstrated that alterations in the sulfation pattern and chain length of CS/DS might contribute to CRC cell growth and progression (Daidouji et al., 2002).

CS/DS chains are composed of alternating blocks of ß-1,3-linked N-acetyl-galactosamine and ß-1,4-linked D-glucuronic acid (or L-iduronic acid, in the case of DS) (Cooney et al., 2011). During their synthesis, sulfate groups can be added to the 4-hydroxyl (4-O-sulfation) and 6-hydroxyl (6-O-sulfation) positions of the N-acetylgalactosamine and/or the 2-hydroxyl (2-O-sulfation) position of the D-glucuronic acid (Nikos Afratis et al., 2012). In CRC, a substantial increase in the amount of 6-O-sulfated and/or non-sulfated disaccharides is normally observed. Interestingly, this phenomenon is accompanied by the reduction of the 4-O-sulfation levels (Pudełko et al., 2019). As a consequence of the prevalence of chondroitin-6-sulfate (C-6-S) isoforms within the tumor stroma, the recruitment of cancer-associated fibroblasts (CAFs) and leukocytes is induced. These cells possess the CD44 receptor, which binds to HA (Figure 7). The resulting C-6-S/HA-rich matrix provides an anti-adhesive microenvironment that contributes to the migration and metastasis of CRC cells (Senbanjo & Chellaiah, 2017).

Although the biological effects of CS/DS are dependent on their structure and concentration, the remodeling of these GAGs constitutes a fundamental event that has been linked to CRC growth and progression (Theocharis, 2002).

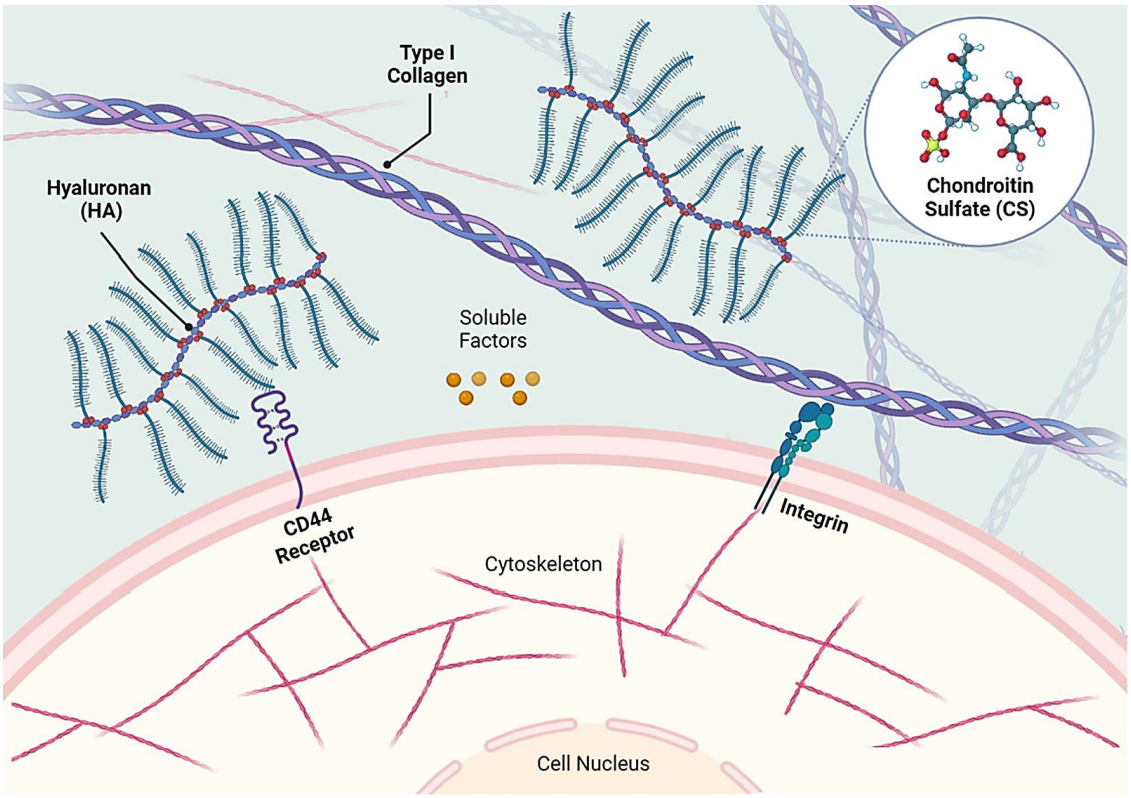

Figure 7 – Roles of chondroitin sulfate (CS) in the modulation of colorectal cancer (CRC). CS is a glycosaminoglycan (GAG) that is frequently overexpressed in the stroma of multiple tumors, either in a free form or linked to proteins. The most abundant CS isoform in CRC is chondroitin-6-sulfate (C-6-S). Abnormal production and deposition of these chains lead to the activation of cancer-associated fibroblasts (CAFs) and tumor-infiltrating cells, which express the CD44 receptor on their membrane. This molecule binds to hyaluronan (HA), producing an anti-adhesive matrix that leads to the detachment/metastasis of CRC cells. *Adapted from (Ewald, 2021). Created with Biorender.com.*

3. Experimental Models for CRC Research

3.1. *In Vivo* Models

In vivo models have been historically applied in fundamental biology and translational medicine to estimate individual responses to therapy and/or disease (Leenaars et al., 2019). For instance, modeling human cancers in animals, including *Drosophila*, zebrafish, chicken, monkey, dog, and/or rabbit, allowed for the comprehension of CRC pathophysiology, identification of new carcinogens, and development of screening assays (Katt et al., 2016). However, rodents, particularly the mouse, have been the most important contributors in this field, owing to their accessibility, small size, high reproductive rate, short lifespan, ease of manipulation, and low consumption of test compounds. Additionally, human and murine genomes share a high level of homology (average of 85%), and the function of their genes is evolutionarily conserved (Mendes et

al., 2020). At the moment, the most used *in vivo* CRC models are chemically induced, genetically engineered, and transplantable animal models (Figure 8). It is worth noting that an appropriate CRC model should produce tumors with a high incidence and within a short period of time; support the non-invasive monitoring of the disease and simulate the histological and molecular features of human colorectal lesions.

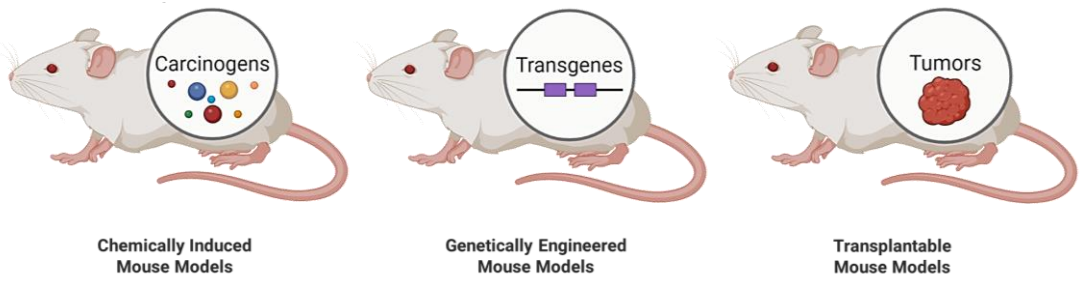

Figure 8 – Schematic representation of the currently available *in vivo* models that are utilized in translational colorectal cancer (CRC) research. Anatomically and physiologically speaking, humans and rodents, particularly mice, are very similar, as they share the same organs and systems, which, in turn, perform equivalent life functions. Given this, *in vivo* mouse models are indispensable in pre-clinical profiling, especially in cancer research. To create these models, natural and/or synthetic chemical carcinogens (chemically induced mouse models), genetic modifications (genetically engineered mouse models), and tumor biopsies (transplantable mouse models) are introduced into these experimental animals. The resulting tumors reflect many key features of the original human cancer. *Adapted from (J. C. Walrath et al., 2010). Created with Biorender.com.*

3.1.1. Chemically Induced Cancer Models

Chemically induced cancer models are generated after prolonged exposures to natural and synthetic compounds, industrial chemicals, environmental pollutants, or food additives, via injection, ingestion, inhalation, and/or dermal adsorption (Liu et al., 2015). One of the first works that assured the involvement of chemical compounds in the development of CRC was conducted by Lorenz and Stewart, who demonstrated that rodents fed with 1,2,5,6-dibenzanthracene and 20-methyleholanthrene could develop lesions in the forestomach and small intestine (Rosenberg et al., 2009). Since then, several chemicals, particularly N-methyl-N-nitrosourea (MNU), N-methyl-N-nitrosoguanidine (MNNG), 1,2-dimethylhydrazine (DMH), methylazoxymethanol (MAM), 3,2′-dimethyl-4-aminobiphenyl (DMAB), azoxymethane (AOM) and 2-amino-1-methyl-6-phenylimidazo(4,5-b)pyridine (PhIP) have been explored to create sporadic lesions in experimental animals (Oliveira et al., 2020). These carcinogens can break down into electrophilic species that react with nucleophilic centers in the DNA, or are exploited by enzymatic reactions, to be converted into an active mutagenic form (Tanaka, 2009).

Regardless of their mode of action, chemically induced cancer models are simple and inexpensive tools that enable the characterization of the biomolecular mechanisms involved in CRC progression. Also, they potentially provide the evaluation of preventive effects concerning different substances, while allowing for the validation of numerous therapeutic agents (Yoshimi et al., 2012).

3.1.2. Genetically Engineered Cancer Models

Genetically engineered mouse models (GEMMs) are strains that have had their genomes modified by transgenic and/or gene-targeting techniques (J. C. Walrath et al., 2010). Constitutive knockouts have been developed to remove/inactivate genes in all the cells/tissues (Cheon & Orsulic, 2011). In the last years, conditional knockouts have emerged as a more sophisticated technology, in which genes are inactivated in a specific cell/tissue or in a time-controlled manner (J. C. Walrath et al., 2010). The Cre-*LoxP* system is the most adopted conditional knockout for engineering the genome of experimental animals (Cheon & Orsulic, 2011). For instance, it is recognized that familial adenomatous polyposis (FAP), a hereditary form of CRC, is induced by the loss of function of the *APC* gene. Following this, Moser *et al*. established the $APC^{Min/+}$ model using the background of a C57BL/6 mouse. The $APC^{Min/+}$ has a nonsense mutation in the codon 850 of the *APC* gene, which is responsible for the development of multiple intestinal neoplasias (Min). Despite its success, most lesions were benign and confined to the small intestine (Lehman & Stairs, 2015). Aiming at shifting carcinogenesis into the large intestine, alternative *APC* mutants (e.g., $APC^{\Delta 716}$, $APC^{\Delta 242}$, APC^{1638} APC^{1309}, $APC^{\Delta 580}$, and $APC^{\Delta 474}$) carrying aberrations in other genes (e.g., *KRAS*) have been conceived (Kwong & Dove, 2009).

Parallel to FAP research, several attempts have been taken to recapitulate the features of hereditary nonpolyposis colorectal cancer (HNPCC, Lynch Syndrome), which arises when inherited mutations in MMR genes, particularly *MSH2*, are present (Cohen & Leininger, 2014). Although increasing the mutational burden, the deletion of these genes may give rise to hematological malignancies, which reduce the survival of the animals (Johnson & Fleet, 2013). To overcome this limitation, Kucherlapati *et al*. created a conditional knockout ($VCMSH2^{LoxP}$), wherein the *MSH2* inactivation was achieved after associating the *LoxP*-flanked allele with a Villin-Cre transgene. This genetic construct was combined with an HNPCC-related missense mutation, resulting in a phenotype equivalent to that observed in human disease (Kucherlapati et al., 2010).

3.1.3. Transplantable Cancer Models

Transplantable models are created from sustained *in vitro* cultures of tumor-derived cell lines or fragments, which are further implanted in mice (Guerin et al., 2020). There are two types of transplantable models, which include the xenotransplantation of human cancers into immunocompromised mice (xenografts) and the allotransplantation of murine cancers into immunocompetent mice (allografts) (Gengenbacher et al., 2017). Cell line-derived xenografts (CDX) were the first transplantable models explored for CRC research. CDX are generated from cell lines that are harvested and inoculated subcutaneously (ectopic), intrasplenically into the renal capsule (heterotopic), or directly into the colorectum (orthotopic) of hosts carrying an impaired immune system (Jung, 2014). Nonetheless, in an ectopic CDX model cells are not placed into the original site of the tumor. Therefore, alternative techniques involving surgical orthotopic implantation have been developed (Mendes et al., 2020). Furthermore, orthotopic CDX share many features of metastatic cancers, hence promoting fast tumor growth, angiogenesis, and hyperpermeability of blood vessels (Johnson & Fleet, 2013). In association with CDX, patient-derived xenografts (PDX) emerged as more predictive models that preserve the stromal composition and the histopathological features of the original tumor (Mendes et al., 2020). PDX are typically used as avatars for patient-personalized treatments, as well as platforms for evaluating drug candidates and cancer-associated resistance (Bürtin et al., 2020). Alternatively, the inoculation of major histocompatibility complex (MHC)-matched tumors into hosts that can produce an immune response has been performed to form syngeneic models. These allografts have been used to identify new targets, stratify patients, as well as characterize the potential of therapeutic strategies targeting immune checkpoint molecules (Mendes et al., 2020).

3.2. *In Vitro* Models

Although preclinical studies deeply rely on *in vivo* models, animal tumors demonstrate some limitations (Table 1). Another strategy that could improve our knowledge of CRC while simultaneously avoiding the variability between donors involves the use of *in vitro* models. *In vitro* refers to a system in which cells are extracted from living tissues and/or organs into an artificial environment (Albritton & Miller, 2017). These platforms are crucial for translational research, drug testing, and/or target validation since they support the control of multiple experimental variables (e.g., efficacy, toxicity, safety, and dosage) and data reproducibility (Mirabelli et al., 2019).

Table 1 – Main limitations of the presented *in vivo* models.

Model	Limitations	References
Chemically Induced Cancer Models	– Long response times and high penetrance variability. – Unpredictable in terms of tumor location, number, and size. – Lack of invasive and metastatic phenotypes. – Occupational hazards to the operating personnel.	(Bürtin et al., 2020; Oliveira et al., 2020)
Genetically Engineered Cancer Models	– Reduced tumor heterogeneity and low mutation burden. – Variability in tissue-specific responses *in vivo*. – Risk of synchronous overexpression. – Long response times and unpredictable tumor behavior.	(Cheon & Orsulic, 2011; Jessica C. Walrath et al., 2010)
Cell Line Derived Xenografts	– Genetic and cellular heterogeneity is not replicated. – Requirement of an immunocompromised background. – Limited predictability, particularly in solid tumors.	(Bürtin et al., 2020; Oliveira et al., 2020)
Patient Derived Xenografts	– Long response times and high variability. – Limited genetic complexity. – Replacement of the human stroma after *in vivo* passaging. – Requirement of an immunocompromised background.	(Gengenbacher et al., 2017)
Syngeneic Mouse Allografts	– Absence of a human immune system and human targets. – Low number of metastases. – Inability to develop chronically inflamed environments. – Reduced genetic complexity and low mutation burden.	(Gengenbacher et al., 2017; Oliveira et al., 2020)

3.2.1. Two-Dimensional *vs*. Three-Dimensional Cell Models

Two-dimensional (2D) *in vitro* models refer to cells that are cultured as a monolayer onto a flat substrate, such as glass or tissue culture polystyrene (TCPS) (Hoarau-Véchot et al., 2018). Despite providing a controlled environment, these systems do not contemplate the complexity of the ECM or the dynamic interactions of the tumor microenvironment (TME) (Rodrigues et al., 2021). This leads to modifications in the tissue-specific structure (e.g., flattened cell shape and constrained polarity) and cellular responses to stimuli (Hoarau-Véchot et al., 2018). Alternatively, three-dimensional (3D) *in vitro* models overcome the existing gap between experimental tractability and physiological significance (Rodrigues et al., 2021). There is a growing recognition that these platforms recapitulate the morphological, biochemical, and mechanical aspects that define a tumor (e.g., cellular and molecular density, stiffness, concentration gradients, cell-cell/cell-matrix contacts, cell intravasation, and extravasation) (Albritton & Miller, 2017). The most used 3D systems for studying CRC are *ex vivo* organotypic

cultures, scaffold-based cell cultures, tumor spheroids and organoids, 3D bioprinting, and microfluidic platforms (Figure 9).

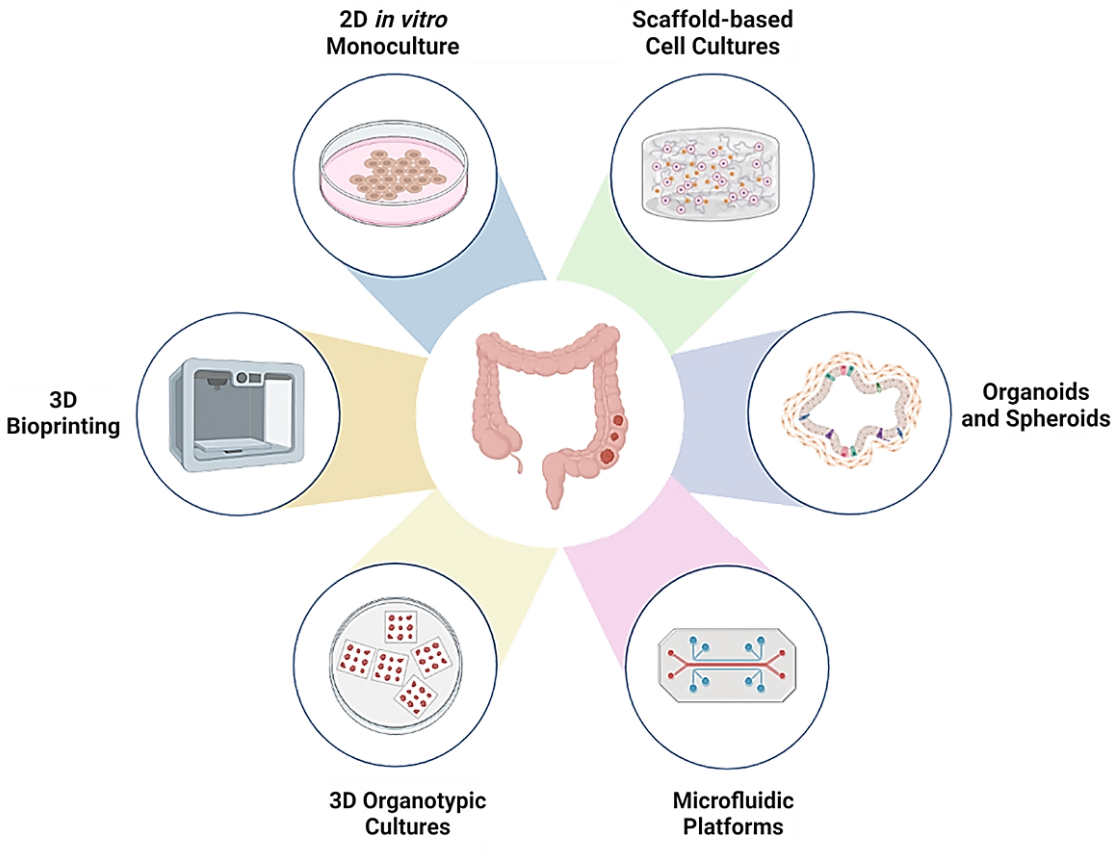

Figure 9 – Schematic representation of the currently available *in vitro* models that are utilized in translational colorectal cancer (CRC) research. In contrast to *in vivo* models, *in vitro* models capture limited aspects of the surrounding tumor microenvironment (TME). Nonetheless, they allow for the control of several experimental variables, therefore supporting the realization of quantitative analysis. Recently, *in vitro* models have been enhanced to allow for the incorporation of multiple cell types, extracellular matrix (ECM) elements, and soluble factors. Because of their biochemical and architectural complexity, tumor *in vitro* models have been considered primary substitutes for animal models, particularly in the early stages of research. *Adapted from (Rodrigues et al., 2021). Created with Biorender.com.*

3.2.2. *Ex Vivo* Organotypic Cultures

Culturing biopsy-derived tumors *ex vivo* constitutes an attractive approach for modeling patient-specific diseases, namely cancer (Rodenhizer et al., 2018). To establish an *ex vivo* CRC organotypic culture, tumor samples must be sectioned into thin slices that preserve the structural and phenotypic characteristics (e.g., 3D architecture and cell-matrix interactions), the proliferative capacity, and the metabolic activity of the native tissues and organs (Misra et al., 2019). These slices incorporate various cell types, such as tumor-infiltrating immune cells, hence simulating the heterogeneity

that is inherent to the primary colorectal lesion (Sivakumar et al., 2019). In this sense, they constitute a good platform for measuring the responsivity of CRC to immunomodulatory therapeutic agents, namely immune checkpoint blockers (Martin et al., 2019).

3.2.3. Scaffold-Based Cell Cultures

Tumor cells cultured in scaffold-based natural/synthetic polymers are reported to support the simulation of CRC *in vitro* (Rodenhizer et al., 2018). The most widespread natural polymers are Matrigel®, collagen, chitosan, alginate, and peptide-based hydrogels. Nonetheless, these materials incorporate highly undefined variables, which might affect the reproducibility of the experimental data. In contrast, synthetic polymers, such as polyethylene glycol (PEG), polystyrene (PS), polycaprolactone (PCL), poly(lactic-co-glycolic acid) (PLGA), and poly(hydroxyethyl methacrylate) (PHEMA) provide more control over the properties of the scaffolds (Rodrigues et al., 2021). In addition, synthetic polymers can be functionalized with natural peptides, such as RGD (Arginine-Glycine-Aspartate), GFOGER (Glycine-Phenylalanine-Hydroxyproline-Glycine-Glutamic Acid-Arginine), and IKVAV (Isoleucine-Lysine-Valine-Alanine-Valine). According to their structural, chemical, and mechanical properties, these molecules can impact the morphology, metabolic activity, growth, proliferation, and invasion of cultured CRC cells (Taubenberger et al., 2016).

3.2.4. Tumor Spheroids and Organoids

Spheroids are powerful tools for CRC research and drug screening because of their high-throughput capabilities and simple workflow (Jeppesen et al., 2017). Spheroids are dense self-assembled clusters of cellular material that can be formed by 3D bioprinting, matrix encapsulation, hanging drop methods, magnetic levitation, and following culture in nonadherent surfaces (Rodrigues et al., 2021). In recent years, multicellular tumor spheroids (MCTS) have been gaining popularity since they can incorporate heterogeneous cell populations. Additionally, MCTS are shown to recapitulate the ECM-TME, signaling pathways, and gene expression patterns of many forms of cancers, including CRC (Ramzy et al., 2020). MCTS include a proliferative zone at the surface, a middle layer with normoxic quiescent cells, and a hypoxic area in the core that is obtained upon an increase in their size. Owing to this, they are frequently employed to study avascular tumors and model micro-metastases (Däster et al., 2017). Similarly, tumor organoids incorporate different cell types and possess an arrangement identical to that of the original tissue from which they were created (Luo et al., 2022).

Tumor organoids are obtained from patient-derived tumors and circulating tumor cells, pluripotent stem cells, and genetically-modified organoids (Seidlitz & Stange, 2021). Upon embedment into an appropriate matrix, they undergo proliferation and self-organization into 3D cell clusters. Accordingly, CRC organoids represent a promising platform for studying tumor cell invasion and metastasis, exploring tumor-stroma interactions, and performing drug screening assays (Young & Reed, 2016).

3.2.5. 3D Bioprinting

Bioprinting is an additive manufacturing technique that supports the generation of complex 3D geometries with well-defined architectures and compositions (Langer et al., 2019). Common bioprinting techniques include laser-assisted, extrusion-based, and inkjet bioprinting, stereolithography, and electrospinning (Heinrich et al., 2019). In bioprinting, living cells, biomaterials, or ECM components are typically printed onto a receiving substrate or liquid reservoir (Datta et al., 2020). Nevertheless, depending on the selected technique, other bioinks, such as microcarriers or tissue spheroids, can be explored (Rodrigues et al., 2021). This technique can also be carried out in a scaffold-based or scaffold-free manner. Specifically, scaffold-based bioprinting consists of a 3D construct that is formed by using cells encapsulated in biomaterials, normally hydrogels. On the other hand, scaffold-free bioprinting involves a sacrificial biomaterial mold (e.g., alginate or agarose), which is removed once the cells deposit their own ECM (Datta et al., 2020). Regardless, bioprinting opens doors for the fabrication of more sophisticated microenvironments, where the communication between the tumor and the supporting cells, the deposition of the ECM, and the self-organization of the tissue can be analyzed (Datta et al., 2020).

3.2.6. Microfluidic Platforms

Microfluidics revolutionized our ability to simulate the multicellular organization of living tissues and organs *in vitro* (Carvalho et al., 2019). They consist of complex 3D microstructural chambers with dimensions around tens to hundreds of micrometers, in which several parameters (e.g., chemical and oxygen gradients, flow patterns, mechanical forces, and tissue-tissue interfaces) can be individually observed (Rodrigues et al., 2021). Microfluidics can be fabricated using polydimethylsiloxane (PDMS), silicon, plastic, or glass. In addition, depending on the application or type of biomaterial, different manufacturing techniques can be explored (Bhatia & Ingber, 2014). Overall, these platforms allow for the incorporation of cancer, stromal, and/or infiltrating cell

types, whose viability is ensured by the continuous perfusion of culture media through the microfluidic channels (Pinho et al., 2021). Therefore, these tools have been considered to recapitulate several aspects of CRC (e.g., cell migration, invasion, and metastasis, angiogenic recruitment, responsivity to gradients and therapeutic agents, and the pathological remodeling of the ECM of the source tissue) (Strelez et al., 2021).

4. Decellularized Extracellular Matrices (dECMs)

4.1. General Applications

Despite the progress achieved in the domain of disease models, our ability to recapitulate the ECM of human solid tumors using 3D *in vitro* systems remains highly challenging (Table 2) (Ferreira et al., 2020). An emerging technique that supports the generation of more complex and physiologically relevant cancer models involves the use of decellularized ECM (dECM)-based biomaterials (Hoshiba et al., 2010). Decellularization consists of the removal of cellular, nuclear, and immunogenic materials from tissues or organs. This approach makes it possible to preserve the main constituents of the ECM, the vascular networks, and the architecture of the native structures (Taylor et al., 2018). Therefore, it constitutes a promising tool for the development of dynamic and instructive scaffolds that retain tissue-specific properties and can be used in different applications, including grafts for tissue engineering and wound healing, injectable and implantable delivery systems, and 3D cell culture models (Figure 10) (McCrary et al., 2020). The process of decellularization usually begins with the physical disruption of the cell membranes, followed by the enzymatic separation of cellular components from the ECM, chemical solubilization of cytoplasmatic and/or nuclear material, and removal of cellular detritus from the tissues (Heath, 2019). The first decellularization protocols were projected to obtain acellular homogenates from muscles and to isolate the basement membrane of blood vessels. Subsequently, numerous dECM-based scaffolds began to be generated from different tissues, including the skin, small intestine submucosa (SIS), heart valves, and urinary bladder (Hussey, Dziki, et al., 2018). Remarkably, the decellularization of these tissues provided the basis for the decellularization of whole organs, particularly the heart, lung, kidney, and liver, which can be repopulated with functional parenchymal and selected progenitor cells (Badylak et al., 2011).

Table 2 - Main limitations of the presented *in vitro* models.

Model	Limitations	References
Tumor Spheroids	- Poor uniformity in size and morphology. - Diffusional restrictions. - Destruction during analysis and manipulation.	(Katt et al., 2016; Rodrigues et al., 2021)
Tumor Organoids	- Difficulty in achieving *in vivo*-like maturity. - High variability between experiments. - Lack of vasculature and stromal components.	(Rodrigues et al., 2021)
3D Bioprinting	- Low reproducibility and control over cell number and types. - Slow speeds and high-stress levels might be observed. - Requires specialized equipment and skills.	(Langer et al., 2019; Rodrigues et al., 2021)
Microfluidic Platforms	- External technical impairments. - Edge effects and shear stresses. - Requires specialized equipment and skills.	(Rodrigues et al., 2021)
***Ex Vivo* Organotypic Cultures**	- Difficult to maintain in culture for an extended period. - Difficult to achieve sufficient perfusion with the medium. - Requires significant optimization.	(Rodenhizer et al., 2018)
Scaffold-Based Cell Cultures	- High variability and low control over the mechanical and biochemical properties of natural matrices. - Poor cellular adhesion in synthetic matrices.	(Rodenhizer et al., 2018)

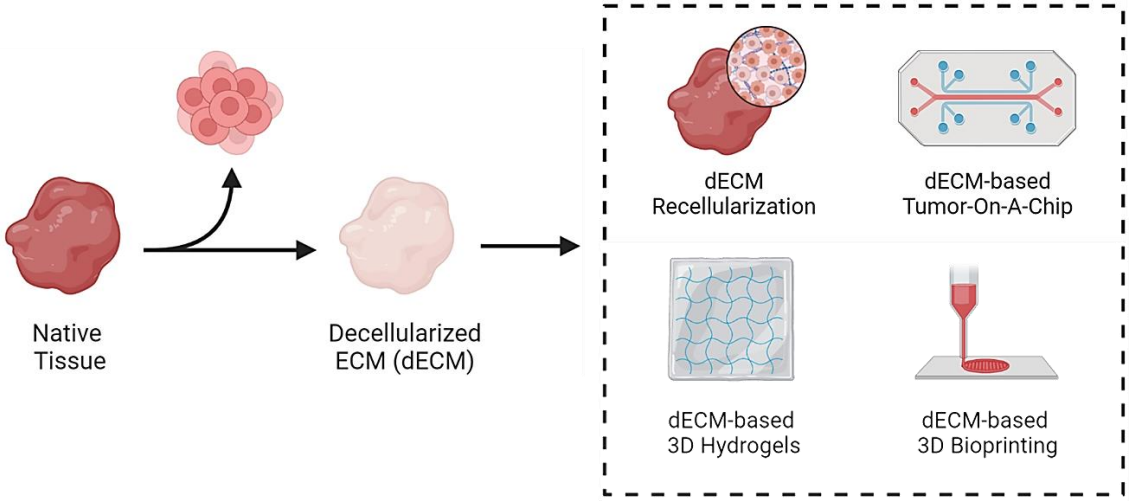

Figure 10 – **Decellularized extracellular matrix (dECM)-based biomaterials used in cancer research.** In the past decades, dECM-based biomaterials have been processed into recellularizable scaffolds, three-dimensional (3D) hydrogels, bioinks for 3D bioprinting, and bioactive constructs for microfluidic platforms. These *in vitro* platforms are structurally sophisticated, yet easy to analyze. Due to their biomimicry and physiological relevance, they have been further explored in the field of cancer modeling for the recapitulation of the critical interactions that define the evolution, progression, and metastasis of human solid tumors. *Adapted from (Ferreira et al., 2020). Created with Biorender.com.*

These materials have been recently engineered to manufacture dECM-based slurries, self-gelling hydrogels, coatings for cell culture substrates, as well as bioinks for the bioprinting of shape-controlled biomimetic constructs (Heath, 2019). Furthermore, the application of novel decellularization methodologies combined with the analytic capacity of omics-based technologies is paving the way for the guided reconstitution of the ECM composition in a patient-personalized manner (Ferreira et al., 2020).

4.2. Decellularization Methods

The most effective decellularization protocols include a combination of physical, chemical, and enzymatic treatments, which have a substantial effect on the composition of the ECM and host responses to the produced scaffolds (Gilbert et al., 2006). Physical treatments use sonication, agitation, electroporation, mechanical delamination, supercritical carbon dioxide (CO_2), high hydrostatic pressures, and freeze-thaw cycles to disrupt cell membranes and facilitate the removal of intracellular components and cell detritus (Hussey, Dziki, et al., 2018). Alternatively, chemical treatments consist of non-ionic (e.g., Triton X-100), ionic (e.g., Triton X-200 and sodium dodecyl sulfate), and zwitterionic (e.g., CHAPS) detergents, hypotonic and hypertonic solutions (e.g., sodium chloride), acids (e.g., acetic acid) and bases (e.g., calcium, ammonium, and sodium hydroxide), organic solvents (e.g., alcohols), and chelating agents (e.g., EDTA) (Crapo et al., 2011). These methods breakdown lipid-protein, protein-protein, and lipid-lipid interactions, induce osmotic shock, solubilize cytoplasmic and nuclear membranes, dissociate the DNA, and induce cell lysis (McCrary et al., 2020). Lastly, enzymatic treatments encompassing proteins with catalytic activity (e.g., DNAse and RNAse, trypsin, dispase, phospholipase A2, thermolysin, and α-galactosidase) are used for targeted removal of particular cellular and molecular components from the ECM (Heath, 2019). These steps can be associated with antegrade and retrograde perfusion, mechanical agitation, immersion, and pressure gradients to improve the penetrance of the decellularization agents (Heath, 2019).

The choice of the decellularization protocol is also determined by multiple factors, particularly the tissue, cellularity, composition, density, and thickness of the tissue of interest, aside from the degree of conservation desired (e.g., IM/BM, macro/microstructure, and growth factors) (Gilbert et al., 2006). For example, thin tissues, such as the pericardium, the intestine, or the urinary bladder, are mechanically processed, decellularized by freezing/thawing cycles and brief exposures (1-2 hours) to easily removed detergents or acids and rinsed to remove the remaining residues. Alternatively,

dense tissues, in particular, the dermis, trachea, and tendons require more extensive exposures to biochemical agents (12-72 hours) and longer rinsing times (Crapo et al., 2011). Nonetheless, many studies have shown that long exposures to detergents, acids, bases, and proteinases may lead to the removal of different extents materials. These include GAGs, fibronectin, laminin, elastin, and collagen. Ultimately, their loss affects the architecture, biochemical composition, and biomechanical properties (e.g., tensile strength and elastic modulus) of the ECM (Mendoza-Novelo et al., 2011). Such a decrease is recognized as a result of the co-location of these components in the bilipid membrane, which is disrupted during the decellularization process (Gilpin & Yang, 2017). Similarly, high concentrations of residual detergents and other agents are shown to be toxic to the host cells upon *in vivo* implantation of the scaffolds, since they hinder cell proliferation and differentiation (Keane et al., 2015). Still, there are no frameworks that recognize which mechanisms will result in the optimal decellularization of a biological structure. In this context, the extraction, production, and processing of dECMs must be planned and optimized to minimize the disruption of the components of the ECM, while simultaneously assuring maximum cell removal (Hoshiba et al., 2010).

4.3. Characterization of the Decellularization Efficiency

At the moment, the most popular strategies to determine the efficiency of decellularization include the assessment of cell, nuclei, and DNA removal. Importantly, the preservation of the composition and structure of the native ECM should be evaluated (Gilpin & Yang, 2017).

4.3.1. Cell and Nuclei Removal

Cell and nuclei removal can be assessed through Hematoxylin and Eosin (H&E) histological staining, wherein fixed tissue specimens exhibit dark blue or purple nuclei and a pink cytoplasm and ECM (Gilbert et al., 2006). Alternatively, the investigation for the presence of DNA can be executed by staining live or fixed cells with nuclear-specific dyes, including Hoechst and 4',6'-diamino-2-fenil-indol (DAPI). Similarly, treatments with PicoGreen™ and Propidium Iodide fluorophores have been proposed to allow for the quantification of cellular DNA content (Gilbert et al., 2006). More recently, Gilbert *et al*. showed that several commercially available dECM-based scaffolds contained traces of remnant DNA. Interestingly, DNA was only present in the form of small fragments, which are not likely to trigger adverse responses (Gilbert et al., 2009).

Nonetheless, to ensure the safety of the decellularization, Crapo *et al*. established the following minimum criteria: (1) less than 50 nanograms (ng) of double-strand (ds) DNA (dsDNA) per milligram (mg) of dry ECM, (2) less than 200 base pair (bp) DNA fragment length, and (3) lack of visible nuclear material in tissue sections (Crapo et al., 2011). These criteria focus on the content of nuclear material, as DNA is the principal responsible for the functional failure and *in vivo* rejection of the dECM scaffolds, is present across all types of tissue, and is easily estimated using standard methods (Heath, 2019).

4.3.2. Compositional and Biological Preservation

Regarding the compositional characterization of dECMs, mass spectrometry analysis and biochemical assays involving histological staining (e.g., Picrosirius Red, Alcian Blue, Masson's Trichome, and Movat's Pentachrome) have been used to estimate the preservation degree of ECM macromolecules (e.g., collagens, proteoglycans, GAGs, elastin, and fibrin) (Gupta et al., 2018). Additionally, immunohistochemical methods comprising specific antibodies can be employed to detect specific cytoplasmic proteins (e.g., fibrous actin and vimentin) (Hoshiba, 2019). Over the past years, several reports established a connection between cytoplasmic/membrane-associated molecules and adverse host responses. For example, residual phospholipids in combination with the high concentration of calcium in decellularized tissues have been associated with calcium phosphate crystallization and calcification (Pathak et al., 2004). Furthermore, α-gal epitopes and mitochondrial material exhibit the potential to trigger complement cascades and MHC complexes, leading to undesirable pro-inflammatory and immune responses (Gilpin & Yang, 2017). Thus, the criteria mentioned above must be extensively optimized to guarantee the effectiveness of the decellularization methods and to facilitate the interpretation and comparison of both *in vitro* and *in vivo* outcomes (Crapo et al., 2011). In 2018, Kawecki *et al*. proposed the following supplementary criteria: (1) maintenance of undamaged ECM components, (2) lack of intracellular and cell membrane elements, and (3) absence of cytotoxicity in the dECMs (Kawecki et al., 2018). Nonetheless, these cannot provide a rigorous and quantifiable measure for the evaluation of the decellularization efficiency. Therefore, the search for the most relevant quality control criteria is still being conducted.

4.3.3. Structural and Mechanical Preservation

For the examination of the architectural organization and biomechanical characteristics of the dECMs, scanning electron microscopy (SEM) and transmission electron

microscopy (TEM) analysis are frequently performed (Hoshiba, 2019). Furthermore, the integrity of the vascular network of the tissue following the decellularization can be assessed by angiography, MicroCT, dye perfusion assays, and/or corrosion casting techniques (Garreta et al., 2017). Contrarily, atomic force microscopy (AFM) is frequently employed to characterize the resistance of the dECMs to deformation at sub-micrometer scales (Alcaraz et al., 2018). Additional mechanical properties (e.g., compression, tensile, flexure, and torsion strength) can be assessed using a rheometer (Kawecki et al., 2018). Finally, fast Fourier transform analysis can be carried out to identify the alignment of ECM fibers (Hoshiba, 2019).

5. Application of dECM-based Biomaterials in CRC Research

The recapitulation of human tumors constitutes a promising approach for the study of the genetic and molecular mechanisms underlying cancer cell growth, proliferation, invasion, metastasis, angiogenesis, immune cell activity, and therapeutic resistance (Ferreira et al., 2020). Indeed, over the past decades, dECMs have been explored as models of primary tumors (same source of the cultured cells) and metastatic sites (different source of the cultured cells) (Hoshiba, 2019). These materials are normally obtained from either native tissues and/or organs or from cells cultured *in vitro*. Tissue/organ-derived dECMs represent important 3D *in vitro* models since they recapitulate the composition and microstructure of the native ECM (Hoshiba et al., 2010). Nonetheless, the low availability of samples and batch-to-batch variability, which is even present in tissues derived from patients diagnosed with the same form of cancer, restrict their application on a larger scale (Hoshiba et al., 2016). Alternatively, dECMs obtained from *in vitro* cultured cells are reproducible and modifiable, since there is greater control of the culture parameters, substrates, cell types, and passage numbers (Hoshiba et al., 2010). Currently, these platforms have been employed to evaluate the mechanisms underlying the maintenance of tissue-specific functions, differentiation of stem cells, and cancer cell chemoresistance (Hoshiba, 2021). However, they evidence limited biochemical and structural complexity, as they can only reconstitute particular regions of the ECM (Hoshiba et al., 2016).

As mentioned before, compared to conventional synthetic and natural biomaterials, dECM-based platforms are more reliable models that can support the viability, morphology, and functionality of normal and cancer cell cultures, while guiding their behavior *in vitro*. For example, Piccoli *et al*. demonstrated that a cyclic decellularization treatment involving short exposures to 4% sodium deoxycholate (SDC), 2000 kU

DNAse I, and 1M NaCl represents an attractive approach for obtaining an intact ECM from both healthy colon mucosa and CRC biopsies. With this procedure, the complete removal of the cells was achieved. Moreover, tissue-specific stimulating factors and crucial proteins were maintained inside the ECM. These molecules possessed biological activity, therefore supporting the migration of the HT-29 CRC cell line, the activation of the DEFA3-mediated signaling pathway, and the expression of the IL-8 immune mediator. Altogether, these events were shown to contribute to CRC cell growth and proliferation, thus confirming the biomimetic effect of the decellularized samples (Piccoli et al., 2018). In a different approach, aiming at simulating the cancer-immune cell dynamics in CRC, Pinto *et al.* developed human-derived colon dECMs, where the polarization of macrophages and the invasive capacity of cancer cells were investigated. To this end, both healthy and tumor tissues were selected from colon-derived surgical resections. Their decellularization was conducted using hypotonic solutions, 0.1% SDS, and 50 U/mL DNase I. Following the analysis of the samples, the results demonstrated that tumor-derived dECMs promoted the transformation of resident macrophages towards an M2-like anti-inflammatory phenotype. These cells produced the CCL18 chemokine, which promoted the migration of CRC cells (RKO, SW420, SW620, and HCT15). The observed increase in invasion resulted not only from the communication between the macrophages but also from the modulatory effect that was exerted by the cancer-derived dECMs (Pinto et al., 2017).

In addition to the permissive cues originated from the ECM-TME, the neoplastic conversion of normal cells into CRC cells may also be influenced by genetic and epigenetic alterations acquired during the early stages of the disease. To validate this premise, Chen *et al.* prepared decellularized colon matrices and investigated the genes that seemed to drive CRC progression and invasion. First, healthy patient-derived colons obtained from surgical resections were decellularized in 1% SDS and 1% Triton X-100. The produced scaffolds were repopulated with myofibroblasts, human colonic epithelial cells (hCECs), and endothelial cells. Remarkably, this physiologically active platform retained the tissue-specific architecture, cell-matrix contacts, and the co-location of the differentiated cell types. With this model, the authors identified 38 cancer-causing genes that were responsible for the submucosal invasion of hCECs via cooperation with *APC* and *KRAS* mutants. Six of these genes (*PAX7, ASXL2*, *MITF, CAMTA1*, *FXR1,* and *DDX20*) have not been described before and are now known to have a role in the epigenetic regulation and metastatic capacity of CRC (Chen et al., 2016).

Decellularization has been also proven to replicate the modifications that are observed in the structure and composition of the ECM-TME during carcinogenesis. Based on the idea that the phenotype of cancer cells may be altered in the absence of the appropriate biomimetic signals, Genovese *et al*. decellularized the mucosa of healthy, perilesional, and cancerous human colons. Following washes with ionic/nonionic detergents, hypotonic/hypertonic solutions, and endonucleases, the obtained platforms were cultured with primary monocytes and one out of three epithelial CRC cell lines (HT-29, LoVo, SW480). The proliferation and invasion of LoVo and SW480 cells were increased in both perilesional and cancerous-derived dECMs, although the latter provided a better outcome. HT-29 cells did not invade any of the scaffolds, possibly due to the lack of the plasminogen activator (uPA). In addition, the 3D distribution of stromal proteins and glycoproteins in the dECMs supported the organization, proliferation, and polarization of monocytes and cancer cells. These findings highlight the contribution of the different ECMs during the process of carcinogenesis (Genovese et al., 2014).

The application of dECM-based platforms in CRC research has been recently extended to the investigation of the primary mechanisms that are involved in the acquisition of drug resistance. In this sense, to test the resistance of CRC cells to treatments with 5-fluorouracil (5-FU) and to simulate the characteristics of the ECM at different phases of malignancy, three cultured cell-derived dECMs were prepared. Decellularization of invasive (HT-29), non-invasive (SW480), and normal (CCD-841-CoN) CRC cell lines in 0.5% Triton X-100, 20 mM NH_4OH, and 100 µg/ml DNase I/RNase A successfully produced acellular scaffolds. After culturing CRC cells in the dECMs derived from the invasive HT-29 cell line, which simulated the compositional complexity of highly malignant tumors, 5-FU resistance increased. Furthermore, HT-29 cells activated the *AKT* signaling pathway and the *ABCB1* and *ABCC1* genes, which can contribute to the pathological remodeling of the ECM (Hoshiba & Tanaka, 2016). Following this work, a CRC metastasis model was developed. Its goal was to predict the responses of two samples derived from different metastatic sites (lung and liver) to three therapeutic agents: 5-FU, irinotecan, and oxaliplatin. First, rat-derived lung and liver ECMs were decellularized in 1% SDC with phospholipase and 3.5M NaCl. Three CRC cell lines (HT-29, SW480, and Caco2) were seeded onto the obtained dECMs. Compared to Matrigel® and a 3D collagen-based model, cells cultured onto the dECMs evidenced a morphology and a metastatic potential equivalent to that observed *in vivo*. Additionally, depending on the substrate in which the cells were placed, different responses to the previous drugs

were achieved. Altogether, these results reinforce the role of particular elements of the ECM in the regulation of the behavior of CRC cells (Tian et al., 2018).

5.1. dECM-based Hydrogels

One of the major advances in the engineering of dECM-based biomaterials is the capacity to fabricate hydrogels through chemical and enzymatic digestion of the ECM into protein monomeric components and subsequent neutralization to a physiological pH, temperature, and salt concentration (Hussey, Dziki, et al., 2018). Hydrogels are defined as 3D networks of crosslinked polymers that preserve their structural integrity by establishing covalent or non-covalent bonds between their molecular chains (Saldin et al., 2017). These materials possess the unique ability to absorb and hold more than 30% (v/w) of water content, owing to the presence of hydrophilic functional groups (e.g., $-NH_2$, -COOH, -OH, $-CONH_2$, -CONH, $-SO_3H$) along their backbone (Bashir et al., 2020). However, the amount of water they retain depends on various parameters, including the structure of the polymer and its molecular weight, the crosslinking density and strength, the chemical composition, and the polymerization technique employed to fabricate the hydrogel (Catoira et al., 2019). To date, dECM-derived hydrogels have been used as 3D organotypic culture models, which recapitulate the *in vivo* microenvironment of the native tissues, while supporting the differentiation and viability of the cultured cells (Hussey, Dziki, et al., 2018).

For instance, Romero-López *et al*. demonstrated the molecular components present within hydrogels derived from dECMs can promote the growth and proliferation of CRC cells, in addition to their shift towards a more glycolytic metabolism. Indeed, the decellularization of both normal colons and tumors that had metastasized to the liver led to a retention of the architecture and composition of the native tissues. Following digestion in 0.1 M HCl and a mixture with fibrinogen, a hybrid hydrogel was obtained. Apart from supporting the growth of GFP-transduced SW620 CRC cells and endothelial colony-forming cells (ECFC), the results revealed these tumor-derived platforms appear to have the capacity to form capillary networks. Furthermore, SW620 cells exhibited an upregulation of *GLUT1* and *HK1* glycolysis genes, thereby highlighting the effect of the ECM on both the tumor cells and vasculature (Romero-López et al., 2017). In another study, porcine-derived SIS/submucosa was decellularized using a detergent-enzymatic treatment (DET). The obtained platforms were then digested to produce 3D hydrogels with different architectures and porosity, depending on the final concentration of ECM. The authors demonstrated that DET maintained the majority of both ECM

and non-ECM components. Apart from sustaining the culture and survival of human gastrointestinal organoids, these materials supported the expression of specific intestinal markers that define the crypt-villi signature. The organoids retained their function *in viv*o and promoted angiogenesis 2.5 weeks after their transplantation into *CD1* and *LGR5-DTR-EGFP* mice. These results show the clinical potential of dECM-derived hydrogels for organoid growth and transplantation (Giobbe et al., 2019). Similarly, Kim *et al*. isolated, decellularized, and solubilized porcine-derived stomachs and small intestines to fabricate self-gelling hydrogels. Compared to Matrigel®, these biomaterials were more effective at promoting the morphological and functional development of both gastric and intestinal organoids. This was mainly due to the preservation of non-matrisome components after the decellularization process. This work strengthens the relevance of tissue-mimetic microenvironments for the stimulation and culture of cancer cells and organoids. Furthermore, it proposes an alternative to Matrigel® that can be applied to model gastrointestinal diseases (Kim et al., 2022).

5.2. Relevance of dECM-based Hydrogels

Regardless of the improvements achieved in the CRC field, such as the decrease in prevalence, incidence, and mortality rates, the available preclinical platforms do not provide enough information. Desirable, evidence on how the cellular and molecular heterogeneity of the ECM-TME may affect the evolution of this form of cancer, particularly at metastatic stages. The lack of appropriate, reproducible, and patient-specific approaches to study CRC compromises the representation of the various disease phenotypes and the capacity to predict the biological responses of the affected individuals (Brockway-Lunardi et al., 2020).

In this sense, the presented work proposes the development of a 3D *in vitro* model that, by mimicking the ECM of the native intestine, can be explored as a cell culture substrate to test drugs and analyze the behavior of cancer cells.

Chapter 2

Aims

Given that the decellularization of native tissues and/or organs constitutes a recent field of research, the widespread application of decellularized scaffolds as platforms for studying cancer cells is yet to be achieved. In this context, the present work aims to produce a novel 3D biomimetic platform based on the decellularization of the ECM derived from the intestines of healthy Wistar Hannover rats. This biomaterial could emerge as a potential alternative to the currently available *in vitro* models (e.g., Matrigel®), as it works as a natural substrate, in which CRC-derived cells (e.g., SW480) can be maintained. Following this, the main tasks performed include:

(a) The extraction and decellularization of the ECM derived from the intestines of Wistar Hannover rats.
(b) The evaluation of the efficiency of the decellularization with the help of histological and biochemical techniques.
(c) The solubilization and neutralization of the resulting dECMs and the production of bioactive dECM-based hydrogels with different values of stiffness, depending on the dECM concentration.
(d) The culture of CRC-derived cell lines (e.g., SW480) and the evaluation of their viability.
(e) The chemical functionalization of the obtained hydrogels with modified CS and the characterization of their mechanical properties.

As described in the literature, CS is known to play a crucial role during morphogenesis and signaling transduction. In addition, depending on its sulfation pattern (4- or 6- carbon sulfation), CS may also be responsible for the modulation of cell adhesion, migration, proliferation, and differentiation under normal and pathological conditions. In this sense, the chemical functionalization of the hydrogels obtained from decellularized intestinal ECMs constitutes an innovative methodology that increases the biomimicry and mechanical stability of the scaffolds, while simultaneously supporting the study of this disease in a patient-personalized manner.

Chapter 3

Materials and Methods

1. Intestinal Tissue Collection

Male and female Wistar Hannover rats aged 3 to 5 months old were purchased from Charles River Laboratories (Figure 11A). The whole intestine (small intestine, caecum, and large intestine) of the animals was collected. Euthanasia was performed according to the directive 2010/63/EU. Rats were placed inside a chamber connected to a source of CO_2 (Figure 11B). Exposure to increasing concentrations of this gas caused the loss of consciousness and cardiac/respiratory arrest. A cut in the jugular vein was also performed to confirm death. Once sacrificed, the abdomen of the animals was opened with the help of tweezers and surgical scissors (Figure 11C). The mesentery was then sectioned to facilitate the extraction of the target tissue (Figure 11D). The intestines were transferred to a Petri dish and briefly rinsed with Milli-Q® water (Merck Millipore) to eliminate blood and other biological debris. Finally, the intestines were embedded in optimal cutting temperature (O.C.T.) compound (Thermo Scientific™), frozen in liquid nitrogen cooled 2-methylbutane, and stored at -80°C until further use (Figure 11E).

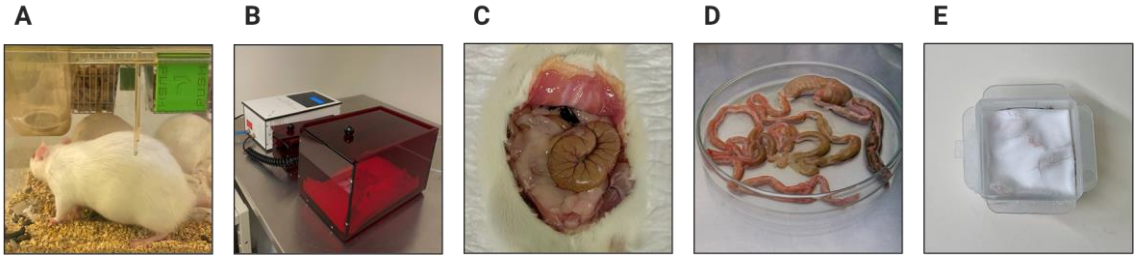

Figure 11 – Intestinal tissue collection. Wistar Hannover rats (A) were placed in a chamber connected to a source of CO_2 (B). Following euthanasia and confirmation of death, the abdomen of these animals was open (C) to allow for the identification and extraction of the whole intestines (small intestine, caecum, and large intestine). The tissues were placed in a Petri dish and washed with Milli-Q® water to remove blood remnants and biological debris (D). Finally, the intestines were embedded in optimal cutting temperature (O.C.T.) compound and stored at -80°C until further use (E).

2. Intestinal Tissue Cleaning

Before decellularization, the collected intestines were thawed at room temperature (25°C), rinsed with Milli-Q® water (Merck Millipore), and unfolded in a Petri dish

with 1x PBS (pH 7.4). Mesenteric fat remnants were separated from the external surface of the tubular structure with the help of a scalpel and tweezers. Afterward, the samples were sectioned into small pieces, with a length of approximately 15 cm. Tissue fragments were opened longitudinally using surgical scissors and the intestinal lumen was scrapped with a surgical blade to mechanically remove the fecal matter from the mucosa. Washes were conducted according to the protocol schematized below (Figure 12). Briefly, the samples were first immersed in increased percentages of ethanol (20%, 50%, and 70%) for a total of 45 minutes (15 minutes in each solution). Following sequential washes in 10x and 1x PBS (pH 7.4), 15-minute treatment with 75% isopropanol was performed. The material was finally washed with 1x PBS (pH 7.4) and Milli-Q® water (Merck Millipore). Once cleaned, the fragmented intestines were placed inside microcentrifuge tubes (one fragment per tube), frozen at -80°C overnight, and lyophilized in the -50°C Freeze Dryer (Labconco Corp.) for 72 hours.

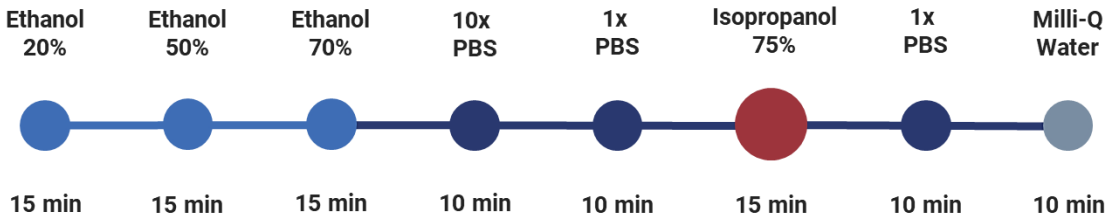

Figure 12 - Intestinal tissue cleaning protocol. Intestinal fragments were first treated with ethanol gradients (20%, 50%, and 70%) for a total of 45 minutes (15 minutes in each solution). In addition, two washes in 10x and 1x PBS (each one with a duration of 10 minutes) were performed. Aiming at improving fat/lipid removal, 15-minute treatment with 75% isopropanol was initiated. Finally, the samples were rinsed with 1x PBS and immersed in Milli-Q® water (10 minutes in each solution).

3. Decellularization of Rat-Derived Intestinal ECMs

The lyophilized intestines were then exposed to the decellularization solutions. To determine the influence of the experimental setting on the efficiency of this process, intestinal fragments were decellularized in 6-well cell culture plates and in 2 mL microcentrifuge tubes (Figure 13). In the first condition, the samples were individually placed inside the wells (one sample per well), while in the second condition, the samples were milled with the M20 Universal Mill (IKA®) and the resulting powder was transferred to the tubes (100 mg of powder per tube). Decellularization was then conducted according to a previously established protocol, which was optimized to allow for the maximal removal of cells and nuclei, while simultaneously producing minimal damage to the architecture of the intestinal tissue (Figure 14, Table 3) (Pinto et al., 2017). Briefly, the process comprehends an 18-hour incubation in a Hypotonic Buffer A (HBA)

solution, succeeded by three washes (1 hour each) in 1x PBS and a 24-hour treatment in a 0.1% SDS solution. The samples were then washed three times (20 minutes each) in a Hypotonic Buffer B (HBB) solution. Importantly, the previous steps were carried out at room temperature (RT) and under mechanical agitation (165 rpm for multi-well plates and 350 rpm for microcentrifuge tubes). In addition, the tissues were digested for 3 hours in a DNAse I Treatment Solution at 37°C and under agitation (165 rpm for multi-well plates and 350 rpm for microcentrifuge tubes). The decellularized intestines were finally washed three times (20 minutes each) in 1x PBS at RT and under agitation (165 rpm for multi-well plates and 350 rpm for microcentrifuge tubes). It is important to note that all the solutions used in this protocol were supplemented with 1% penicillin/streptomycin, 0.5% fungizone, and 0.1% gentamicin (Gibco™, REF. 15710-049). Non-decellularized (native) intestines were also utilized for control purposes.

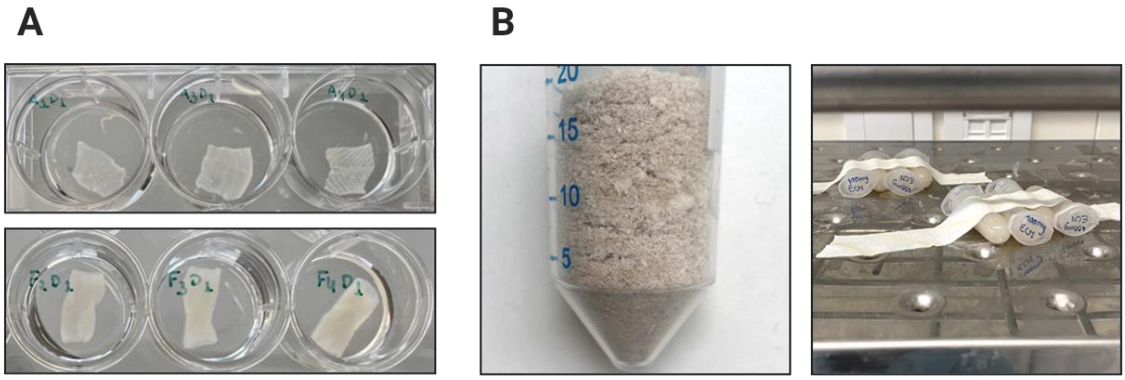

Figure 13 - Experimental settings used for the decellularization of the intestinal tissue. Fragments derived from the small intestine, caecum, and large intestine were lyophilized and individually placed in a 6-well cell culture plate (one tissue sample per well) (A). To completely immerse the samples, 3 mL of the decellularization solutions were added to each well. It is important to note that, with this approach, the different anatomical parts of the intestine can be separated from each other. On the other hand, intestinal fragments can be milled together to create a fine powder, which can be transferred to microcentrifuge tubes (100 mg of powder per tube). The different anatomical parts of the intestines are combined in the same batch, which contains a total of 20 intestines collected from different rats.

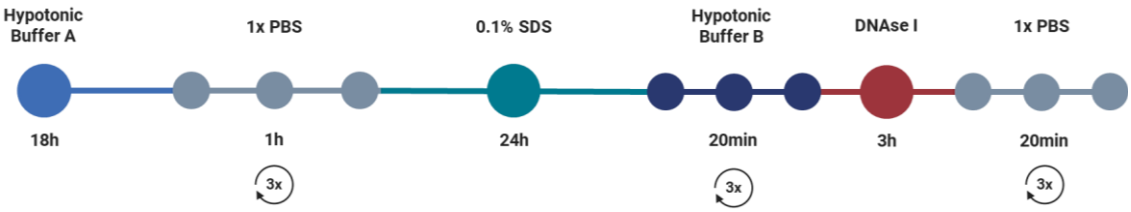

Figure 14 - Intestinal tissue decellularization protocol. The samples were first treated with a Hypotonic Buffer A (HBA) solution for 18 hours, washed three times (1 hour per wash) with 1x PBS, and immersed in a 0.1% SDS solution for 24 hours. Afterward, three washes (20 minutes per wash) in a Hypotonic Buffer B (HBB) solution were conducted. The tissues were then digested with DNAse I for 3 hours at 37°C. Finally, the decellularized samples were washed three times (20 minutes per wash) with 1x PBS.

Table 3 - Composition and pH of the solutions used in the decellularization protocol.

Solution	Composition	pH
1x PBS	NaCl (Fisher Scientific™) KCl (VWR Chemicals) Na_2HPO_4 (Fisher Scientific™) KH_2PO_4 (Fisher Scientific™)	7.4
Hypotonic Buffer A	10 mM Tris-Base (VWR Chemicals) 0.1% EDTA (Sigma-Aldrich®)	7.8
Hypotonic Buffer B	10 mM Tris-Base (VWR Chemicals)	
0.1% SDS Solution	0.1% SDS (Sigma-Aldrich®) 10 mM Tris-Base (VWR Chemicals)	
DNAse I Treatment Solution	20 mM Tris-Base (VWR Chemicals) 2 mM $MgCl_2$ (Merck Millipore) 50 U/mL DNAse I (Fisher Scientific™)	

4. Histological Analysis

Non-decellularized (native) and decellularized samples were fixed in 10% buffered formalin overnight at 4°C. The tissues were transferred to histology cassettes, rinsed with 1x PBS (pH 7.4), and then processed in the Microm STP 120 Spin Tissue Processor (Thermo Scientific™) for 12 hours. The processed samples were impregnated in paraffin blocks and sliced into 5 µm-thick sections. The removal of cellular and nuclear material was assessed by performing standard Hematoxylin and Eosin (H&E) histological staining. Moreover, Alcian Blue and PicroSirius Red dyes were used to determine the preservation degree of primary ECM macromolecules: sulfated proteoglycans/GAGs and type I/III collagen fibrils, respectively. The histological slides were observed under the Light Microscope Olympus DP 25 Camera Software Cell B (Olympus).

5. DNA Staining

The qualitative examination for the presence of DNA was performed by staining the previously obtained tissue sections with the Fluoroshield™ Histology Mounting Medium fortified with 4',6'-diamino-2-fenil-indol (DAPI) (Sigma-Aldrich®, REF. F6057). The DAPI-stained slides were observed under the Axiovert 200M Inverted Fluorescence Microscope (ZEISS).

6. DNA Extraction and Quantification

The double-stranded DNA (dsDNA) of non-decellularized (native) and decellularized samples was isolated and further extracted with the PureLink® Genomic DNA Mini Kit (Invitrogen™, REF: K1820) according to the manufacturer's instructions. To extract the dsDNA, tissue samples were placed inside microcentrifuge tubes, frozen at -80°C overnight, and lyophilized in the -50°C Freeze Dryer (Labconco Corp.) for 72 hours. The lyophilized samples were then incubated with PureLink® Genomic Digestion Buffer and Proteinase K for 4 hours at 55°C. Following digestion and centrifugation, the supernatant was collected, transferred to sterile nuclease-free microcentrifuge tubes, combined with RNase A, and treated with PureLink® Genomic Lysis Buffer mixed with 96-100% ethanol. The dsDNA that adhered to the PureLink® Spin Column was washed to remove impurities and eluted with PureLink® Genomic Elution Buffer. The purified dsDNA was stored at -20°C until further use. dsDNA quantification was performed using the Quant-iT™ PicoGreen® dsDNA kit (Invitrogen™, REF. P7589) according to the manufacturer's instructions. Briefly, high-range (1 ng/mL-2 µg/mL) and low-range (6.25 pg/mL-25 ng/mL) standard curves were prepared. The samples were diluted 25x in a TE Buffer working solution, which was prepared by adding 20x the concentrated buffer to sterile distilled nuclease-free water. A 1x Quant-iT™ PicoGreen® solution was prepared by mixing the concentrated reagent with TE Buffer and added to the standards and samples. After incubating in the dark, the fluorescence was read in the Synergy™ HT Multi-Mode Microplate Reader (BioTek Instruments, Inc.) with an excitation wavelength set at 480 nm and an emission wavelength set at 520 nm, using a black 96-well plate. The concentration of dsDNA in each sample was calculated based on the high and low-range standard curves. The results were presented in nanograms (ng) of dsDNA per milligram (mg) of dry tissue. All standards and samples were run in duplicates.

7. GAG Extraction and Quantification

The sulfated proteoglycans and GAGs (sGAGs) of non-decellularized (native) and decellularized samples were isolated and further extracted with the Blyscan™ Sulfated Glycosaminoglycan Assay (Biocolor Ltd.) according to the manufacturer's instructions. To extract the sGAGs, tissue samples were placed inside microcentrifuge tubes, frozen at -80°C overnight, and lyophilized in the -50°C Freeze Dryer (Labconco Corp.) for 72 hours. The lyophilized samples were then digested in a Papain Extraction Reagent solution (0.1 M sodium acetate, 0.005 M L-cysteine, 0.01 M EDTA, 0.1 mg/mL papain enzyme, pH 6.4) overnight at 65°C. Following incubation and centrifugation, the

supernatant was collected to clean microcentrifuge tubes. For the sGAGs quantification, 10 µL of native-derived and 100 µL of decellularized-derived supernatants were used. A standard curve ranging from 3 µg/mL to 50 µg/mL was also prepared from a stock sGAGs solution. After that, the Blyscan™ Dye Reagent was added to all the standards and samples. Once incubated for 30 minutes, the tubes were centrifuged for 5 minutes, and the liquid was discarded. The remaining pellets (containing the extracted sGAGs) were dissolved using the Blyscan™ Dissociation Reagent. The tubes were finally centrifuged for 5 minutes, and the absorbance was read in the Synergy™ HT Multi-Mode Microplate Reader (BioTek Instruments, Inc.) with the wavelength set at 656 nm, using a 96-well plate. The results were presented in micrograms (µg) of sGAGs per milligrams (mg) of dry tissue. All standards and samples were run in duplicates.

8. Synthesis of Aldehyde-Modified CS

The chemical modification of CS was conducted according to our in-house expertise. Briefly, 616 mg of sodium periodate ($NaIO_4$) (Sigma-Aldrich®, REF. 311448) and 600 mg of CS sodium salt from shark cartilage (Sigma-Aldrich®, REF. C4384) were dissolved in 10 mL of deionized water. The reaction occurred in the dark, for almost 24 hours and under vigorous mechanical agitation (350 rpm). Following this, the solution was transferred to a Spectra/Por®7 1 kD MWCO Dialysis Membrane (Spectrum Laboratories, Inc.) that was placed inside a container with deionized water. Dialysis was carried out for 4 days and under orbital agitation. To maintain the salt gradient, the water inside the container was changed once every day. The contents of the membrane were then frozen at -80°C overnight and lyophilized in the -50°C Freeze Dryer (INEB CI 1781) for 72 hours. Attenuated Total Reflectance-Fourier Transform Infra-Red (ATR-FTIR) and Transmittance of Solids were used for the characterization of the chemical composition of modified and natural CS, respectively. The parameters for all the measurements included a resolution of 1 cm^{-1}, a 4000–400 cm^{-1} spectral range, and 22 scans/samples.

9. dECM-based Hydrogel Fabrication

Following decellularization, the obtained samples were placed inside microcentrifuge tubes, frozen at -80°C overnight, and lyophilized in the -50°C Freeze Dryer (Labconco Corp.) for 72 hours. The material was milled into smaller particles with the help of the M20 Universal Mill (IKA®) and the resulting powder was solubilized using 2.5 mg of pepsin (≥ 3200 U/mg) from porcine gastric mucosa (Sigma-Aldrich®, REF. P6887) and 3% acetic acid to produce pre-gels with a final concentration of 15, 20, and 25 mg/mL

(Figure 15A). The solubilization was performed at 4°C, pH 2.5, under magnetic agitation, and until a homogeneous solution, with no visible particles, was achieved (Figure 15B). The proteolytic activity of the enzyme was later stopped by increasing the pH to a value of 11. After that, the pre-gels were neutralized to a physiological pH (7.4) and salt concentration, by mixing 10 M NaOH and 10x PBS, respectively. Lastly, the hydrogels were placed in a thermostatic bath at 37°C to induce gelation in 30 minutes (Figure 15C). The chemical functionalization of the collagen-based network was performed in 20 and 25 mg/mL pre-gels. After neutralization at 4°C, 5 mg of the aldehyde-modified CS powder was added to the previously solubilized dECMs. The reaction occurred overnight and in the cold. Subsequently, the hydrogels were placed in a thermostatic bath at 37°C to induce gelation in 30 minutes.

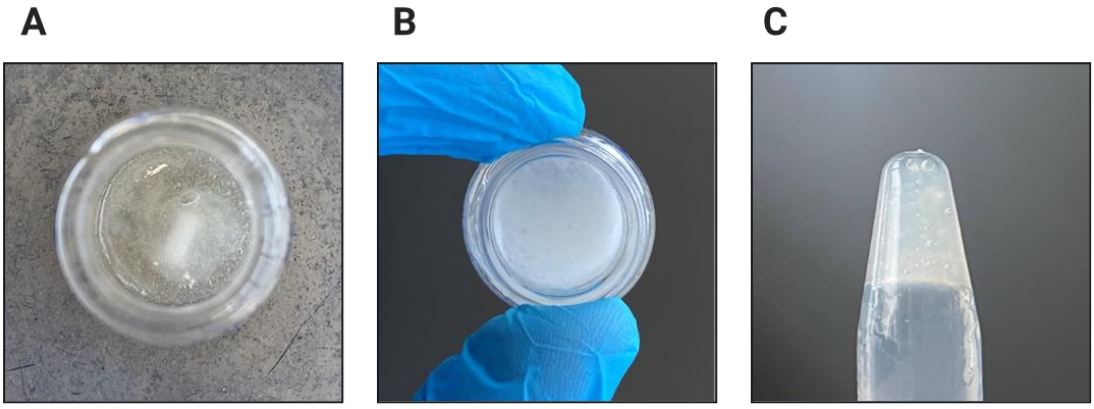

Figure 15 - Hydrogel fabrication. Hydrogel fabrication starts with the solubilization of the previously obtained dECMs under magnetic agitation (A). Solubilization involves the disintegration of type I collagen fibers into monomeric compounds. This is achieved after combining pepsin derived from porcine gastric mucosa with acetic acid, at 4°C, and pH 2.5. Solubilization ends when no visible particles are observed within the pre-gels (B). The sequential addition of NaOH and 10x PBS is further necessary to neutralize the material to a physiological pH and salt concentration, respectively. When placed at 37°C, a crosslinking process is induced, and a structurally stable 3D hydrogel is achieved (C).

10. Turbidity Measurements

The turbidity of the dECM-derived hydrogels was estimated using spectrophotometric techniques. Three hydrogel concentrations (15, 20, 25 mg/mL) were analyzed. The values of the absorbance were measured in the Synergy™ HT Multi-Mode Microplate Reader (BioTek Instruments, Inc.) with the wavelength set at 405 nm and using a 96-well black plate. The measurements were performed once every 2 minutes, for a total of 1 hour and 20 minutes, at 37°C. Readings were normalized to a 1x PBS control using the formula below, where *NA* is the final normalized absorbance, *R* is the absorbance measured at a given time, *Rmin* is the smallest absorbance value recorded, and *Rmax* is the greatest absorbance value recorded.

$$NA = \frac{R - Rmin}{Rmax - Rmin}$$

11. Characterization of the Viscoelastic Properties

The viscoelastic properties of the dECM-based hydrogels were assessed using the Kinexus Pro Rheometer (Malvern Instruments Ltd.). Three hydrogel concentrations (15, 20, 25 mg/mL) were analyzed. Functionalized scaffolds were also tested. On the other hand, Matrigel® (Corning®) was used for control purposes. All the measurements were performed inside the rheometer hood, in a humidified and temperature-controlled environment (37°C), and using 8 mm parallel plates. The linear viscoelastic regions (LVR) of the samples were determined by performing amplitude strain sweeps with a 0.01-100% range of complex sheer strains and a frequency of 1Hz.

12. Cell Line and Culture Conditions

SW480 cells derived from the large intestine of a male Dukes B colorectal carcinoma patient were purchased from the American Type Culture Collection (ATCC, USA). Cells were cultured in monolayer in a 75 cm^2 cell culture flask and maintained in Dulbecco's Modified Eagle's Medium (DMEM) (Gibco™, REF. 31885049) supplemented with 10% fetal bovine serum (FBS) (Sigma-Aldrich®, REF. F7524) and 1% P/S, in a temperature-controlled (37°C) and 5% CO_2 humidified environment. The medium was changed every two days. At confluence, cells were detached with 0.05% trypsin and seeded at a concentration of $0.01x10^6$ cells/well in a 96-well plate. Cells were cultured in a humidified atmosphere with 5% CO_2 at 37°C. Three different conditions were tested: cells cultured on top of Matrigel®; cells cultured on top of 20 mg/mL dECM-based hydrogel; and cells cultured on top of 25 mg/mL of dECM-based hydrogel (Figure 16). For control purposes, cells were cultured alone. Both cells and conditioned medium were further collected at 24 hours (1 day), 72 hours (3 days), and 7 days.

13. Cytotoxicity and Metabolic Activity Assays

The resazurin assay was performed to assess the metabolic activity of the dECM-based hydrogels. SW480 cells were seeded at a cell density of $0.01x10^6$ cells/well in 96 well-plates. 10% (v/v) of resazurin redox dye (0.01 mg/mL, Sigma-Aldrich®) was added to each well and incubated for 3h in the dark and in a humidified atmosphere with 5% CO_2 at 37°C. The supernatant was then collected and transferred to a black 96 well-

plate, and the reduction of resazurin (non-fluorescent blue dye) into resorufin (pink fluorescent) was measured at an excitation wavelength of 530 nm and an emission wavelength of 590 nm, using the Synergy™ HT Multi-Mode Microplate Reader (BioTek Instruments, Inc.). Three biological replicates were performed for each condition and time point. Cytotoxicity was evaluated using the CytoTox 96® Non-Radioactive Cytotoxicity Assay (Promega Corporation, REF. G1780), which quantifies lactate dehydrogenase (LDH), a stable cytosolic enzyme that is released upon cell membrane lysis. The amount of LDH released into the culture supernatant was measured after a 30-minute coupled enzymatic assay, during which the conversion of a tetrazolium salt into red formazan products is observed. A positive control (1% BSA in 1x PBS with CytoTox 96® LDH Positive Control), a negative control (culture medium), and a blank (CytoTox 96® Reagent with Stop Solution) were also included. The absorbance was measured in the Synergy™ HT Multi-Mode Microplate Reader (BioTek Instruments, Inc.) with a wavelength set at 490 nm. Three biological replicates were performed for each condition and time point.

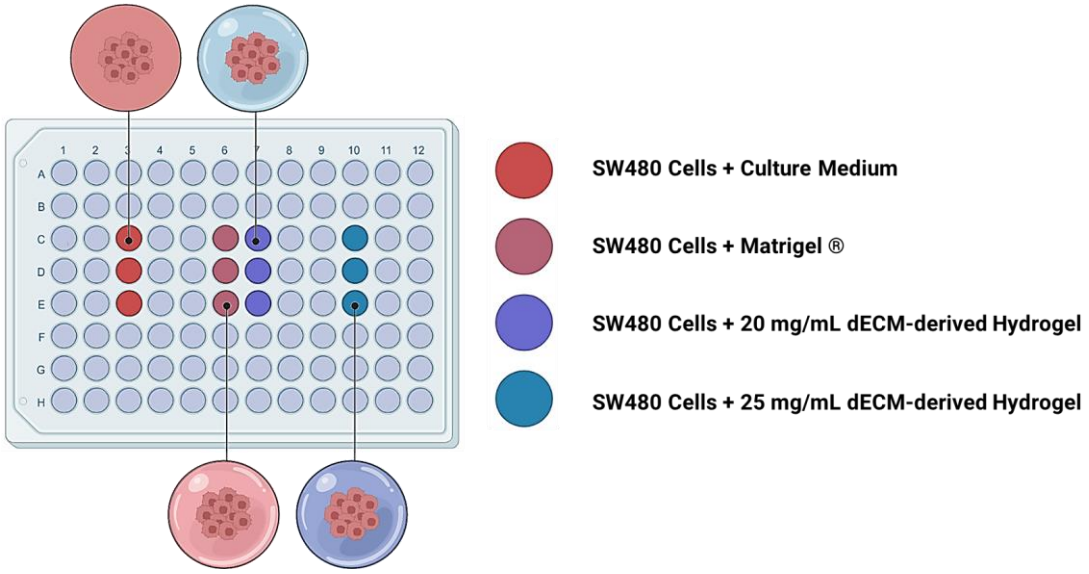

Figure 16 – Experimental setting of the resazurin assay. The resazurin was used to measure the metabolic activity of SW480 cells in four different conditions. A cell suspension containing 0.01×10^6 cells/well and 200 µL of supplemented culture medium was added to empty wells (just cells) and wells containing Matrigel® and two concentrations of dECM-based hydrogels (20 and 25 mg/mL).

14. Statistical Evaluation

All graphs and statistical analysis were performed using GraphPad Prism Software v.8.4.3 (GraphPad-trial version). The presented data were analyzed by performing the One-way ANOVA with Dunn-Sidàk Multiple Test Correction or the Two-way ANOVA with Dunnet's Multiple Test Correction (for multiple comparisons).

Chapter 4

Results

1. Characterization of the Efficiency of the Decellularization

1.1. Cell and Nuclei Removal

The intestines derived from Wistar Hannover rats were cleaned and then decellularized according to the experimental protocol that is described in the "Materials and Methods" section. In this context, non-decellularized (native) intestinal samples were used for control purposes. Compared to the native controls, decellularized intestines became macroscopically whiter and more translucent as a consequence of the removal of cellular/nuclear components from the tissue. To microscopically validate this premise, the efficiency of the decellularization was assessed by staining the intestinal samples with standard H&E and nuclear-specific dyes, particularly DAPI. H&E staining confirmed the successful elimination of the cells from the fragments that were washed in organic solvents (e.g., ethanol-based gradients and 75% isopropanol) and treated with the 0.1% SDS-based protocol. Indeed, following decellularization, both the small intestine and the caecum demonstrated little-to-none cytoplasmic and nuclear material, as seen by the absence of dark blue or purple spots and the presence of a weak pink color (Figure 17A). Interestingly, the large intestine seemed to constitute an exception to this rule, as its histological analysis highlighted the permanence of many cells throughout the mucosa and around the intestinal crypts (Figure 17A). Nonetheless, since the nuclei were fragmented and the cytoplasmatic membranes were disrupted, the cells in the acellular scaffolds were considered unviable. To further support these findings, the nuclear content of the previous intestines was labeled with DAPI (Figure 17B). As perceived by this staining, there was a marked reduction in the fluorescence signal from non-decellularized to decellularized tissue fragments, including the ones derived from the large intestine, therefore corroborating the efficiency of the process, independently of the anatomical origin of the biological samples (Figure 17B). Similar data were obtained when analyzing the tissue fragments that were milled into a fine powder before decellularization. Despite not retaining the native structure, the decellularization of powdered intestines produced a better outcome in terms of cell and nuclei

removal (Figure 17A). These results were, once again, confirmed through DAPI staining, which revealed a reduction in the number of bright fluorescent dots in the powder that underwent the proposed decellularization treatments (Figure 17B).

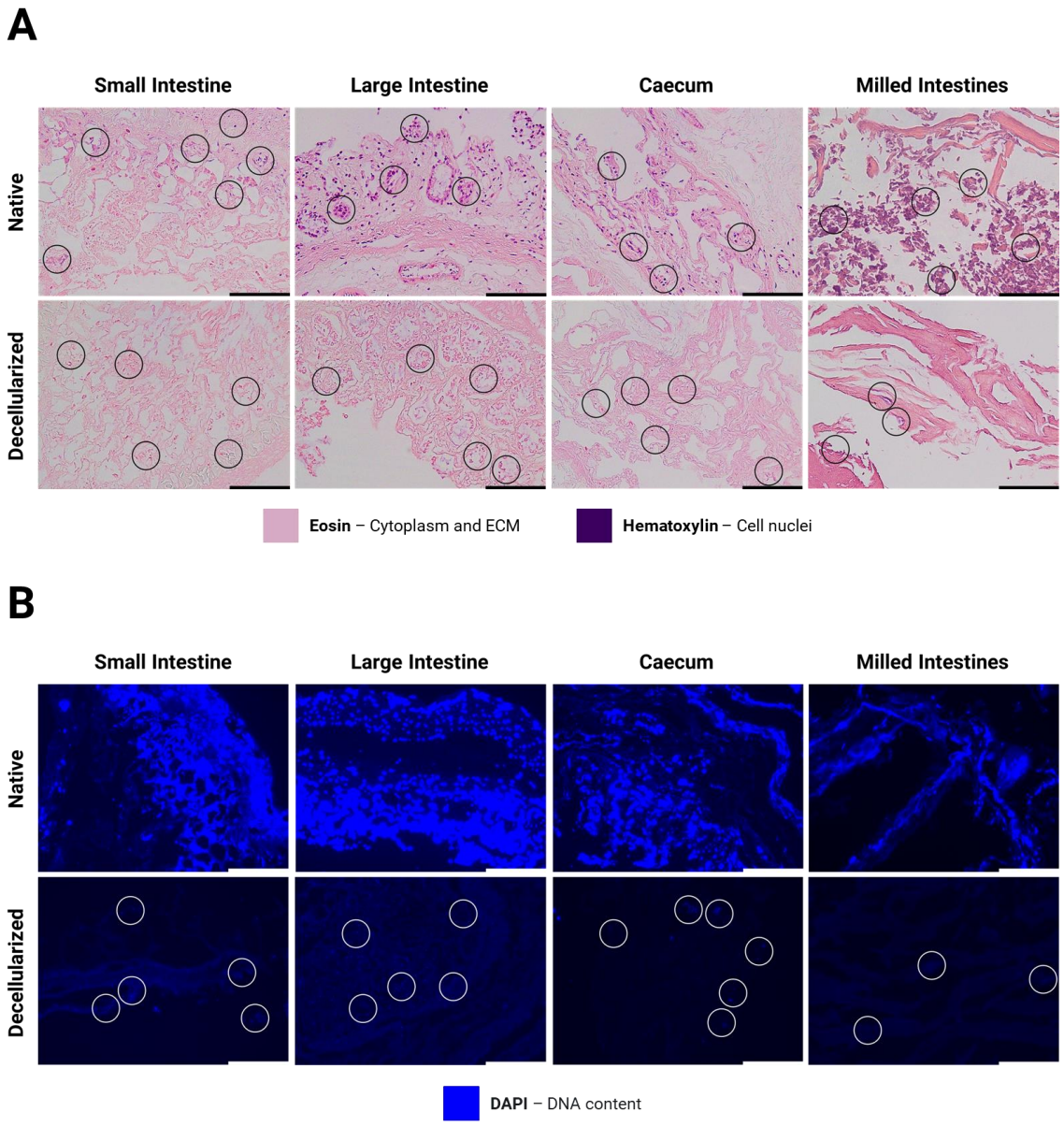

Figure 17 - Characterization of the efficiency of the decellularization: cell and nuclei removal. Non-decellularized (native) and decellularized rat-derived intestines were stained with hematoxylin and eosin (H&E) (A) and 4',6'-diamino-2-fenil-indol (DAPI) (B). Decellularization led to the removal of cells and nuclei from the samples. An exception to this rule was observed in the large intestine, which retained some cells along the mucosa and around the crypts. However, the cells present in all the acellular scaffolds were not viable, as they were not labeled with DAPI. This means that their nuclei and cytoplasmic membranes were disrupted. Milled intestines were also efficiently decellularized, confirming the potential of the 0.1% SDS-based decellularization protocol. All images were acquired with 20x magnifications. Scale bar = 100 μm. Some of the observed nuclei are highlighted with black (H&E) and white (DAPI) circles.

1.2. DNA Removal

In conformity with the results from the H&E/DAPI staining, the dsDNA quantification with the PicoGreen® solution evidenced a dramatic reduction in the dsDNA content. Thus, when comparing the native controls with the intestinal samples that were cleaned with organic solvents and treated with the 0.1% SDS-based decellularization protocol. Once again, this outcome was seen in the tissue fragments obtained from the small intestine, caecum, and large intestine (Figure 18). Notably, the removal of nuclear material from non-decellularized to decellularized samples was in accordance with the criteria proposed by Crapo *et al*. (2011), as all the conditions retained less than 50 ng of dsDNA per mg of dry dECM weight (Figure 18). Nevertheless, although not exceeding the previous threshold, the percentage of dsDNA removal was significantly higher in the intestinal fragments that were milled into a powder before decellularization (Figure 18).

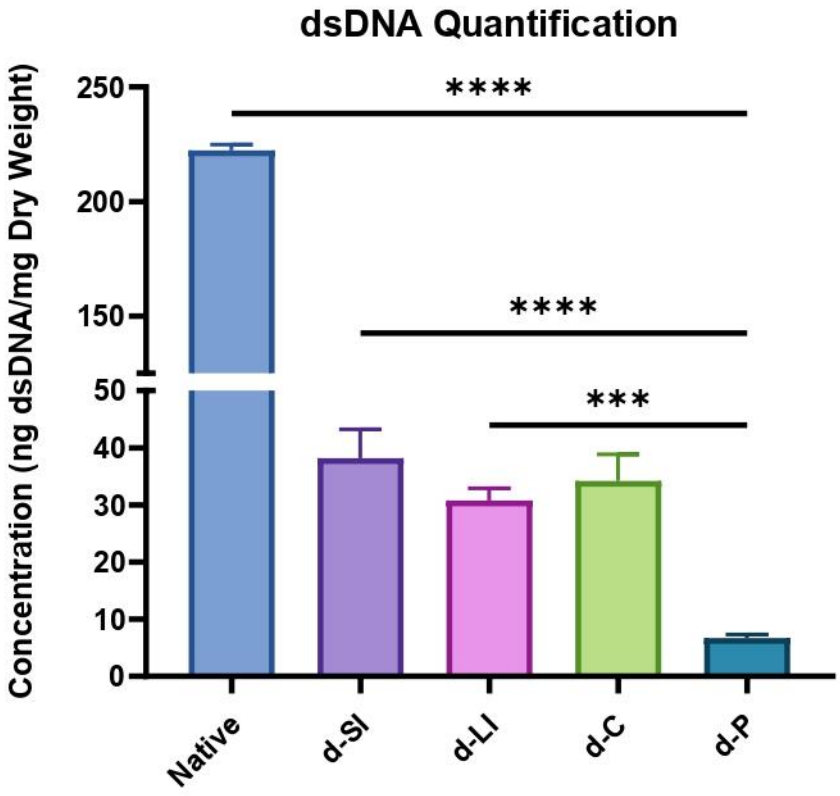

Figure 18 - Quantification of the content of dsDNA in the decellularized rat-derived intestines. Quantification of dsDNA was performed in tissue fragments derived from the small intestine (d-SI), large intestine (d-LI), and caecum (d-C), as well as in powdered intestines (d-P). Non-decellularized (native) intestines were also utilized for control purposes. All standards and samples were run in duplicates. The results are presented in nanograms (ng) of dsDNA per milligram (mg) of dry dECM weight. According to Crapo *et al. (2011)*, optimal decellularization occurs when less than 50 ng of dsDNA is present per mg of dry dECM weight. Statistical analysis: One-way ANOVA with Dunn-Sidàk multiple test correction. Asterisk denotes significance (****$P < 0.0001$; ***$P < 0.001$). Mean ± S.D. ($n = 5$ batches of intestines).

1.3. Structural and Compositional Preservation

Except for milled intestines, whose architecture was intentionally disrupted, the histological analysis confirmed the preservation of the native structure in the acellular samples (Figure 19). Indeed, the intestinal fragments that were decellularized in multi-well cell culture plates evidenced a partially-to-completely intact mucosa, submucosa, muscularis propria, and serosa or adventitia. In this context, the use of organic solvents, particularly ethanol gradients and 75% isopropanol, was responsible for the removal of lipids and undigested food, which are known to impair the performance of decellularization solutions. Although providing a delipidating effect, the combination of the previous treatments with the 0.1% SDS-based protocol led to alterations in the macrostructure of the tissue, namely in the small intestine and the caecum, and an increase in the size of the spaces between the ECM fibers (Figure 19). Concerning the characterization of the composition of the decellularized scaffolds, PicroSirius Red and Alcian Blue staining revealed the maintenance of the collagen-based network and the loss of variable amounts of sGAGs, respectively (Figure 19). Despite being generalized, the depletion of these molecules was more evident in the small intestine and caecum.

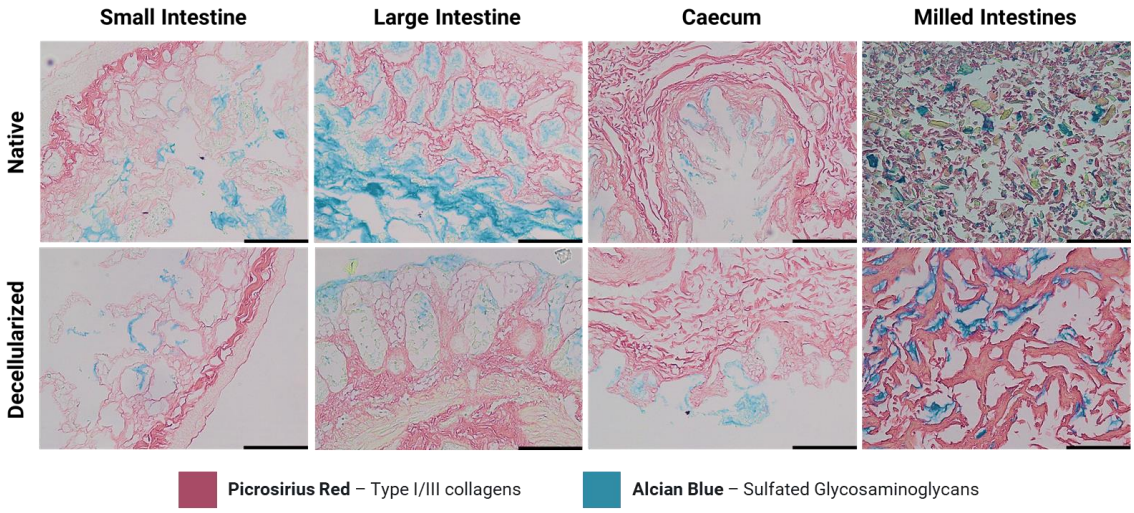

Figure 19 - Characterization of the efficiency of the decellularization: structural and compositional preservation. Non-decellularized (native) and decellularized rat-derived intestines were stained with PicroSirius Red and Alcian Blue. Decellularization led to the overall conservation of the macrostructure of the ECM. An exception to this rule was observed in the small intestine and the caecum, which possessed damaged mucosa. The collagen-based network of these samples was also maintained after the washes. However, a significant amount of sulfated glycosaminoglycans (sGAGs) was loss during the 0.1% SDS-based protocol. All images were acquired with 20x magnifications. Scale bar = 200 µm.

1.4. GAG Preservation

In conformity with the results from the Alcian Blue staining, the sGAGs quantification with the Blyscan™ reagent evidenced a pronounced reduction in the sGAGs content when comparing the native controls with the intestinal samples that were cleaned with organic solvents and treated with the 0.1% SDS-based decellularization protocol. Once again, this effect was observed in the tissue fragments obtained from the small intestine, caecum, and large intestine. Nevertheless, it was proven to be more evident in the small intestine and caecum (Figure 20). Although exhibiting low amounts of sGAGs, especially when compared to non-decellularized intestines, the concentration of these macromolecules was higher in the intestinal fragments that were milled into a powder before decellularization. The large intestine constituted an exception to this rule, as the differences with the powdered intestines were not statistically relevant. Because decellularized milled intestines displayed the best results so far, they were selected for the fabrication of the dECM-based hydrogels.

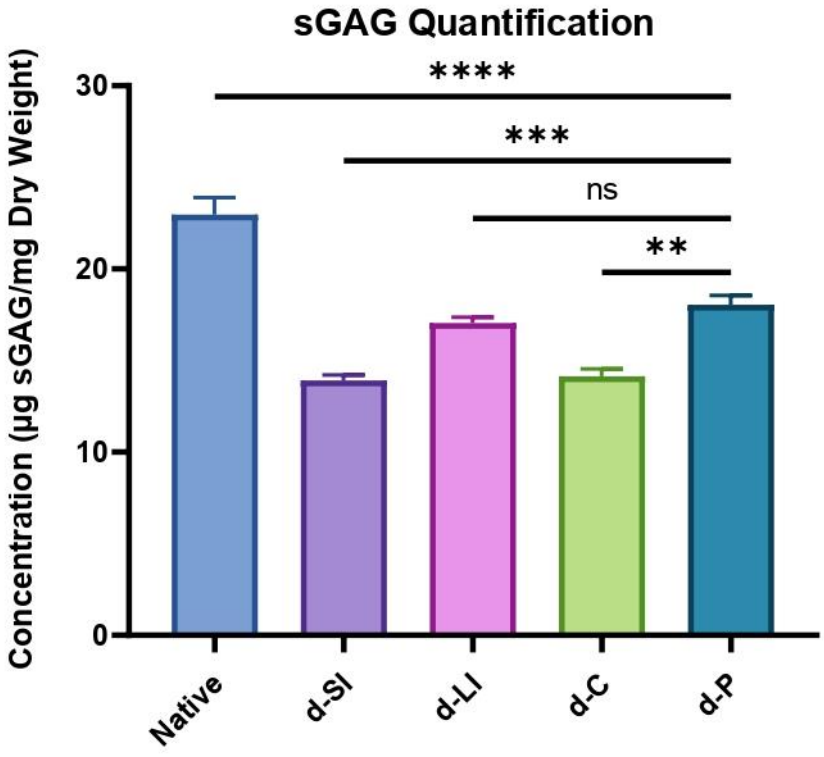

Figure 20 – Quantification of the content of sGAGs in the decellularized rat-derived intestines. Quantification of sGAGs was performed in tissue fragments derived from the small intestine (d-SI), large intestine (d-LI), and caecum (d-C), as well as in milled intestines (d-P). Non-decellularized (native) intestines were also utilized for control purposes. All standards and samples were run in duplicates. The results are presented in micrograms (µg) of sGAGs per milligrams (mg) of dry dECM weight. Statistical analysis: One-way ANOVA with Dunn-Sidàk multiple test correction. Asterisk denotes significance (****P < 0.0001; ***P < 0.001; **P < 0.01; *ns* = not significant). Mean ± S.D. (n = 4 batches of intestines).

2. dECM-based Hydrogel Fabrication and Functionalization

According to the previous results, dECM-based hydrogels were prepared from the enzymatic solubilization and chemical neutralization of intestinal fragments that were milled into a powder before decellularization. In this context, three concentrations of dECMs (15, 20, and 25 mg/mL) were used to evaluate the impact of this parameter on the polymerization kinetics, macroscopic appearance, and rheological properties of the resulting platforms. Despite the dECM concentration, the combination of washes in ethanol gradients and 75% isopropanol with the 0.1% SDS-based decellularization protocol allowed for the fabrication of homogeneous hydrogels that were able to reach 90% of gelation 30 minutes (t_{growth}) after being placed at 37°C (Figure 20). In addition, based on the *quasi*-sigmoidal curve acquired from the normalization of turbidimetric results to the 1x PBS control, the time necessary to reach this plateau (t_{lag}) was lower in hydrogels derived from higher dECM concentrations (Figure 21).

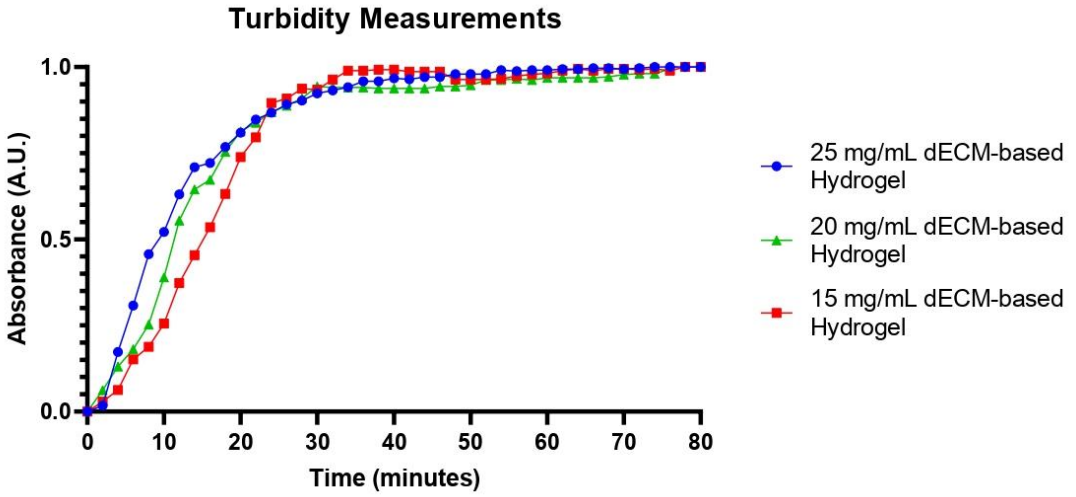

Figure 21 – Turbidity measurements of the dECM-based hydrogels. Spectrophotometry tools were used to assess the turbidity of three dECM-based hydrogels (15, 20, and 25 mg/mL) during the gelation process. A *quasi*-sigmoidal curve was obtained. In all three conditions, polymerization occurred approximately 30 minutes (t_{growth}) after placing the hydrogels at 37°C. Moreover, the time necessary to reach the plateau (t_{lag}) was reported to increase in the scaffolds that resulted from lower dECM concentrations. Data was normalized to a 1x PBS control. $n = 3$ batches of dECM-based hydrogels.

As a consequence of the removal of the biological material from the tissues, the hydrogels derived from all three conditions revealed a translucid appearance, with no visible dark spots or accumulation of lipids. Moreover, higher dECM concentrations resulted in stiffer structures, with well-defined edges, that could be handled without breaking. Alternatively, when the concentration of the dECM decreased, the polymeric network became softer and the constructs displayed rounder edges. Despite that, the physical integrity of these platforms was preserved for approximately 7 days. However,

after that time, the hydrogels became less viscous, running down the wall of the flask where they were stored after applying a mechanical stimulus (e.g., shaking). However, the gel-like appearance was sustained for more than one week (Figure 22A).

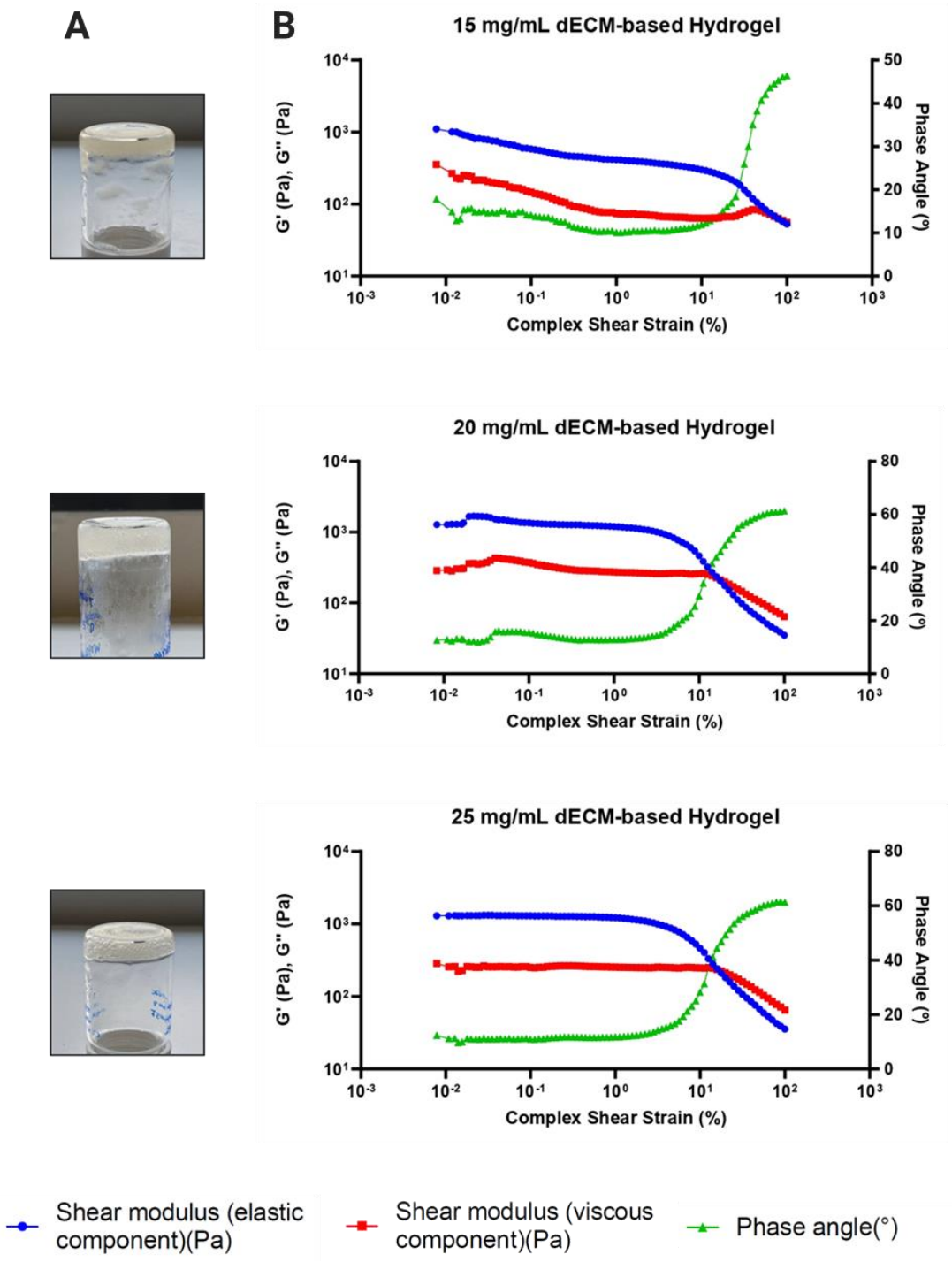

Figure 22 – **Structural and biomechanical characteristics of the dECM-based hydrogels.** The macroscopical appearance of the dECM-based hydrogels after being placed at 37°C for 7 days (A). The viscoelastic properties of these materials were assessed by rheological analysis (B). In this context, amplitude strain sweeps with a 0.01-100% range of complex sheer strains and a fixed frequency of 1Hz were iteratively performed to determine the linear viscoelastic region (LVR) of the scaffolds. G' (Pa): storage/elastic modulus. G'' (Pa): loss/viscous modulus. *n* = 1 batch of dECM-based hydrogels.

To corroborate the previous results, the viscoelastic characteristics of the dECM-based hydrogels were assessed by oscillatory rheology analysis. In this case, amplitude strain sweeps were iteratively performed using a 0.01-100% range of complex sheer strains and a fixed frequency of 1Hz. According to the obtained data, all the platforms derived from the three concentrations of dECMs exhibited gel-like properties at 37°C. This was further confirmed by the presence of higher storage (elastic) modulus (G') in comparison to the loss (viscous) modulus (G''). Despite that, the physical integrity of these materials seemed to be variable. Indeed, the linear viscoelastic region (LVR) in the 20 mg/mL dECM-based hydrogels was restricted to the 0.2 to 1% strain ranges. On the other hand, in the 25 mg/mL dECM-based hydrogels, this parameter oscillated from 0.01 to 1% strain ranges. Notably, 15 mg/mL dECM-based hydrogels did not present a marked LVR, as a result of their instability when placed under stress (Figure 22B). Because the 20 and 25 mg/mL dECM-based hydrogels displayed the best results so far, they were selected for the execution of the next steps.

Aiming at increasing the biomimicry and improving the biomechanical properties of the scaffolds, the previous gels were functionalized with an aldehyde-modified CS. To investigate the incorporation of the aldehyde group within the CS chemical structure, an ATR-FTIR analysis was performed. The resulting spectrum was equivalent to the one achieved for the natural CS, with the only noticeable difference being the presence of an absorption peak at 1728.3 cm^{-1} in modified CS molecules (Figure 24). This band resulted from the conversion of hydroxyl groups into carbonyl groups, which occurs during oxidation with $NaIO_4$. Accordingly, the changes in the vibrational energy at this wavenumber confirmed the successful appearance of aldehyde moieties along the CS backbone (Figure 24).

For comparison purposes, the complex shear modulus (G*) obtained from the amplitude strain sweeps was analyzed. In this case, the hydrogels derived from the two dECM concentrations, with and without the chemical functionalization, were compared to standard Matrigel® cell culture substrates (Figure 23). The results revealed that the solubilization and neutralization of non-functionalized intestinal dECMs could give rise to a set of materials with greater stiffness and tensile strength than Matrigel® (Figure 23). This parameter varied proportionally with the amount of biological material used to form the hydrogels, with 25 mg/mL concentrations producing the stiffest scaffolds. Although being more resistant to mechanical deformation, particularly at lower ranges of shear strains, non-functionalized dECM-based hydrogels lost their physical integrity

with the increase in tension (Figure 23). On the other hand, when looking at the functionalized platforms, a decrease in the density and tensile strength was observed. Interestingly, the addition of the aldehyde-modified CS to the 20 mg/mL dECM-based hydrogels generated a hybrid material possessing a viscoelastic profile similar to that of Matrigel®. Overall, despite being less rigid, the functionalized hydrogels were more stable than their counterparts, even at higher complex shear strain rates (Figure 23).

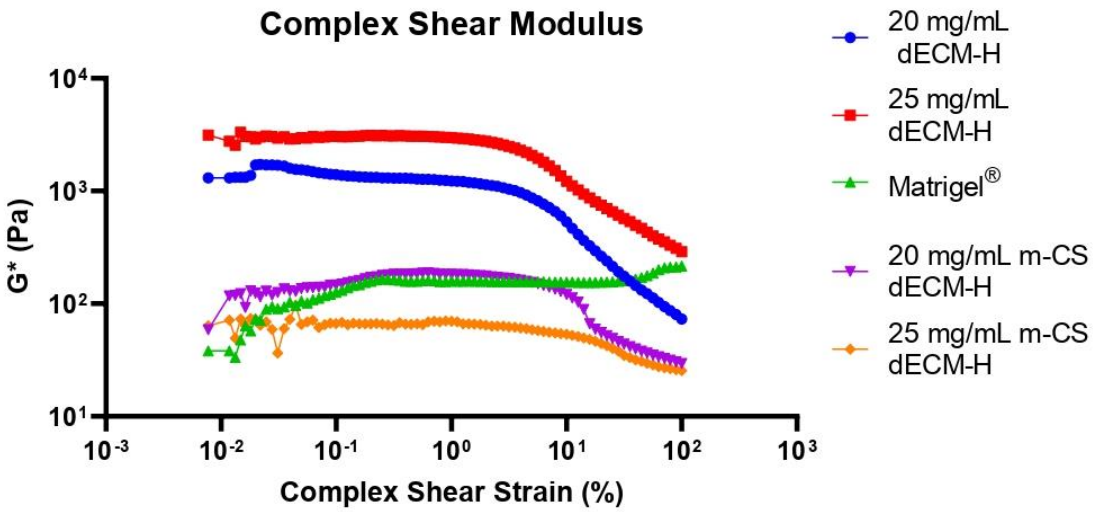

Figure 23 - Variations of the complex shear modulus (G*) of the dECM-based hydrogels and Matrigel®. The complex modulus (G*) represents the relation between the storage (G') and the loss (G'') components of viscoelastic materials. Additionally, it gives information about their resistance to deformation, whether that deformation is recoverable (elastic) or non-recoverable (viscous). Here, the G* profile of the scaffolds derived from the three dECM concentrations, with and without functionalization with aldehyde-modified CS (m-CS), was compared to the one of Matrigel®. *n* = 1 batch of dECM-based hydrogels.

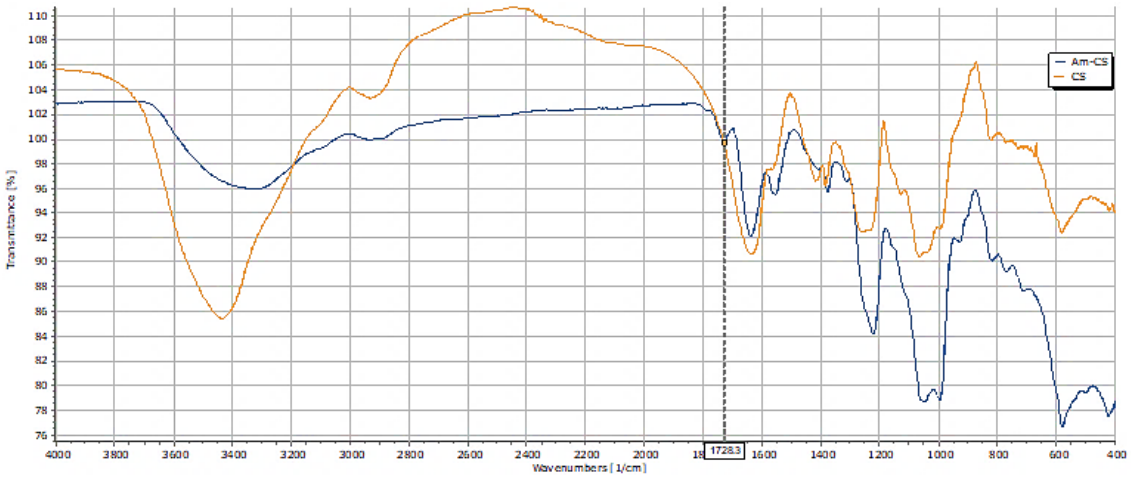

Figure 24 - Attenuated Total Reflectance-Fourier Transform Infra-Red (ATR-FTIR) spectra of modified and non-modified chondroitin sulfate (CS). CS modification was performed by inducing the oxidation of hydroxyl groups with $NaIO_4$. The conversion into carbonyl groups led to the establishment of an aldehyde group in the chemical structure of CS. The stretching vibration of the previous functional group at 1728.3 cm^{-1} shows that the reaction was successfully conducted. *n* = 1 batch of CS and modified CS.

3. Culture of CRC cells in the dECM-based Hydrogels

To determine the safety and biocompatibility of the hydrogels produced from the decellularization, solubilization, and neutralization of rat-derived intestinal ECMs, cell cultures using the SW480 CRC cell line were performed. In this context, the cells were seeded on top of the 20 and 25 mg/mL non-functionalized dECM-based hydrogels, and their viability was assessed 24 hours (1 day), 72 hours (3 days), and 7 days after culture using the resazurin and LDH assays (Figure 24). For control purposes, these materials were, once again, compared with standard Matrigel® substrates (Figure 24).

The resazurin assay was used to estimate the impact of the tested biomaterials on the viability of SW480 cells through the measurement of their metabolic activity levels. In this context, a positive control consisting of cells with culture medium was used for the normalization of the experimental data. All the dECM-based hydrogels exhibited a noticeable stimulatory effect on SW480 cells, particularly when compared to Matrigel®. However, the percentages of metabolic activity in the three experimental conditions were lower than in the control, which, after normalization, was considered to be 100%. Remarkably, this outcome was shown to be dependent on the concentration of dECMs used (Figure 25). Accordingly, the metabolic activity of SW480 cells was higher in 25 mg/mL dECM-based hydrogels for the tested time points. Nevertheless, from 24 hours to 7 days, a general reduction in the fluorescence intensity was observed, hence suggesting an increase in cell renovation and/or death. This trend was further observed in cancer cells cultured in Matrigel® (Figure 25). However, in this case, the values were even lower. To determine if the previous changes in the metabolic activity of cultured SW480 cells were a consequence of the increased cytotoxicity of the tested biomaterials, the search for the presence of the LDH enzyme in the culture medium was conducted (Figure 26). Equivalently to the resazurin assay, a positive control consisting of cells and culture medium was used for the normalization of the experimental data. In spite of exhibiting higher percentages than in the control, which was considered to be null, the dECM-based hydrogels were reported to induce negligible cytotoxicity in the SW480 cells. Overall, the survival of these cells did not seem to change between conditions. Nonetheless, when compared to Matrigel®, the cytotoxicity of the dECMs was slightly higher, especially at 72 hours and after 7 days (Figure 26). An exception to this trend was observed in the 24 hours time point when SW480 cells appeared to release more LDH to the culture medium when in contact with Matrigel®. These effects were, once again, dependent on the concentration of dECMs used, with the 25 mg/mL dECM-based hydrogels being the most cytotoxic material (Figure 26).

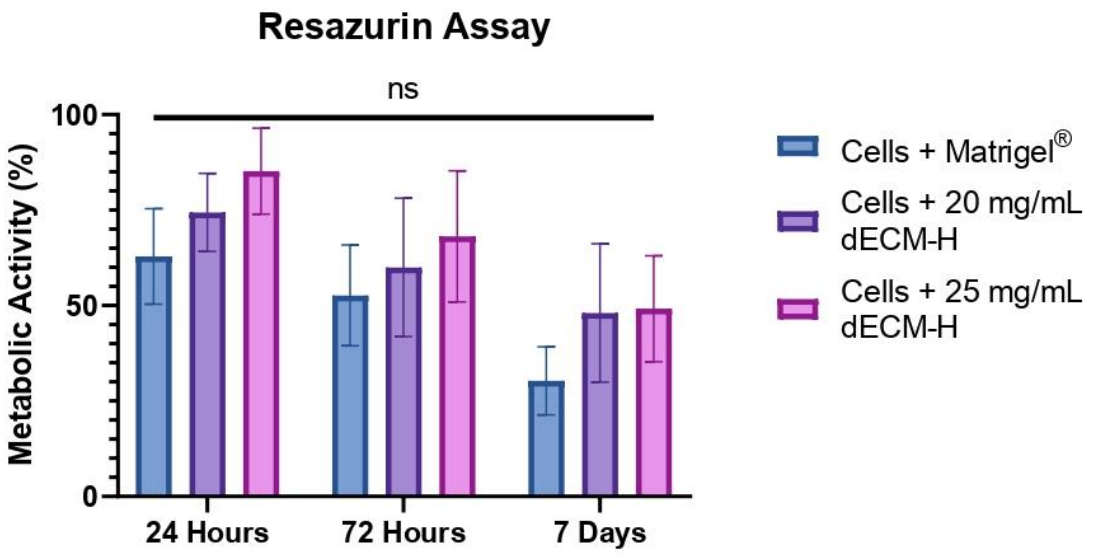

Figure 25 – Quantification of the percentage of cell viability using the resazurin assay. The resazurin assay was performed 24 hours (1 day), 72 hours (3 days), and 7 days after culturing SW480 cancer cells on top of Matrigel®, 20 mg/mL, and 25 mg/mL dECM-based hydrogels. The obtained results were normalized to a control containing just cells and culture medium, which was considered to possess 100% of metabolic activity. Statistical analysis: Two-way ANOVA with Dunnet's multiple test correction (*ns* = not significant). *n* = 1 batch of dECM-based hydrogels and Matrigel®.

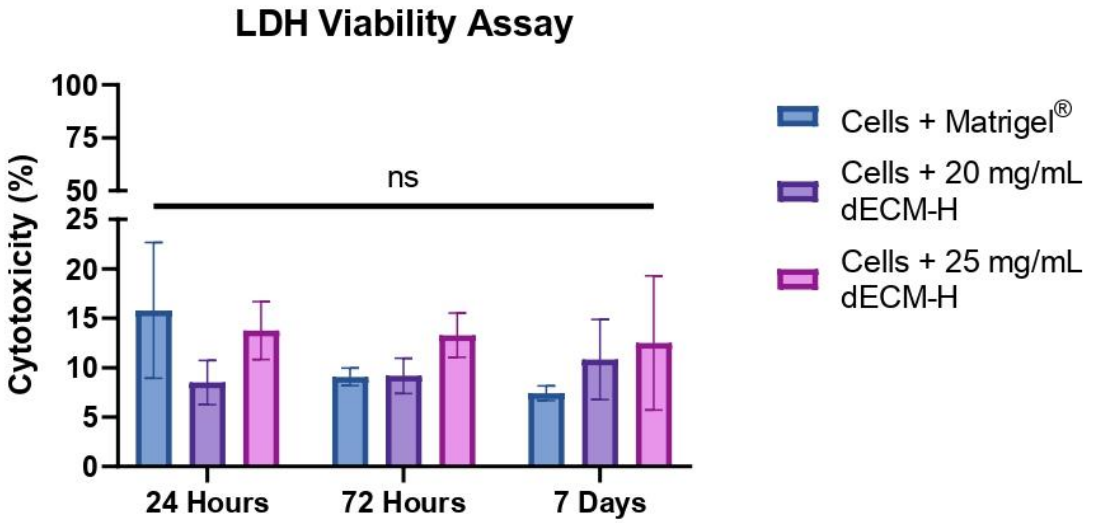

Figure 26 - Quantification of the percentage of cytotoxicity using the lactate dehydrogenase (LDH) assay. The LDH assay was performed 24 hours (1 day), 72 hours (3 days), and 7 days after culturing SW480 cancer cells on top of Matrigel®, 20 mg/mL, and 25 mg/mL dECM-based hydrogels. The obtained results were normalized to a control containing just cells and culture medium, which was considered to possess null cytotoxicity. Statistical analysis: Two-way ANOVA with Dunnet's multiple test correction (*ns* = not significant). *n* = 1 batch of dECM-based hydrogels and Matrigel®.

The evaluation of the morphological appearance of SW480 cells was in accordance with the previous findings. Indeed, as mentioned before, cells in culture medium form

a confluent monolayer. At 24 hours, their shape is undifferentiated and heterogeneous, as seen by the presence of both round and elongated structures. Moreover, aggregates of post-confluency suspended cells could be observed in this condition. After 72 hours in culture, colonies containing round and refractile cells were identified. Despite possessing a morphology that is characteristic of standard cultures, a reduction in the cell density was observed in this condition over time (Figure 27). This was ultimately confirmed by the high number of intercellular spaces. On the other hand, cells cultured in Matrigel® self-assembled into 3D aggregates, which decreased in size from 24 to 72 hours. When compared to this material, dECM-based hydrogels evidenced a similar cell density. This parameter did not seem to be dependent on the dECM concentration or the tested time point. Nevertheless, after 24 hours, 20 mg/mL dECM-based hydrogels seemed to induce a higher proliferative effect. In this condition, SW480 cells exhibited colony-forming features. This tendency was further extended to the 25 mg/mL dECM-based hydrogels. In this case, cancer cells started to evidence invasive characteristics after 72 hours of culture (Figure 27).

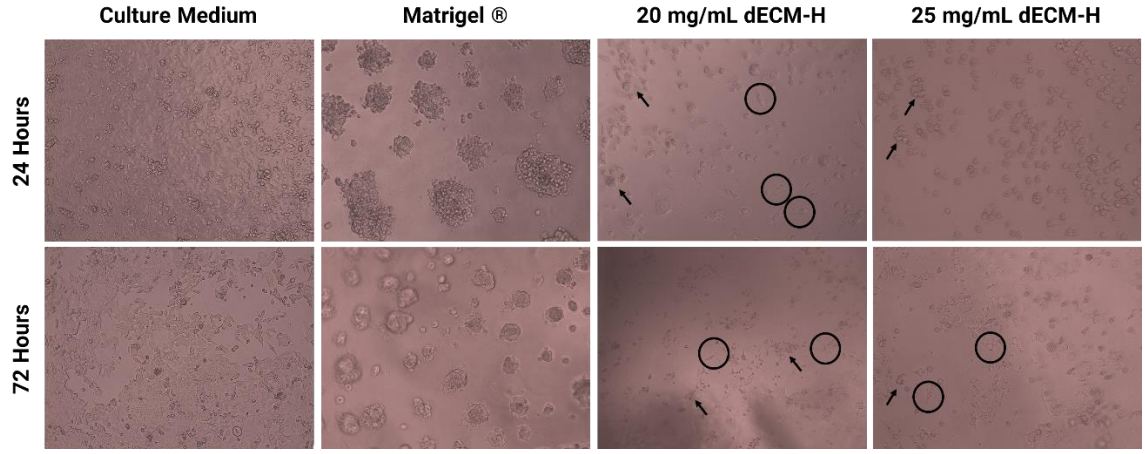

Figure 27 – Morphological evaluation of SW480 CRC cells. Cancer cells were seeded on top of the tested biomaterials and their morphology was evaluated after 24 hours (1 day) and 72 hours (3 days) in culture. An experimental condition, containing cells with just culture medium, was used for control purposes. Cells in Matrigel® evidenced invasive features, as seen by the presence of 3D aggregates. These were not observed in 20 and 25 mg/mL dECM-based hydrogels (dECM-H). Nevertheless, these scaffolds induced a proliferative effect on SW480 cells, which was confirmed by the presence of refractile structures. Arrows are highlighting cell aggregates, while circles are highlighting elongated cells. All images were acquired with 10x magnifications.

It is important to note that these results are preliminary, as new studies with CRC cells must be carried out in order to validate the potential of the proposed materials.

Chapter 5

Discussion

Although CRC incidence and mortality rates have been decreasing in many developed countries due to the implementation of improved screening assays, only a negligible fraction of the patients reveals a positive response to conventional anti-cancer therapies (Chapelle et al., 2020) Therefore, a comprehensive understanding of the biological, biophysical, and biochemical mechanisms underlying cancer cell proliferation, growth, migration, and metastasis could contribute to the discovery of novel biomarkers and targeted agents for the diagnosis and treatment of this disease (Jiacheng Huang et al., 2021). In the last years, the decellularization of native tissues and organs has been explored as a promising technique to produce biocompatible stable scaffolds. These are shown to have suitable mechanical and biodegradable properties, retaining major soluble factors and ECM macromolecules (Saldin et al., 2017). Accordingly, many works studied the effect of physical, chemical, and enzymatic-based methods on the decellularization of the kidney, heart, lung, liver, urinary bladder, skin, and SIS extracted from humans and/or animals (e.g., mice, rats, or pigs) (Gilbert et al., 2006). Furthermore, several techniques have been reported to administer the decellularization solutions, hence conferring an additional layer of complexity to this process. For instance, the decellularization of tubular structures, such as the intestine, has been performed by continuous perfusion through the lumen or by arterial cannulation (Gupta et al., 2018). Nonetheless, this can constitute an approach that is difficult to perform on a daily basis, as it requires specific equipment. Because the intestine is a soft and relatively thin tissue, its immersion in decellularization agents and combination with mechanical agitation may constitute a simpler, faster, and more effective alternative to the previous approach (Crapo et al., 2011). Having this in mind, we aimed at producing a novel dECM-based biomaterial by immersing the ECM derived from male and female Wistar Hannover rat intestines in hypotonic buffers (HBA and HBB), detergents (0.1% SDS), saline solutions (1x PBS) and enzymatic treatments (DNAse I). Since rat intestines have a multi-layered structure possessing high amounts of lipids and other biological debris derived from digested and/or undigested food, additional washing steps with increasing concentrations of ethanol (20%, 50%, and 70%) and 75% isopropanol were carried out before decellularization. Additionally, because the preservation

of the macrostructure of this tissue is not required for the fabrication of the hydrogels, the milling of the whole intestine into a thin powder was also considered.

In this study, SDS was employed as the primary decellularization agent. SDS is an ionic surfactant that contains a negatively charged sulfate (SO_4^-) head group (White et al., 2017). This polar head group is responsible for binding the positively charged hydrophobic residues that are found in membrane proteins and phospholipids, therefore leading to their denaturation and solubilization (Keane et al., 2015). However, despite being acknowledged as one of the most effective chemical solutions for removing cells from a given tissue, SDS must be cautiously used, as it can also disrupt the macrostructure and modify the composition of the ECM (Gilpin & Yang, 2017). Indeed, depending on the concentration and exposure time, SDS is reported to damage the triple helix of type I/III collagen fibrils. Furthermore, it is responsible for the solubilization of different extents of sulfated proteoglycans and GAGs. In this sense, the preservation degree of these constituents after decellularization was qualitatively assessed by performing histological staining with PicroSirius Red and Alcian Blue dyes, respectively. Indeed, compared to non-decellularized controls, the loss of sGAGs was ubiquitously observed in all the decellularized samples, independently of the chosen experimental setting or anatomical origin. The reduction observed in the concentration of these macromolecules was also confirmed by quantification techniques using the Blyscan™ assay. Interestingly, this effect was not completely unexpected, since sGAGs are connected to the surface of the bilipid membrane, which is destroyed throughout the decellularization process (Gilpin & Yang, 2017). In this sense, to prevent the occurrence of these events, multiple washes, with shorter exposure times and low detergent concentrations, must be employed (Mendibil et al., 2020). Another consequence of sGAG depletion, is the exposure of collagen fibers to the decellularization solutions, particularly acids. This causes the denaturation of these proteins and the impairment in the packing features of the ECM molecules, causing an increase in the pore sizes (Meyer, 2019). For this reason, the intestinal fragments treated with the 0.1% SDS-based decellularization protocol exhibited a looser ECM when compared to the native samples.

Rodents, namely rats, are fed *ad libitum*, which means that food is constantly available to the animals. Normally, an adult rat eats 10 to 30 grams of food every day. As a result of their feeding behavior, some strains of laboratory rats achieve high body weights, which often leads to obesity. This is also due to their diet, which is particularly rich in fats and fibers. Consequently, these animals exhibit an accumulation of

visceral adipose tissue around the tubular structure of the intestine and greater amounts of fatty acids and triglycerides within the tissue (Martin et al., 2010). Because the decellularization solutions *per se* are incapable of efficiently removing these debris, washing steps with increasing concentrations of ethanol and 75% isopropanol were introduced in this protocol. Particularly, isopropanol is indicated to remove grease, as well as cells and DNA. However, when used in a concentration higher than 70%, which is the case, it causes fixation of the tissues and precipitation of the proteins (Ventura et al., 2019). In a different work, Gonzalez *et al.* also indicated that this organic solvent can adsorb onto the surface of the type I collagen triple helix, thereby decreasing the lateral distance of the fibers (Gonzalez et al., 2012). For this reason, a brief wash of 15 minutes was implemented to avoid the previous repercussions.

The primary goal of decellularization is to avoid functional failure and the *in vivo* rejection of the dECMs, which are mainly triggered by dsDNA (Heath, 2019). As seen by the staining with H&E, the removal of the nuclear and cellular material was achieved after treatments with the 0.1% SDS-based protocol. This result was independent of the anatomical origin of the material and the experimental setting is chosen. The only exception to this trend was seen in the large intestine fragments, which retained cells in the crypts and the mucosa. Importantly, these were further recognized as non-viable, as they displayed fragmented nuclei and membranes. Since these findings are merely qualitative, Crapo *et al.* established criteria that restrict the adequate concentration of dsDNA after decellularization to a maximum of 50 ng per mg of dry dECM weight (Crapo et al., 2011). Despite exhibiting some variability, which is due to the use of different animals, none of the tested conditions surpassed the above threshold.

The previous analysis was further extended to the intestines that were milled into a powder before decellularization. A fundamental aspect of the powdered materials is their high surface area-to-volume ratio, which, in this case, allows for better elimination of cells, nuclei, and biological debris from the ECM (Mendibil et al., 2020). Interestingly, despite disrupting the native architecture and exposing many ECM elements to decellularization solutions, the milling allowed for the general retention of structural and functional molecules, including collagens and sGAGs. Lastly, another advantage of powdered materials is their extended shelf life and the possibility to use standard sterilization techniques (e.g., exposures to peracetic acid and ethanol) (Tao

et al., 2021). This is even more relevant considering that the main application of these samples involves their processing into a hydrogel-based cell culture substrate.

Hydrogels are viscoelastic and hydrophilic networks that evidence the unique ability to absorb and hold more than 30% (v/w) water content (Bashir et al., 2020). These materials can be obtained from a variety of natural or synthetic polymers. Matrigel® is the most used hydrogel for cell culture applications. However, it is limited in terms of applications, due to its biological origin (since it is derived from a murine sarcoma), batch-to-batch variability, modified mechanical properties, and high costs (Aisenbrey & Murphy, 2020). In recent years, various reports have shown that dECM-based hydrogels could represent an appropriate alternative to Matrigel® scaffolds since they retain the physicochemical characteristics and stimulatory properties of the native ECM (J. Huang et al., 2021). The most popular method used to prepare a dECM-based hydrogel involves the lyophilization and milling of the dECM into a powder that is digested with a pepsin-based solution (White et al., 2017). Pepsin is a protease derived from porcine gastric juices, which cleaves the telopeptides in the collagen triple helix (Jafari et al., 2020). These domains contain hydroxylysine residues, which are enzymatically converted into highly reactive aldehydes. The condensation of these chemical groups creates divalent crosslinking points that connect adjacent collagen fibrils under appropriate environmental conditions (Sarrigiannidis et al., 2021). In the past decades, various studies reported that acid-based collagen digestion might lead to faster reactions compared with pepsin-based digestion (Antoine et al., 2014). Having this in mind, the current protocols combine porcine-derived pepsin with acidic solutions, particularly acetic and hydrochloric acids (Freytes et al., 2008; Voytik-Harbin et al., 1998). Owing to its weaker nature, 3% acetic acid was considered to aid in the extraction of collagen monomers from intestinal ECMs derived from Wistar Hannover rats. Importantly, apart from promoting a more controlled rearrangement of intermolecular bonds, this solvent is also known to isolate high-purity collagen fibers (Delgado et al., 2017). Following digestion, the extracted collagen molecules were triggered to self-assemble into a 3D polymeric network. For that, a neutralization step involving the adjustment of the pH and temperature to physiological values was required (Saldin et al., 2017). Under these circumstances, the digested pre-gels experience an increase in entropy, which culminates in the formation of collagen aggregates. This phenomenon is supported by the addition of PBS, whose divalent anions cancel the excess of positive charges, avoiding the repulsion of the charged monomers (Sarrigiannidis et al., 2021).

To evaluate the impact of the quantity of collagen in the polymerization kinetics, macroscopic appearance, and viscoelastic characteristics of these *in vitro* platforms, three concentrations of dECMs (15, 20, and 25 mg/mL) were evaluated. The produced scaffolds remained stable when placed at RT. Nonetheless, their polymerization only occurred at 37°C. Several studies have shown that, during this process, the turbidity of the pre-gel solutions increases over time, owing to the accelerated nucleation and lateral aggregation of the collagen monomers (Zhu & Kaufman, 2014). In this sense, by measuring the absorbance at 405 nm and 37°C, the time required to form a stable 3D hydrogel can be determined. Here, the spectrophotometric analysis gave rise to a turbidity curve, containing a *quasi*-sigmoidal shape and distinct growth (t_{growth}) and lag (t_{lag}) phases (Antoine et al., 2014). According to that, the dECM-based hydrogels took approximately 30 minutes to be generated. During this period, the collagen molecules present in the hydrogels scattered progressively higher amounts of light, reaching a plateau by the end of the process. Importantly, the gelation kinetics was dependent on the concentration, as higher amounts of dECMs produced a faster crosslinking.

Macroscopically, the hydrogels derived from higher dECM concentrations (e.g., 20 and 25 mg/mL) were stiffer and more stable. On the other hand, the hydrogels derived from lower dECM concentrations (e.g., 15 mg/mL) were softer and more brittle. Such dosage effect results from the availability and spatial proximity of the collagen fibers, which is proportional to the quantity of acellular milled intestines used (Stojkov et al., 2021). Another explanation for this behavior is the reversible nature of the crosslinking, which relies on hydrogen bonding and hydrophobic interactions to hold the polymeric network together (Wang & Heilshorn, 2015). Following this, the viscoelastic properties of the dECM-hydrogels were analyzed by amplitude strain sweep tests. In this case, the G' and G'' moduli are determined by performing experiments with increasing oscillatory strains and a constant frequency. Importantly, these variables give insights into the LVRs of the tested biomaterials, which characterize the behavior of the materials under stress/tension (Stojkov et al., 2021). The results suggested that dECM-based hydrogel samples behaved like viscoelastic solids, since G' > G''. Furthermore, it was shown that the increase in the concentration of the dECMs led to higher stiffnesses and well-defined LVRs. This was consistent with other works that have stated that the viscoelastic characteristics of collagen-rich materials are proportional to the concentration of material in high-stress deformation regimens (Licup et al., 2015). This tendency was particularly evident in 20 and 25 mg/mL dECM-hydrogels. In fact, since these platforms possessed a more flexible collagen-based network, the maintenance of the

physical integrity over broader ranges of complex shear stresses was guaranteed (Storm et al., 2005). Despite this, these hydrogels behaved like viscoelastic fluids when the applied forces were higher than 10%, as seen by G'' > G'. This phenomenon is defined as shear thinning and is a common characteristic of these scaffolds (Fernández-Pérez & Ahearne, 2019). Based on the previous findings, 20 and 25 mg/mL dECM-based hydrogels were chosen to be functionalized with an aldehyde-modified CS. Their viscoelastic profiles were then compared to non-functionalized and standard Matrigel® substrates.

As mentioned before, CS chains play pivotal roles in morphogenesis, cytokinesis, and signaling transduction. In addition, they also participate in the modulation of cell adhesion, migration, proliferation, and differentiation (Hayes et al., 2018). Recently, a prognostic value for the clinical outcome of many types of cancers, such as CRC, has been assigned to modifications in the biosynthesis, expression patterns, and metabolism of CS (Yip et al., 2006). Simultaneously, the emerging use of dECM-based scaffolds made it possible to assess the biological impact of these sGAGs on the behavior of CRC cells (Hoshiba, 2018). Considering that native CS is water soluble and easily degraded, a modification of its chemical structure is required to create multi-functional and material-processable CS alternatives (Fang et al., 2022). To achieve this, catechol chemistry, methacrylation, and oxidation techniques are commonly used. In this study, we propose an alternative in-house methodology consisting of the oxidation of a CS sodium with $NaIO_4$. This reaction converts the hydroxyl groups in the CS backbone into intermediate aldehydes. These react with the amines in collagenous proteins, forming imine bonds. As a result, the engraftment of the CS molecules in the polymeric network of the hydrogels is achieved.

To facilitate the comparison between functionalized and non-functionalized platforms, the G* values obtained from the amplitude strain sweeps were analyzed. Standard Matrigel® substrates were used as a control. When compared to their counterparts, particularly Matrigel®, non-functionalized hydrogels showed greater viscoelastic characteristics. Matrigel® is mainly composed of laminins (60%), type IV collagens (30%), entactin (8%), and HSPGs (~2–3%) (Aisenbrey & Murphy, 2020). Owing to the absence of fibrous proteins (e.g., type I/III collagens), this material possesses a lower G*. Consequently, it exhibits more elastic behavior. The functionalized dECM-based hydrogels were also softer when compared to non-functionalized scaffolds. This is probably a result of the water-binding capacity of the CS-bound matrix, which leads to decreased

values of the tensile strength (Aravamudhan et al., 2014) Despite this, these substrates remained relatively stable over a broad range of complex shear strains. Altogether, these findings emphasize the idea that hydrogel polymerization is dependent on the properties of the source tissue, in addition to the ECM components that are preserved after decellularization (e.g. collagen, sGAGs, proteoglycans, growth factors, cytokines, and chemokines) (Brightman et al., 2000).

Lastly, as a proof-of-concept, the safety and biocompatibility of the non-functionalized dECM-based hydrogels were assessed by establishing cell cultures with the SW480 CRC cell line. The measurement of the metabolic activity of these cells and the evaluation of the cytotoxicity of the tested biomaterials were accomplished by the resazurin and LDH assays, respectively. The morphology of the cultures was also evaluated after 24 and 72 hours. SW480 cells, which are derived from a grade III colon adenocarcinoma, can spread over time (L. Genovese et al., 2014). In the presence of a culture medium, a heterogeneous population of undifferentiated cells was achieved. These results were similar to those stated by previous studies (Duranton et al., 2003). Initially, SW480 cells were confluent, possessing a flat polygonal form. However, after 72 hours, round and refractile cells were more predominant (Biazik et al., 2010). After being seeded on Matrigel®, these structures developed colony-forming/invasive features, which arose from the low expression of E-cadherin, allied to the high expression of N-cadherin, vimentin, and ZEB-1 (Feng et al., 2012). Nonetheless, the size of these spherical aggregates of multinucleated cells decreased with time. This was probably due to cell detachment and, consequently, induction of anoikis (Liu et al., 2017). The emergence of SW480 aggregates was not observed in the dECM-based hydrogels. In this case, the morphology was similar to the early stages of standard cultures with medium. Once again, a mixture of round and elongated cells was seen in these conditions. The number of refractile structures was higher in 20 mg/mL dECM-based hydrogels at 24 hours, yet it was surpassed by 25 mg/mL dECM-based hydrogels at 72 hours. These effects have been correlated with integrin activation, which is triggered by the collagen molecules in the dECM-based substrates (Ciasca et al., 2016).

These findings were supported by the resazurin assay, which revealed an increase in cell activity after culture in the dECM-based scaffolds. Indeed, apart from possessing high levels of metabolic activity, the 25 mg/mL dECM-based hydrogels showed equally high percentages of cytotoxicity, as reported by the LDH assay. A similar outcome was obtained for the 20 mg/mL dECM-based hydrogels This is most likely due to the pH of

the scaffolds, whose acidic nature (pH ~6) might have inhibited cell growth and proliferation. However, because acidosis constitutes a hallmark of cancer, the viability of these cells was not fully compromised. Compared to the remaining materials, the d fluorescence intensity in Matrigel® was surprisingly reduced. In this substrate, SW480 cells were organized into multicellular aggregates. As a result of the increased number and size of these colonies, we suspect that oxygen, nutrients, and metabolite gradients were altered, impairing the cancer cell growth and proliferation (Anzai et al., 2021). The cytotoxicity of these materials was assessed by the LDH assay, which confirmed the release of the LDH enzyme into the culture medium. Although noticed in all the conditions, these effects were higher in Matrigel® substrates. Regarding the dECM-based hydrogels, the previous outcomes were shown to vary proportionally with the concentration of the material. Overall, the high percentages of cytotoxicity in the tested scaffolds might be a result of the presence of FBS in the supplemented medium, which is an exogenous source of LDH (Kaja et al., 2017). For this reason, an FBS-reduced medium is commonly employed when conducting this analysis. Nonetheless, the viability of SW480 cells can still be diminished under these circumstances, due to the introduction of false positives (Hartmann et al., 2008). As dECM-based hydrogels did not induce dramatic changes in the viability, metabolic activity, and morphological appearance of SW480 cells, it can be concluded that they could represent an appropriate replacement for standard cell culture substrates, particularly Matrigel®. It is important to note that these results are preliminary, as new studies with CRC cells must be carried out in order to validate the potential of the proposed materials.

Chapter 6

Conclusion

In comparison with the currently available natural and synthetic *in vitro* platforms, hydrogels derived from dECMs have been gathering increasing interest in the last years, due to their biomimicry of the native tissues. Nonetheless, despite being obtained from multiple biological sources, no methods have been proposed to manufacture a hydrogel from decellularized rat intestines. Aiming at surpassing this shortcoming, an innovative protocol was designed to allow for the decellularization, solubilization, and neutralization of intestinal dECMs into self-gelling hydrogels.

The presented findings revealed the main architectural and compositional features of the intestine were preserved after decellularization. Importantly, the maintenance of the tissue-specific structure is not mandatory, as the ultimate purpose of this process is the fabrication of a hydrogel out of a decellularized powder. For this reason, the intestines were milled into smaller particles before being exposed to the 0.1% SDS-based protocol. Because this leads to an increase in the contact surface area, cells and nuclei were more efficiently removed. Following solubilization and neutralization, the powdered intestines gave rise to homogeneous hydrogels, whose mechanical properties varied according to the concentration of material that was initially used. Compared to Matrigel®, these scaffolds possessed higher tensile strengths at standard values of complex shear strains. Furthermore, they could sustain the activity and viability of cultured SW480 CRC cells After functionalization with an aldehyde-modified CS, this parameter evidenced a reduction, due to the swelling of the CS-bound matrix. Nevertheless, their stability, particularly under stress, was increased, compared to non-functionalized hydrogels. Despite the success of the presented approach, it is expected to see this study extended, so that the role of CS in the tumor microenvironment and the modulation of the behavior of CRC cells can be evaluated.

Chapter 7

Future Perspectives

Despite being successful at removing cells and DNA from the intestines, the 0.1% SDS-based decellularization protocol still requires some optimization in order to guarantee better preservation of ECM macromolecules, particularly sGAGs and collagens. Furthermore, to make sure that the differences observed between decellularized and non-decellularized tissues are minimal, SDS-PAGE, Western Blotting, and immunohistochemistry techniques must be performed. Alternative methodologies, including capillary electrophoresis, proteomic analysis, and HPLC have also been recently considered to allow for the identification of tissue-specific elements.

Another issue related to decellularized-based biomaterials is their batch-to-batch variability, which is a result of the differences observed between human and/or animal donors, anatomical regions from which the tissues are extracted, and decellularization protocols. In the future, the use of rats with the same gender, age, and genetic background is advised to maintain the consistency, as well as the significance of the experimental procedures.

When the main goal is to produce an off-the-shelf product to be used on an industrial scale, several guidelines must be accomplished. First, the manufacturing process of the materials should be controllable and reproducible. After that, biochemical and biophysical characterization must be well-defined. Finally, regulatory issues should be established (Alonso et al., 2021). Currently, the preparation of the dECM-based hydrogels is done by adjusting the temperature, pH, and salt concentration to physiological values. However, this method only promotes gelation to a certain extent. Additionally, because this constitutes a reversible process, it can give rise to materials with variable mechanical properties (Zhang et al., 2021). In this context, the introduction of a chemical crosslinking (e.g., genipin) or the combination with a collagen-concentrated solution would be beneficial to increase their stability under experimental conditions. The functionalization of the dECM-based hydrogels could also contribute to the translation of these platforms to load-bearing applications. This can be achieved by improving the strength, elasticity, and/or compliance of the 3D polymeric network. In this report, a

modified CS was engrafted onto the surface of the hydrogels obtained from decellularized rat intestines. As mentioned before, CS participates in the regulation of many cellular functions. Additionally, the expression of this molecule in CRC is higher, especially when compared to healthy tissues. The chain length, metabolism, and sulfation pattern of these macromolecules are also modified in malignant structures (Hoshiba, 2018). The determination of the adequate concentration of CS, which will be used in the functionalization of the scaffolds, represents a key step in protocol optimization. According to it, distinct materials, with various mechanical properties can be generated. This is particularly important, considering that they will ultimately modulate the viability of CRC cells in a different way (Keane et al., 2015).

Concerning the theoretical and practical knowledge within the scientific community, it may prove of great benefit to undertake more cellular studies within these hydrogels. Such studies may require the use of more invasive cell types to assess the relation of various forms of CRC within its microenvironment (Hoshiba & Tanaka, 2016). This will prove fundamental, especially in the identification of treatments (Marques-Magalhães et al., 2022). Moreover, due to the wide use of Matrigel® in organoid cancer models, which are widely sourced from the intestine, the application of this scaffold may provide more relevant findings (Giobbe et al., 2019). Such an assumption may be due to the advantageous features these models have over the use of other cell-based platforms.

As a whole, the presented study stresses the importance of addressing each of the suggestions present in this section to support the establishment of a controllable and well-defined off-the-shelf material that can be applied in multiple pre-clinical applications and point-of-care screenings. In this sense, a successful model can be achieved and widely used by the scientific community.

References

Abancens, M., Bustos, V., Harvey, H., McBryan, J., & Harvey, B. J. (2020). Sexual Dimorphism in Colon Cancer [Review]. *Frontiers in Oncology*, *10*. https://doi.org/10.3389/fonc.2020.607909

Afratis, N., Gialeli, C., Nikitovic, D., Tsegenidis, T., Karousou, E., Theocharis, A. D., Pavão, M. S., Tzanakakis, G. N., & Karamanos, N. K. (2012). Glycosaminoglycans: key players in cancer cell biology and treatment. *The FEBS journal*, *279*(7), 1177-1197. https://doi.org/10.1111/j.1742-4658.2012.08529.x

Afratis, N., Gialeli, C., Nikitovic, D., Tsegenidis, T., Karousou, E., Theocharis, A. D., Pavão, M. S., Tzanakakis, G. N., & Karamanos, N. K. (2012). Glycosaminoglycans: key players in cancer cell biology and treatment. *The FEBS journal*, *279*(7), 1177-1197. https://doi.org/10.1111/j.1742-4658.2012.08529.x

Ahmad, R., Singh, J. K., Wunnava, A., Al-Obeed, O., Abdulla, M., & Srivastava, S. K. (2021). Emerging trends in colorectal cancer: Dysregulated signaling pathways (Review). *International journal of molecular medicine*, *47*(3), 14. https://doi.org/10.3892/ijmm.2021.4847

Aisenbrey, E. A., & Murphy, W. L. (2020). Synthetic alternatives to Matrigel. *Nat Rev Mater*, *5*(7), 539-551. https://doi.org/10.1038/s41578-020-0199-8

Albritton, J. L., & Miller, J. S. (2017). 3D bioprinting: improving *in vitro* models of metastasis with heterogeneous tumor microenvironments. *Disease Models & Mechanisms*, *10*(1), 3. https://doi.org/10.1242/dmm.025049

Alcaraz, J., Otero, J., Jorba, I., & Navajas, D. (2018). Bidirectional mechanobiology between cells and their local extracellular matrix probed by atomic force microscopy. *Seminars in cell & developmental biology*, *73*, 71-81. https://doi.org/https://doi.org/10.1016/j.semcdb.2017.07.020

Alonso, J. M., Andrade del Olmo, J., Perez Gonzalez, R., & Saez-Martinez, V. (2021). Injectable Hydrogels: From Laboratory to Industrialization. *Polymers*, *13*(4), 650. https://www.mdpi.com/2073-4360/13/4/650

Amitay, E. L., Carr, P. R., Jansen, L., Roth, W., Alwers, E., Herpel, E., Kloor, M., Bläker, H., Chang-Claude, J., Brenner, H., & Hoffmeister, M. (2020). Smoking, alcohol consumption and colorectal cancer risk by molecular pathological subtypes and pathways. *British Journal of Cancer*, *122*(11), 1604-1610. https://doi.org/10.1038/s41416-020-0803-0

Antoine, E. E., Vlachos, P. P., & Rylander, M. N. (2014). Review of collagen I hydrogels for bioengineered tissue microenvironments: characterization of mechanics, structure, and transport. *Tissue engineering. Part B, Reviews*, *20*(6), 683-696. https://doi.org/10.1089/ten.TEB.2014.0086

Aragona, M., Panciera, T., Manfrin, A., Giulitti, S., Michielin, F., Elvassore, N., Dupont, S., & Piccolo, S. (2013). A mechanical checkpoint controls multicellular growth through YAP/TAZ regulation by actin-processing factors. *Cell*, *154*(5), 1047-1059. https://doi.org/10.1016/j.cell.2013.07.042

Aravamudhan, A., Ramos, D. M., Nada, A. A., & Kumbar, S. G. (2014). Chapter 4 - Natural Polymers: Polysaccharides and Their Derivatives for Biomedical Applications. In S. G. Kumbar, C. T. Laurencin, & M. Deng (Eds.), *Natural and Synthetic Biomedical Polymers* (pp. 67-89). Elsevier. https://doi.org/https://doi.org/10.1016/B978-0-12-396983-5.00004-1

Armaghany, T., Wilson, J. D., Chu, Q., & Mills, G. (2012). Genetic alterations in colorectal cancer. *Gastrointestinal cancer research : GCR*, *5*(1), 19-27. https://pubmed.ncbi.nlm.nih.gov/22574233

Arnold, M., Park, J. Y., Camargo, M. C., Lunet, N., Forman, D., & Soerjomataram, I. (2020). Is gastric cancer becoming a rare disease? A global assessment of predicted incidence trends to 2035. *Gut*, *69*(5), 823-829. https://doi.org/10.1136/gutjnl-2019-320234

Azzouz, L. L., & Sharma, S. (2022). Physiology, Large Intestine. In *StatPearls*. StatPearls Publishing

Badylak, S. F., Taylor, D., & Uygun, K. (2011). Whole-Organ Tissue Engineering: Decellularization and Recellularization of Three-Dimensional Matrix Scaffolds. *Annual Review of Biomedical Engineering*, *13*(1), 27-53. https://doi.org/10.1146/annurev-bioeng-071910-124743

Baran, B., Mert Ozupek, N., Yerli Tetik, N., Acar, E., Bekcioglu, O., & Baskin, Y. (2018). Difference Between Left-Sided and Right-Sided Colorectal Cancer: A Focused Review of Literature. *Gastroenterology research*, *11*(4), 264-273. https://doi.org/10.14740/gr1062w

Bashir, S., Hina, M., Iqbal, J., Rajpar, A. H., Mujtaba, M. A., Alghamdi, N. A., Wageh, S., Ramesh, K., & Ramesh, S. (2020). Fundamental Concepts of Hydrogels: Synthesis, Properties, and Their Applications. *Polymers*, *12*(11), 2702. https://www.mdpi.com/2073-4360/12/11/2702

Bhatia, S. N., & Ingber, D. E. (2014). Microfluidic organs-on-chips. *Nature biotechnology*, *32*(8), 760-772. https://doi.org/10.1038/nbt.2989

Biazik, J. M., Jahn, K. A., Su, Y., Wu, Y. N., & Braet, F. (2010). Unlocking the ultrastructure of colorectal cancer cells in vitro using selective staining. *World journal of gastroenterology*, *16*(22), 2743-2753. https://doi.org/10.3748/wjg.v16.i22.2743

Brightman, A. O., Rajwa, B. P., Sturgis, J. E., McCallister, M. E., Robinson, J. P., & Voytik-Harbin, S. L. (2000). Time-lapse confocal reflection microscopy of collagen fibrillogenesis and extracellular matrix assembly in vitro. *Biopolymers*, *54*(3), 222-234. https://doi.org/10.1002/1097-0282(200009)54:3<222::Aid-bip80>3.0.Co;2-k

Brockway-Lunardi, L., Nelson, S., Pandiri, A. R., Tricoli, J. V., Umar, A., Wali, A., & Daschner, P. J. (2020). Early-onset colorectal cancer research: gaps and opportunities. *Colorectal Cancer*, *9*(3), CRC34. https://doi.org/10.2217/crc-2020-0028

Bürtin, F., Mullins, C. S., & Linnebacher, M. (2020). Mouse models of colorectal cancer: Past, present and future perspectives. *World journal of gastroenterology*, *26*(13), 1394-1426. https://doi.org/10.3748/wjg.v26.i13.1394

Cardoso, R., Guo, F., Heisser, T., Hackl, M., Ihle, P., De Schutter, H., Van Damme, N., Valerianova, Z., Atanasov, T., Májek, O., Mužík, J., Nilbert, M. C., Tybjerg, A. J., Innos, K., Mägi, M., Malila, N., Bouvier, A.-M., Bouvier, V., Launoy, G., . . . Brenner, H. (2021). Colorectal cancer incidence, mortality, and stage distribution in European countries in the colorectal cancer screening era: an international population-based study. *The Lancet Oncology*, *22*(7), 1002-1013. https://doi.org/10.1016/S1470-2045(21)00199-6

Carvalho, M. R., Barata, D., Teixeira, L. M., Giselbrecht, S., Reis, R. L., Oliveira, J. M., Truckenmüller, R., & Habibovic, P. (2019). Colorectal tumor-on-a-chip system: A 3D tool for precision onco-nanomedicine. *Science Advances*, *5*(5), eaaw1317. https://doi.org/doi:10.1126/sciadv.aaw1317

Catoira, M. C., Fusaro, L., Di Francesco, D., Ramella, M., & Boccafoschi, F. (2019). Overview of natural hydrogels for regenerative medicine applications. *Journal of Materials Science: Materials in Medicine*, *30*(10), 115. https://doi.org/10.1007/s10856-019-6318-7

Chapelle, N., Martel, M., Toes-Zoutendijk, E., Barkun, A. N., & Bardou, M. (2020). Recent advances in clinical practice: colorectal cancer chemoprevention in the average-risk population. *Gut*, *69*(12), 2244-2255. https://doi.org/10.1136/gutjnl-2020-320990

Chen, H. J., Wei, Z., Sun, J., Bhattacharya, A., Savage, D. J., Serda, R., Mackeyev, Y., Curley, S. A., Bu, P., Wang, L., Chen, S., Cohen-Gould, L., Huang, E., Shen, X., Lipkin, S. M., Copeland, N. G., Jenkins, N. A., & Shuler, M. L. (2016). A recellularized human colon model identifies cancer driver genes. *Nature biotechnology*, *34*(8), 845-851. https://doi.org/10.1038/nbt.3586

Cheon, D. J., & Orsulic, S. (2011). Mouse models of cancer. *Annu Rev Pathol*, *6*, 95-119. https://doi.org/10.1146/annurev.pathol.3.121806.154244

Choe, E. K., Kim, D., Kim, H. J., & Park, K. J. (2013). Association of visceral obesity and early colorectal neoplasia. *World journal of gastroenterology*, *19*(45), 8349-8356. https://doi.org/10.3748/wjg.v19.i45.8349

Ciasca, G., Papi, M., Minelli, E., Palmieri, V., & De Spirito, M. (2016). Changes in cellular mechanical properties during onset or progression of colorectal cancer. *World journal of gastroenterology*, *22*(32), 7203-7214. https://doi.org/10.3748/wjg.v22.i32.7203

Cohen, S. A., & Leininger, A. (2014). The genetic basis of Lynch syndrome and its implications for clinical practice and risk management. *The application of clinical genetics*, *7*, 147-158. https://doi.org/10.2147/TACG.S51483

Cooney, C. A., Jousheghany, F., Yao-Borengasser, A., Phanavanh, B., Gomes, T., Kieber-Emmons, A. M., Siegel, E. R., Suva, L. J., Ferrone, S., Kieber-Emmons, T., & Monzavi-Karbassi, B. (2011). Chondroitin sulfates play a major role in breast cancer metastasis: a role for CSPG4 and CHST11gene expression in forming surface P-selectin ligands in aggressive breast cancer cells. *Breast Cancer Research*, *13*(3), R58. https://doi.org/10.1186/bcr2895

Crapo, P. M., Gilbert, T. W., & Badylak, S. F. (2011). An overview of tissue and whole organ decellularization processes. *Biomaterials*, *32*(12), 3233-3243. https://doi.org/10.1016/j.biomaterials.2011.01.057

Crotti, S., Piccoli, M., Rizzolio, F., Giordano, A., Nitti, D., & Agostini, M. (2017). Extracellular Matrix and Colorectal Cancer: How Surrounding Microenvironment Affects Cancer Cell Behavior? *J Cell Physiol*, *232*(5), 967-975. https://doi.org/10.1002/jcp.25658

Daidouji, K., Takagaki, K., Yoshihara, S., Matsuya, H., Sasaki, M., & Endo, M. (2002). Neoplastic changes in saccharide sequence of dermatan sulfate chains derived from human colon cancer. *Dig Dis Sci*, *47*(2), 331-337. https://doi.org/10.1023/a:1013718021713

Däster, S., Amatruda, N., Calabrese, D., Ivanek, R., Turrini, E., Droeser, R. A., Zajac, P., Fimognari, C., Spagnoli, G. C., Iezzi, G., Mele, V., & Muraro, M. G. (2017). Induction of hypoxia and necrosis in multicellular tumor spheroids is associated with resistance to chemotherapy treatment. *Oncotarget*, *8*(1), 1725-1736. https://doi.org/10.18632/oncotarget.13857

Datta, P., Dey, M., Ataie, Z., Unutmaz, D., & Ozbolat, I. T. (2020). 3D bioprinting for reconstituting the cancer microenvironment. *npj Precision Oncology*, *4*(1), 18. https://doi.org/10.1038/s41698-020-0121-2

Davies, R. J., Miller, R., & Coleman, N. (2005). Colorectal cancer screening: prospects for molecular stool analysis. *Nat Rev Cancer*, *5*(3), 199-209. https://doi.org/10.1038/nrc1569

Dekker, E., Tanis, P. J., Vleugels, J. L. A., Kasi, P. M., & Wallace, M. B. (2019). Colorectal cancer. *Lancet*, *394*(10207), 1467-1480. https://doi.org/10.1016/s0140-6736(19)32319-0

Delgado, L. M., Shologu, N., Fuller, K., & Zeugolis, D. I. (2017). Acetic acid and pepsin result in high yield, high purity and low macrophage response collagen for biomedical applications. *Biomed Mater*, *12*(6), 065009. https://doi.org/10.1088/1748-605X/aa838d

Duranton, B., Holl, V., Schneider, Y., Carnesecchi, S., Gossé, F., Raul, F., & Seiler, N. (2003). Polyamine metabolism in primary human colon adenocarcinoma cells (SW480) and their lymph node metastatic derivatives (SW620). *Amino Acids*, *24*(1-2), 63-72. https://doi.org/10.1007/s00726-002-0333-5

Ewald, C. Y. (2021). Drug Screening Implicates Chondroitin Sulfate as a Potential Longevity Pill. *Front Aging*, *2*, 741843. https://doi.org/10.3389/fragi.2021.741843

Fang, Y., Zhou, W., He, J., Zhai, X., He, F., & Wei, W. (2022). Effect of chemical modification on physicochemical and biological properties of chondroitin sulfate. *Polymer Testing*, *115*, 107747. https://doi.org/https://doi.org/10.1016/j.polymertesting.2022.107747

Fernández-Pérez, J., & Ahearne, M. (2019). The impact of decellularization methods on extracellular matrix derived hydrogels. *Sci Rep*, *9*(1), 14933. https://doi.org/10.1038/s41598-019-49575-2

Ferreira, L. P., Gaspar, V. M., & Mano, J. F. (2020). Decellularized Extracellular Matrix for Bioengineering Physiomimetic 3D in Vitro Tumor Models. *Trends Biotechnol*, *38*(12), 1397-1414. https://doi.org/10.1016/j.tibtech.2020.04.006

Freytes, D. O., Martin, J., Velankar, S. S., Lee, A. S., & Badylak, S. F. (2008). Preparation and rheological characterization of a gel form of the porcine urinary bladder matrix. *Biomaterials*, *29*(11), 1630-1637. https://doi.org/https://doi.org/10.1016/j.biomaterials.2007.12.014

Gabriel, E., Attwood, K., Al-Sukhni, E., Erwin, D., Boland, P., & Nurkin, S. (2018). Age-related rates of colorectal cancer and the factors associated with overall survival. *Journal of gastrointestinal oncology*, *9*(1), 96-110. https://doi.org/10.21037/jgo.2017.11.13

Garreta, E., Oria, R., Tarantino, C., Pla-Roca, M., Prado, P., Fernández-Avilés, F., Campistol, J. M., Samitier, J., & Montserrat, N. (2017). Tissue engineering by decellularization and 3D bioprinting. *Materials Today*, *20*(4), 166-178. https://doi.org/https://doi.org/10.1016/j.mattod.2016.12.005

Gengenbacher, N., Singhal, M., & Augustin, H. G. (2017). Preclinical mouse solid tumour models: status quo, challenges and perspectives. *Nature Reviews Cancer*, *17*(12), 751-765. https://doi.org/10.1038/nrc.2017.92

Genovese, L., Zawada, L., Tosoni, A., Ferri, A., Zerbi, P., Allevi, R., Nebuloni, M., & Alfano, M. (2014). Cellular localization, invasion, and turnover are differently influenced by healthy and tumor-derived extracellular matrix. *Tissue engineering. Part A*, *20*(13-14), 2005-2018. https://doi.org/10.1089/ten.TEA.2013.0588

Gilbert, T. W., Freund, J. M., & Badylak, S. F. (2009). Quantification of DNA in biologic scaffold materials. *The Journal of surgical research*, *152*(1), 135-139. https://doi.org/10.1016/j.jss.2008.02.013

Gilbert, T. W., Sellaro, T. L., & Badylak, S. F. (2006). Decellularization of tissues and organs. *Biomaterials*, *27*(19), 3675-3683. https://doi.org/https://doi.org/10.1016/j.biomaterials.2006.02.014

Gilpin, A., & Yang, Y. (2017). Decellularization Strategies for Regenerative Medicine: From Processing Techniques to Applications. *BioMed Research International*, *2017*, 9831534. https://doi.org/10.1155/2017/9831534

Giobbe, G. G., Crowley, C., Luni, C., Campinoti, S., Khedr, M., Kretzschmar, K., De Santis, M. M., Zambaiti, E., Michielin, F., Meran, L., Hu, Q., van Son, G., Urbani, L., Manfredi, A., Giomo, M., Eaton, S., Cacchiarelli, D., Li, V. S. W., Clevers, H., . . . De Coppi, P. (2019). Extracellular matrix hydrogel derived from decellularized tissues enables endodermal organoid culture. *Nature Communications*, *10*(1), 5658. https://doi.org/10.1038/s41467-019-13605-4

Gonzalez, L. G., Hiller, J., Terrill, N. J., Parkinson, J., Thomas, K., & Wess, T. J. (2012). Effects of isopropanol on collagen fibrils in new parchment. *Chem Cent J*, *6*, 24. https://doi.org/10.1186/1752-153x-6-24

Guerin, M. V., Finisguerra, V., Van den Eynde, B. J., Bercovici, N., & Trautmann, A. (2020). Preclinical murine tumor models: a structural and functional perspective. *Elife*, *9*. https://doi.org/10.7554/eLife.50740

Gupta, S. K., Mishra, N. C., & Dhasmana, A. (2018). Decellularization Methods for Scaffold Fabrication. In K. Turksen (Ed.), *Decellularized Scaffolds and Organogenesis: Methods and Protocols* (pp. 1-10). Springer New York. https://doi.org/10.1007/7651_2017_34

Hartmann, M., Zimmermann, D., & Nolte, J. (2008). Changes of the metabolism of the colon cancer cell line SW-480 under serum-free and serum-reduced growth conditions. *In Vitro Cell Dev Biol Anim*, *44*(10), 458-463. https://doi.org/10.1007/s11626-008-9133-x

Hayes, A., Sugahara, K., Farrugia, B., Whitelock, J. M., Caterson, B., & Melrose, J. (2018). Biodiversity of CS-proteoglycan sulphation motifs: chemical messenger recognition modules with roles in information transfer, control of cellular behaviour and tissue morphogenesis. *Biochem J*, *475*(3), 587-620. https://doi.org/10.1042/bcj20170820

Heath, D. E. (2019). A Review of Decellularized Extracellular Matrix Biomaterials for Regenerative Engineering Applications. *Regenerative Engineering and Translational Medicine*, *5*(2), 155-166. https://doi.org/10.1007/s40883-018-0080-0

Heinrich, M. A., Liu, W., Jimenez, A., Yang, J., Akpek, A., Liu, X., Pi, Q., Mu, X., Hu, N., Schiffelers, R. M., Prakash, J., Xie, J., & Zhang, Y. S. (2019). 3D Bioprinting: from Benches to Translational Applications. *Small (Weinheim an der Bergstrasse, Germany)*, *15*(23), e1805510-e1805510. https://doi.org/10.1002/smll.201805510

Henderson, R. H., French, D., Maughan, T., Adams, R., Allemani, C., Minicozzi, P., Coleman, M. P., McFerran, E., Sullivan, R., & Lawler, M. (2021). The economic burden of colorectal cancer across Europe: a population-based cost-of-illness study. *The Lancet Gastroenterology & Hepatology*, *6*(9), 709-722. https://doi.org/10.1016/S2468-1253(21)00147-3

Hoarau-Véchot, J., Rafii, A., Touboul, C., & Pasquier, J. (2018). Halfway between 2D and Animal Models: Are 3D Cultures the Ideal Tool to Study Cancer-Microenvironment Interactions? *International journal of molecular sciences*, *19*(1). https://doi.org/10.3390/ijms19010181

Hong, Q., Li, B., Cai, X., Lv, Z., Cai, S., Zhong, Y., & Wen, B. (2021). Transcriptomic Analyses of the Adenoma-Carcinoma Sequence Identify Hallmarks Associated With the Onset of Colorectal Cancer. *Frontiers in Oncology*, *11*. https://doi.org/10.3389/fonc.2021.704531

Hoshiba, T. (2018). An extracellular matrix (ECM) model at high malignant colorectal tumor increases chondroitin sulfate chains to promote epithelial-mesenchymal transition and

chemoresistance acquisition. *Exp Cell Res*, *370*(2), 571-578. https://doi.org/10.1016/j.yexcr.2018.07.022

Hoshiba, T. (2019). Decellularized Extracellular Matrix for Cancer Research. *Materials (Basel)*, *12*(8). https://doi.org/10.3390/ma12081311

Hoshiba, T. (2021). Cultured cell-derived decellularized extracellular matrix (cultured cell-derived dECM): Future applications and problems — a mini review. *Current Opinion in Biomedical Engineering*, *17*, 100256. https://doi.org/https://doi.org/10.1016/j.cobme.2020.100256

Hoshiba, T., Chen, G., Endo, C., Maruyama, H., Wakui, M., Nemoto, E., Kawazoe, N., & Tanaka, M. (2016). Decellularized Extracellular Matrix as an In Vitro Model to Study the Comprehensive Roles of the ECM in Stem Cell Differentiation. *Stem cells international*, *2016*, 6397820-6397820. https://doi.org/10.1155/2016/6397820

Hoshiba, T., Lu, H., Kawazoe, N., & Chen, G. (2010). Decellularized matrices for tissue engineering. *Expert Opin Biol Ther*, *10*(12), 1717-1728. https://doi.org/10.1517/14712598.2010.534079

Hoshiba, T., & Tanaka, M. (2016). Decellularized matrices as in vitro models of extracellular matrix in tumor tissues at different malignant levels: Mechanism of 5-fluorouracil resistance in colorectal tumor cells. *Biochimica et Biophysica Acta (BBA) - Molecular Cell Research*, *1863*(11), 2749-2757. https://doi.org/https://doi.org/10.1016/j.bbamcr.2016.08.009

Huang, J., Zhang, L., Wan, D., Zhou, L., Zheng, S., Lin, S., & Qiao, Y. (2021). Extracellular matrix and its therapeutic potential for cancer treatment. *Signal Transduct Target Ther*, *6*(1), 153. https://doi.org/10.1038/s41392-021-00544-0

Huang, J., Zhang, L., Wan, D., Zhou, L., Zheng, S., Lin, S., & Qiao, Y. (2021). Extracellular matrix and its therapeutic potential for cancer treatment. *Signal Transduction and Targeted Therapy*, *6*(1), 153. https://doi.org/10.1038/s41392-021-00544-0

Hussey, G. S., Cramer, M. C., & Badylak, S. F. (2018). Extracellular Matrix Bioscaffolds for Building Gastrointestinal Tissue. *Cellular and Molecular Gastroenterology and Hepatology*, *5*(1), 1-13. https://doi.org/https://doi.org/10.1016/j.jcmgh.2017.09.004

Hussey, G. S., Dziki, J. L., & Badylak, S. F. (2018). Extracellular matrix-based materials for regenerative medicine. *Nature Reviews Materials*, *3*(7), 159-173. https://doi.org/10.1038/s41578-018-0023-x

Jafari, H., Lista, A., Siekapen, M. M., Ghaffari-Bohlouli, P., Nie, L., Alimoradi, H., & Shavandi, A. (2020). Fish Collagen: Extraction, Characterization, and Applications for Biomaterials Engineering. *Polymers (Basel)*, *12*(10). https://doi.org/10.3390/polym12102230

Jeppesen, M., Hagel, G., Glenthoj, A., Vainer, B., Ibsen, P., Harling, H., Thastrup, O., Jørgensen, L. N., & Thastrup, J. (2017). Short-term spheroid culture of primary colorectal cancer cells as an in vitro model for personalizing cancer medicine. *PLoS One*, *12*(9), e0183074. https://doi.org/10.1371/journal.pone.0183074

Johnson, R. L., & Fleet, J. C. (2013). Animal models of colorectal cancer. *Cancer metastasis reviews*, *32*(1-2), 39-61. https://doi.org/10.1007/s10555-012-9404-6

Jung, J. (2014). Human tumor xenograft models for preclinical assessment of anticancer drug development. *Toxicol Res*, *30*(1), 1-5. https://doi.org/10.5487/tr.2014.30.1.001

Kaja, S., Payne, A. J., Naumchuk, Y., & Koulen, P. (2017). Quantification of Lactate Dehydrogenase for Cell Viability Testing Using Cell Lines and Primary Cultured Astrocytes. *Curr Protoc Toxicol*, *72*, 2.26.21-22.26.10. https://doi.org/10.1002/cptx.21

Katt, M. E., Placone, A. L., Wong, A. D., Xu, Z. S., & Searson, P. C. (2016). In Vitro Tumor Models: Advantages, Disadvantages, Variables, and Selecting the Right Platform. *Frontiers in Bioengineering and Biotechnology*, *4*, 12-12. https://doi.org/10.3389/fbioe.2016.00012

Kawecki, M., Łabuś, W., Klama-Baryla, A., Kitala, D., Kraut, M., Glik, J., Misiuga, M., Nowak, M., Bielecki, T., & Kasperczyk, A. (2018). A review of decellurization methods caused by an urgent need for quality control of cell-free extracellular matrix' scaffolds and their role in regenerative medicine. *J Biomed Mater Res B Appl Biomater*, *106*(2), 909-923. https://doi.org/10.1002/jbm.b.33865

Keane, T. J., Swinehart, I. T., & Badylak, S. F. (2015). Methods of tissue decellularization used for preparation of biologic scaffolds and in vivo relevance. *Methods*, *84*, 25-34. https://doi.org/https://doi.org/10.1016/j.ymeth.2015.03.005

Keum, N., & Giovannucci, E. (2019). Global burden of colorectal cancer: emerging trends, risk factors and prevention strategies. *Nature Reviews Gastroenterology & Hepatology*, *16*(12), 713-732. https://doi.org/10.1038/s41575-019-0189-8

Kim, S.-E., Paik, H. Y., Yoon, H., Lee, J. E., Kim, N., & Sung, M.-K. (2015). Sex- and gender-specific disparities in colorectal cancer risk. *World journal of gastroenterology*, *21*(17), 5167-5175. https://doi.org/10.3748/wjg.v21.i17.5167

Kim, S., Min, S., Choi, Y. S., Jo, S.-H., Jung, J. H., Han, K., Kim, J., An, S., Ji, Y. W., Kim, Y.-G., & Cho, S.-W. (2022). Tissue extracellular matrix hydrogels as alternatives to Matrigel for culturing gastrointestinal organoids. *Nature Communications*, *13*(1), 1692. https://doi.org/10.1038/s41467-022-29279-4

Kucherlapati, M. H., Lee, K., Nguyen, A. A., Clark, A. B., Hou, H., Jr., Rosulek, A., Li, H., Yang, K., Fan, K., Lipkin, M., Bronson, R. T., Jelicks, L., Kunkel, T. A., Kucherlapati, R., & Edelmann, W. (2010). An Msh2 conditional knockout mouse for studying intestinal cancer and testing anticancer agents. *Gastroenterology*, *138*(3), 993-1002.e1001. https://doi.org/10.1053/j.gastro.2009.11.009

Kwong, L. N., & Dove, W. F. (2009). APC and its modifiers in colon cancer. *Adv Exp Med Biol*, *656*, 85-106. https://doi.org/10.1007/978-1-4419-1145-2_8

Langer, E. M., Allen-Petersen, B. L., King, S. M., Kendsersky, N. D., Turnidge, M. A., Kuziel, G. M., Riggers, R., Samatham, R., Amery, T. S., Jacques, S. L., Sheppard, B. C., Korkola, J. E., Muschler, J. L., Thibault, G., Chang, Y. H., Gray, J. W., Presnell, S. C., Nguyen, D. G., & Sears, R. C. (2019). Modeling Tumor Phenotypes In Vitro with Three-Dimensional Bioprinting. *Cell reports*, *26*(3), 608-623.e606. https://doi.org/10.1016/j.celrep.2018.12.090

Leenaars, C. H. C., Kouwenaar, C., Stafleu, F. R., Bleich, A., Ritskes-Hoitinga, M., De Vries, R. B. M., & Meijboom, F. L. B. (2019). Animal to human translation: a systematic scoping review of reported concordance rates. *Journal of Translational Medicine*, *17*(1), 223. https://doi.org/10.1186/s12967-019-1976-2

Lehman, H. L., & Stairs, D. B. (2015). Single and Multiple Gene Manipulations in Mouse Models of Human Cancer. *Cancer growth and metastasis*, *8*(Suppl 1), 1-15. https://doi.org/10.4137/CGM.S21217

Licup, A. J., Münster, S., Sharma, A., Sheinman, M., Jawerth, L. M., Fabry, B., Weitz, D. A., & MacKintosh, F. C. (2015). Stress controls the mechanics of collagen networks. *Proceedings of the National Academy of Sciences*, *112*(31), 9573-9578. https://doi.org/doi:10.1073/pnas.1504258112

Liu, Y., Yin, T., Feng, Y., Cona, M. M., Huang, G., Liu, J., Song, S., Jiang, Y., Xia, Q., Swinnen, J. V., Bormans, G., Himmelreich, U., Oyen, R., & Ni, Y. (2015). Mammalian models of chemically induced primary malignancies exploitable for imaging-based preclinical theragnostic research. *Quant Imaging Med Surg*, *5*(5), 708-729. https://doi.org/10.3978/j.issn.2223-4292.2015.06.01

Liu, Y., Zhang, Y., Wu, H., Li, Y., Zhang, Y., Liu, M., Li, X., & Tang, H. (2017). miR-10a suppresses colorectal cancer metastasis by modulating the epithelial-to-mesenchymal transition and anoikis. *Cell Death & Disease*, *8*(4), e2739-e2739. https://doi.org/10.1038/cddis.2017.61

Luo, L., Ma, Y., Zheng, Y., Su, J., & Huang, G. (2022). Application Progress of Organoids in Colorectal Cancer [Review]. *Frontiers in Cell and Developmental Biology*, *10*. https://doi.org/10.3389/fcell.2022.815067

Mármol, I., Sánchez-de-Diego, C., Pradilla Dieste, A., Cerrada, E., & Rodriguez Yoldi, M. J. (2017). Colorectal Carcinoma: A General Overview and Future Perspectives in Colorectal Cancer. *International journal of molecular sciences*, *18*(1), 197. https://doi.org/10.3390/ijms18010197

Marques-Magalhães, Â., Cruz, T., Costa, Â. M., Estêvão, D., Rios, E., Canão, P. A., Velho, S., Carneiro, F., Oliveira, M. J., & Cardoso, A. P. (2022). Decellularized Colorectal Cancer Matrices as Bioactive Scaffolds for Studying Tumor-Stroma Interactions. *Cancers*, *14*(2), 359. https://www.mdpi.com/2072-6694/14/2/359

Martin, B., Ji, S., Maudsley, S., & Mattson, M. P. (2010). "Control" laboratory rodents are metabolically morbid: why it matters. *Proc Natl Acad Sci U S A*, *107*(14), 6127-6133. https://doi.org/10.1073/pnas.0912955107

Martin, S. Z., Wagner, D. C., Hörner, N., Horst, D., Lang, H., Tagscherer, K. E., & Roth, W. (2019). Ex vivo tissue slice culture system to measure drug-response rates of hepatic

metastatic colorectal cancer. *BMC cancer*, *19*(1), 1030. https://doi.org/10.1186/s12885-019-6270-4

McCrary, M. W., Bousalis, D., Mobini, S., Song, Y. H., & Schmidt, C. E. (2020). Decellularized tissues as platforms for in vitro modeling of healthy and diseased tissues. *Acta Biomaterialia*, *111*, 1-19. https://doi.org/https://doi.org/10.1016/j.actbio.2020.05.031

Mendes, N., Dias Carvalho, P., Martins, F., Mendonça, S., Malheiro, A. R., Ribeiro, A., Carvalho, J., & Velho, S. (2020). Animal Models to Study Cancer and Its Microenvironment. *Adv Exp Med Biol*, *1219*, 389-401. https://doi.org/10.1007/978-3-030-34025-4_20

Mendibil, U., Ruiz-Hernandez, R., Retegi-Carrion, S., Garcia-Urquia, N., Olalde-Graells, B., & Abarrategi, A. (2020). Tissue-Specific Decellularization Methods: Rationale and Strategies to Achieve Regenerative Compounds. *International journal of molecular sciences*, *21*(15). https://doi.org/10.3390/ijms21155447

Mendoza-Novelo, B., Avila, E. E., Cauich-Rodríguez, J. V., Jorge-Herrero, E., Rojo, F. J., Guinea, G. V., & Mata-Mata, J. L. (2011). Decellularization of pericardial tissue and its impact on tensile viscoelasticity and glycosaminoglycan content. *Acta Biomater*, *7*(3), 1241-1248. https://doi.org/10.1016/j.actbio.2010.11.017

Meran, L., Baulies, A., & Li, V. S. W. (2017). Intestinal Stem Cell Niche: The Extracellular Matrix and Cellular Components. *Stem Cells Int*, *2017*, 7970385. https://doi.org/10.1155/2017/7970385

Meyer, M. (2019). Processing of collagen based biomaterials and the resulting materials properties. *Biomed Eng Online*, *18*(1), 24. https://doi.org/10.1186/s12938-019-0647-0

Mirabelli, P., Coppola, L., & Salvatore, M. (2019). Cancer Cell Lines Are Useful Model Systems for Medical Research. *Cancers*, *11*(8), 1098. https://doi.org/10.3390/cancers11081098

Misra, S., Moro, C. F., Del Chiaro, M., Pouso, S., Sebestyén, A., Löhr, M., Björnstedt, M., & Verbeke, C. S. (2019). Ex vivo organotypic culture system of precision-cut slices of human pancreatic ductal adenocarcinoma. *Scientific Reports*, *9*(1), 2133. https://doi.org/10.1038/s41598-019-38603-w

Morla, S. (2019). Glycosaminoglycans and Glycosaminoglycan Mimetics in Cancer and Inflammation. *International journal of molecular sciences*, *20*(8), 1963. https://doi.org/10.3390/ijms20081963

Oliveira, R. C., Abrantes, A. M., Tralhão, J. G., & Botelho, M. F. (2020). The role of mouse models in colorectal cancer research—The need and the importance of the orthotopic models. *Animal Models and Experimental Medicine*, *3*(1), 1-8. https://doi.org/https://doi.org/10.1002/ame2.12102

Pathak, C. P., Adams, A. K., Simpson, T., Phillips, R. E., Jr., & Moore, M. A. (2004). Treatment of bioprosthetic heart valve tissue with long chain alcohol solution to lower calcification potential. *J Biomed Mater Res A*, *69*(1), 140-144. https://doi.org/10.1002/jbm.a.20129

Piccoli, M., D'Angelo, E., Crotti, S., Sensi, F., Urbani, L., Maghin, E., Burns, A., De Coppi, P., Fassan, M., Rugge, M., Rizzolio, F., Giordano, A., Pilati, P., Mammano, E., Pucciarelli, S., & Agostini, M. (2018). Decellularized colorectal cancer matrix as bioactive microenvironment for in vitro 3D cancer research [https://doi.org/10.1002/jcp.26403]. *Journal of Cellular Physiology*, *233*(8), 5937-5948. https://doi.org/https://doi.org/10.1002/jcp.26403

Pinho, D., Santos, D., Vila, A., & Carvalho, S. (2021). Establishment of Colorectal Cancer Organoids in Microfluidic-Based System. *Micromachines (Basel)*, *12*(5). https://doi.org/10.3390/mi12050497

Pinto, M. L., Rios, E., Silva, A. C., Neves, S. C., Caires, H. R., Pinto, A. T., Durães, C., Carvalho, F. A., Cardoso, A. P., Santos, N. C., Barrias, C. C., Nascimento, D. S., Pinto-do-Ó, P., Barbosa, M. A., Carneiro, F., & Oliveira, M. J. (2017). Decellularized human colorectal cancer matrices polarize macrophages towards an anti-inflammatory phenotype promoting cancer cell invasion via CCL18. *Biomaterials*, *124*, 211-224. https://doi.org/10.1016/j.biomaterials.2017.02.004

Pompili, S., Latella, G., Gaudio, E., Sferra, R., & Vetuschi, A. (2021). The Charming World of the Extracellular Matrix: A Dynamic and Protective Network of the Intestinal Wall [Review]. *Frontiers in Medicine*, *8*. https://doi.org/10.3389/fmed.2021.610189

Pretzsch, E., Bösch, F., Neumann, J., Ganschow, P., Bazhin, A., Guba, M., Werner, J., & Angele, M. (2019). Mechanisms of Metastasis in Colorectal Cancer and Metastatic Organotropism: Hematogenous versus Peritoneal Spread. *J Oncol*, *2019*, 7407190. https://doi.org/10.1155/2019/7407190

Pudełko, A., Wisowski, G., Olczyk, K., & Koźma, E. M. (2019). The dual role of the glycosaminoglycan chondroitin-6-sulfate in the development, progression and metastasis of cancer. *The FEBS journal*, *286*(10), 1815-1837. https://doi.org/10.1111/febs.14748

Ramzy, G. M., Koessler, T., Ducrey, E., McKee, T., Ris, F., Buchs, N., Rubbia-Brandt, L., Dietrich, P.-Y., & Nowak-Sliwinska, P. (2020). Patient-Derived In Vitro Models for Drug Discovery in Colorectal Carcinoma. *Cancers*, *12*(6), 1423. https://doi.org/10.3390/cancers12061423

Rodenhizer, D., Dean, T., D'Arcangelo, E., & McGuigan, A. P. (2018). The Current Landscape of 3D In Vitro Tumor Models: What Cancer Hallmarks Are Accessible for Drug Discovery? *Adv Healthc Mater*, *7*(8), e1701174. https://doi.org/10.1002/adhm.201701174

Rodrigues, J., Heinrich, M. A., Teixeira, L. M., & Prakash, J. (2021). 3D In Vitro Model (R)evolution: Unveiling Tumor–Stroma Interactions. *Trends in Cancer*, *7*(3), 249-264. https://doi.org/10.1016/j.trecan.2020.10.009

Romero-López, M., Trinh, A. L., Sobrino, A., Hatch, M. M., Keating, M. T., Fimbres, C., Lewis, D. E., Gershon, P. D., Botvinick, E. L., Digman, M., Lowengrub, J. S., & Hughes, C. C. (2017). Recapitulating the human tumor microenvironment: Colon tumor-derived extracellular matrix promotes angiogenesis and tumor cell growth. *Biomaterials*, *116*, 118-129. https://doi.org/10.1016/j.biomaterials.2016.11.034

Rosenberg, D. W., Giardina, C., & Tanaka, T. (2009). Mouse models for the study of colon carcinogenesis. *Carcinogenesis*, *30*(2), 183-196. https://doi.org/10.1093/carcin/bgn267

Saldin, L. T., Cramer, M. C., Velankar, S. S., White, L. J., & Badylak, S. F. (2017). Extracellular matrix hydrogels from decellularized tissues: Structure and function. *Acta Biomaterialia*, *49*, 1-15. https://doi.org/https://doi.org/10.1016/j.actbio.2016.11.068

Sarrigiannidis, S. O., Rey, J. M., Dobre, O., González-García, C., Dalby, M. J., & Salmeron-Sanchez, M. (2021). A tough act to follow: collagen hydrogel modifications to improve mechanical and growth factor loading capabilities. *Mater Today Bio*, *10*, 100098. https://doi.org/10.1016/j.mtbio.2021.100098

Sartore-Bianchi, A., Loupakis, F., Argilés, G., & Prager, G. W. (2016). Challenging chemoresistant metastatic colorectal cancer: therapeutic strategies from the clinic and from the laboratory. *Annals of Oncology*, *27*(8), 1456-1466. https://doi.org/10.1093/annonc/mdw191

Seely, K. D., Morgan, A. D., Hagenstein, L. D., Florey, G. M., & Small, J. M. (2022). Bacterial Involvement in Progression and Metastasis of Colorectal Neoplasia. *Cancers*, *14*(4), 1019. https://www.mdpi.com/2072-6694/14/4/1019

Seidlitz, T., & Stange, D. E. (2021). Gastrointestinal cancer organoids—applications in basic and translational cancer research. *Experimental & Molecular Medicine*, *53*(10), 1459-1470. https://doi.org/10.1038/s12276-021-00654-3

Senbanjo, L. T., & Chellaiah, M. A. (2017). CD44: A Multifunctional Cell Surface Adhesion Receptor Is a Regulator of Progression and Metastasis of Cancer Cells. *Front Cell Dev Biol*, *5*, 18. https://doi.org/10.3389/fcell.2017.00018

Siegel, R. L., Miller, K. D., Fuchs, H. E., & Jemal, A. (2021). Cancer Statistics, 2021. *CA: a cancer journal for clinicians*, *71*(1), 7-33. https://doi.org/10.3322/caac.21654

Simon, K. (2016). Colorectal cancer development and advances in screening. *Clinical interventions in aging*, *11*, 967-976. https://doi.org/10.2147/CIA.S109285

Siri, S., Zhao, Y., Maier, F., Pierce, D. M., & Feng, B. (2020). The Macro- and Micro-Mechanics of the Colon and Rectum I: Experimental Evidence. *Bioengineering*, *7*(4), 130. https://www.mdpi.com/2306-5354/7/4/130

Sivakumar, R., Chan, M., Shin, J. S., Nishida-Aoki, N., Kenerson, H. L., Elemento, O., Beltran, H., Yeung, R., & Gujral, T. S. (2019). Organotypic tumor slice cultures provide a versatile platform for immuno-oncology and drug discovery. *Oncoimmunology*, *8*(12), e1670019-e1670019. https://doi.org/10.1080/2162402X.2019.1670019

Smit, W. L., Spaan, C. N., Boer, R. J. d., Ramesh, P., Garcia, T. M., Meijer, B. J., Vermeulen, J. L. M., Lezzerini, M., MacInnes, A. W., Koster, J., Medema, J. P., Brink, G. R. v. d., Muncan, V., & Heijmans, J. (2020). Driver mutations of the adenoma-carcinoma sequence govern the intestinal epithelial global translational capacity. *Proceedings of the National Academy of Sciences*, *117*(41), 25560-25570. https://doi.org/doi:10.1073/pnas.1912772117

Stojkov, G., Niyazov, Z., Picchioni, F., & Bose, R. K. (2021). Relationship between Structure and Rheology of Hydrogels for Various Applications. *Gels*, *7*(4). https://doi.org/10.3390/gels7040255

Storm, C., Pastore, J. J., MacKintosh, F. C., Lubensky, T. C., & Janmey, P. A. (2005). Nonlinear elasticity in biological gels. *Nature*, *435*(7039), 191-194. https://doi.org/10.1038/nature03521

Strelez, C., Chilakala, S., Ghaffarian, K., Lau, R., Spiller, E., Ung, N., Hixon, D., Yoon, A. Y., Sun, R. X., Lenz, H.-J., Katz, J. E., & Mumenthaler, S. M. (2021). Human colorectal cancer-on-chip model to study the microenvironmental influence on early metastatic spread. *iScience*, *24*(5), 102509. https://doi.org/https://doi.org/10.1016/j.isci.2021.102509

Stukalin, I., Ahmed, N. S., Fundytus, A. M., Singh, S., & Ma, C. (2021). Prevalence-adjusted trends in U.S. healthcare spending on colorectal cancer, 1996-2016. *Journal of Clinical Oncology*, *39*(15_suppl), e18819-e18819. https://doi.org/10.1200/JCO.2021.39.15_suppl.e18819

Sung, H., Ferlay, J., Siegel, R. L., Laversanne, M., Soerjomataram, I., Jemal, A., & Bray, F. (2021). Global Cancer Statistics 2020: GLOBOCAN Estimates of Incidence and Mortality Worldwide for 36 Cancers in 185 Countries. *CA: a cancer journal for clinicians*, *71*(3), 209-249. https://doi.org/https://doi.org/10.3322/caac.21660

Swiderska, M., Choromańska, B., Dąbrowska, E., Konarzewska-Duchnowska, E., Choromańska, K., Szczurko, G., Myśliwiec, P., Dadan, J., Ladny, J. R., & Zwierz, K. (2014). The diagnostics of colorectal cancer. *Contemporary oncology (Poznan, Poland)*, *18*(1), 1-6. https://doi.org/10.5114/wo.2013.39995

Tanaka, T. (2009). Colorectal carcinogenesis: Review of human and experimental animal studies. *Journal of carcinogenesis*, *8*, 5-5. https://doi.org/10.4103/1477-3163.49014

Tanjore, H., & Kalluri, R. (2006). The role of type IV collagen and basement membranes in cancer progression and metastasis. *The American journal of pathology*, *168*(3), 715-717. https://doi.org/10.2353/ajpath.2006.051321

Tao, M., Ao, T., Mao, X., Yan, X., Javed, R., Hou, W., Wang, Y., Sun, C., Lin, S., Yu, T., & Ao, Q. (2021). Sterilization and disinfection methods for decellularized matrix materials: Review, consideration and proposal. *Bioact Mater*, *6*(9), 2927-2945. https://doi.org/10.1016/j.bioactmat.2021.02.010

Taubenberger, A. V., Bray, L. J., Haller, B., Shaposhnykov, A., Binner, M., Freudenberg, U., Guck, J., & Werner, C. (2016). 3D extracellular matrix interactions modulate tumour cell growth, invasion and angiogenesis in engineered tumour microenvironments. *Acta Biomater*, *36*, 73-85. https://doi.org/10.1016/j.actbio.2016.03.017

Taylor, D. A., Sampaio, L. C., Ferdous, Z., Gobin, A. S., & Taite, L. J. (2018). Decellularized matrices in regenerative medicine. *Acta Biomaterialia*, *74*, 74-89. https://doi.org/https://doi.org/10.1016/j.actbio.2018.04.044

Taylor, K. R., & Gallo, R. L. (2006). Glycosaminoglycans and their proteoglycans: host-associated molecular patterns for initiation and modulation of inflammation. *The FASEB Journal*, *20*(1), 9-22. https://doi.org/https://doi.org/10.1096/fj.05-4682rev

Thanikachalam, K., & Khan, G. (2019). Colorectal Cancer and Nutrition. *Nutrients*, *11*(1), 164. https://doi.org/10.3390/nu11010164

Theocharis, A. D. (2002). Human colon adenocarcinoma is associated with specific post-translational modifications of versican and decorin. *Biochimica et Biophysica Acta (BBA) - Molecular Basis of Disease*, *1588*(2), 165-172. https://doi.org/https://doi.org/10.1016/S0925-4439(02)00161-8

Tian, X., Werner, M. E., Roche, K. C., Hanson, A. D., Foote, H. P., Yu, S. K., Warner, S. B., Copp, J. A., Lara, H., Wauthier, E. L., Caster, J. M., Herring, L. E., Zhang, L., Tepper, J. E., Hsu, D. S., Zhang, T., Reid, L. M., & Wang, A. Z. (2018). Organ-specific metastases obtained by culturing colorectal cancer cells on tissue-specific decellularized scaffolds. *Nat Biomed Eng*, *2*(6), 443-452. https://doi.org/10.1038/s41551-018-0231-0

Ventura, R. D., Padalhin, A. R., Park, C. M., & Lee, B. T. (2019). Enhanced decellularization technique of porcine dermal ECM for tissue engineering applications. *Materials Science and Engineering: C*, *104*, 109841. https://doi.org/https://doi.org/10.1016/j.msec.2019.109841

Voytik-Harbin, S. L., Brightman, A. O., Waisner, B. Z., Robinson, J. P., & Lamar, C. H. (1998). Small Intestinal Submucosa: A Tissue-Derived Extracellular Matrix That Promotes

Tissue-Specific Growth and Differentiation of Cells in Vitro. *Tissue Engineering*, *4*(2), 157-174. https://doi.org/10.1089/ten.1998.4.157

Walrath, J. C., Hawes, J. J., Van Dyke, T., & Reilly, K. M. (2010). Genetically engineered mouse models in cancer research. *Advances in cancer research*, *106*, 113-164. https://doi.org/10.1016/S0065-230X(10)06004-5

Walrath, J. C., Hawes, J. J., Van Dyke, T., & Reilly, K. M. (2010). Genetically engineered mouse models in cancer research. *Adv Cancer Res*, *106*, 113-164. https://doi.org/10.1016/s0065-230x(10)06004-5

Walter, F. M., Emery, J. D., Mendonca, S., Hall, N., Morris, H. C., Mills, K., Dobson, C., Bankhead, C., Johnson, M., Abel, G. A., Rutter, M. D., Hamilton, W., & Rubin, G. P. (2016). Symptoms and patient factors associated with longer time to diagnosis for colorectal cancer: results from a prospective cohort study. *British Journal of Cancer*, *115*(5), 533-541. https://doi.org/10.1038/bjc.2016.221

Wang, H., & Heilshorn, S. C. (2015). Adaptable hydrogel networks with reversible linkages for tissue engineering. *Adv Mater*, *27*(25), 3717-3736. https://doi.org/10.1002/adma.201501558

Wargovich, M. J., Brown, V. R., & Morris, J. (2010). Aberrant Crypt Foci: The Case for Inclusion as a Biomarker for Colon Cancer. *Cancers*, *2*(3), 1705-1716. https://www.mdpi.com/2072-6694/2/3/1705

Wei, J., Hu, M., Huang, K., Lin, S., & Du, H. (2020). Roles of Proteoglycans and Glycosaminoglycans in Cancer Development and Progression. *International journal of molecular sciences*, *21*(17), 5983. https://doi.org/10.3390/ijms21175983

White, L. J., Taylor, A. J., Faulk, D. M., Keane, T. J., Saldin, L. T., Reing, J. E., Swinehart, I. T., Turner, N. J., Ratner, B. D., & Badylak, S. F. (2017). The impact of detergents on the tissue decellularization process: A ToF-SIMS study. *Acta Biomater*, *50*, 207-219. https://doi.org/10.1016/j.actbio.2016.12.033

Winkler, J., Abisoye-Ogunniyan, A., Metcalf, K. J., & Werb, Z. (2020). Concepts of extracellular matrix remodelling in tumour progression and metastasis. *Nature Communications*, *11*(1), 5120. https://doi.org/10.1038/s41467-020-18794-x

Xi, Y., & Xu, P. (2021). Global colorectal cancer burden in 2020 and projections to 2040. *Translational Oncology*, *14*(10), 101174. https://doi.org/https://doi.org/10.1016/j.tranon.2021.101174

Xie, Y.-H., Chen, Y.-X., & Fang, J.-Y. (2020). Comprehensive review of targeted therapy for colorectal cancer. *Signal Transduction and Targeted Therapy*, *5*(1), 22. https://doi.org/10.1038/s41392-020-0116-z

Xu, S., Xu, H., Wang, W., Li, S., Li, H., Li, T., Zhang, W., Yu, X., & Liu, L. (2019). The role of collagen in cancer: from bench to bedside. *Journal of Translational Medicine*, *17*(1), 309. https://doi.org/10.1186/s12967-019-2058-1

Yamamoto, S., Nakase, H., Matsuura, M., Honzawa, Y., Matsumura, K., Uza, N., Yamaguchi, Y., Mizoguchi, E., & Chiba, T. (2013). Heparan sulfate on intestinal epithelial cells plays a critical role in intestinal crypt homeostasis via Wnt/β-catenin signaling. *American journal of physiology. Gastrointestinal and liver physiology*, *305*(3), G241-G249. https://doi.org/10.1152/ajpgi.00480.2012

Yang, L., Wang, S., Lee, J. J.-K., Lee, S., Lee, E., Shinbrot, E., Wheeler, D. A., Kucherlapati, R., & Park, P. J. (2019). An enhanced genetic model of colorectal cancer progression history. *Genome Biology*, *20*(1), 168. https://doi.org/10.1186/s13059-019-1782-4

Yoshimi, K., Hashimoto, T., Niwa, Y., Hata, K., Serikawa, T., Tanaka, T., & Kuramoto, T. (2012). Use of a chemically induced-colon carcinogenesis-prone Apc-mutant rat in a chemotherapeutic bioassay. *BMC Cancer*, *12*, 448-448. https://doi.org/10.1186/1471-2407-12-448

Young, M., & Reed, K. R. (2016). Organoids as a Model for Colorectal Cancer. *Curr Colorectal Cancer Rep*, *12*(5), 281-287. https://doi.org/10.1007/s11888-016-0335-4

Zhang, W., Du, A., Liu, S., Lv, M., & Chen, S. (2021). Research progress in decellularized extracellular matrix-derived hydrogels. *Regen Ther*, *18*, 88-96. https://doi.org/10.1016/j.reth.2021.04.002

Zhu, J., & Kaufman, L. J. (2014). Collagen I self-assembly: revealing the developing structures that generate turbidity. *Biophysical journal*, *106*(8), 1822-1831. https://doi.org/10.1016/j.bpj.2014.03.011